Available online at www.sciencedirect.com

ScienceDirect

Acta Materialia 62 (2014) 1–48

Acta MATERIALIA

www.elsevier.com/locate/actamat

Overview No. 152

Grain boundary complexions

Patrick R. Cantwell [a], Ming Tang [b,1], Shen J. Dillon [c], Jian Luo [d], Gregory S. Rohrer [e], Martin P. Harmer [a,*]

[a] Department of Materials Science and Engineering, Center for Advanced Materials and Nanotechnology, Lehigh University, Bethlehem, PA 18015, USA
[b] Condensed Matter and Materials Division, Lawrence Livermore National Laboratory, Livermore, CA 94550, USA
[c] Department of Materials Science and Engineering, University of Illinois Urbana-Champaign, Urbana, IL 61801, USA
[d] Department of NanoEngineering, Program of Materials Science and Engineering, University of California, San Diego, La Jolla, CA 92093-0448, USA
[e] Department of Materials Science and Engineering, Carnegie Mellon University, Pittsburgh, PA 15213, USA

Received 3 May 2013; received in revised form 20 July 2013; accepted 22 July 2013
Available online 4 September 2013

Abstract

Grain boundaries exhibit phase-like behavior in which their structure, chemistry and properties may change discontinuously at critical values of thermodynamic parameters such as temperature, pressure and chemical potential. Therefore, grain boundaries (and other interfaces such as surfaces and heterophase boundaries) can be treated as thermodynamically stable interfacial states. To differentiate these interfacial states from bulk phases, the term "complexion" has been introduced. A variety of terminology has been used to describe complexions and complexion transitions. In many cases, several terms exist that describe essentially the same phenomenon. We give an overview of complexion-related terminology, suggest a preferred nomenclature and discuss a classification framework that can be used to categorize complexions and complexion transitions. The field of grain boundary complexions has evolved rapidly in the past decade due to advances in experimental equipment – in particular, aberration-corrected transmission electron microscopy – and progress in computational simulation methods. Grain boundary complexion transitions are the root cause of a wide variety of materials phenomena – such as abnormal grain growth, grain boundary embrittlement and activated sintering – that have defied mechanistic explanation for years. In this overview, we review the history and theory of grain boundary complexion transitions, their role in materials processing and their effect on materials properties.

Keywords: Grain boundary; Complexions; Phases; Transitions; Kinetics

1. Introduction

Grain boundaries strongly influence the properties and behavior of polycrystalline materials during processing and in service [1]. Grain boundary energy, mobility, diffusivity, cohesive strength and sliding resistance – all of which depend upon local structure and chemistry – determine bulk materials behavior and properties such as superplasticity, creep, fatigue, corrosion, strength and conductivity [2]. Grain boundary specialists have long recognized that grain boundaries can be considered as quasi-two-dimensional "phases" that may undergo phase-like transitions in which their structure and chemistry changes abruptly at critical values of thermodynamic parameters [1,3–11]. As predicted by Hart [5], the grain boundary properties most strongly affected by these transitions will be the non-equilibrium properties, such as mobility, diffusivity, intergranular cohesive strength and grain boundary sliding resistance. Equilibrium grain boundary properties, such as energy, specific volume and adsorption, will also be affected, but in general are less accessible to experiment than non-equilibrium grain boundary properties. If a significant fraction of the grain boundaries in a polycrystalline material undergo a transition, the cumulative effect can be a dramatic and rather sudden change in macroscopic properties [5].

* Corresponding author. Tel.: +1 610 758 4227.
E-mail address: mph2@lehigh.edu (M.P. Harmer).
[1] Present address: Shell Technology Center, Houston, TX 77082, USA.

1359-6454/$36.00 © 2013 Acta Materialia Inc. Published by Elsevier Ltd. All rights reserved.
http://dx.doi.org/10.1016/j.actamat.2013.07.037

Grain boundary complexion transitions have traditionally been called grain boundary "phase transitions", in analogy to bulk phase transitions. Interfaces such as grain boundaries can be analyzed using equilibrium thermodynamics [12] and may transform in a manner analogous to bulk phase transitions, but equilibrium interfacial states do not satisfy the Gibbs definition of a phase because they are inhomogeneous and may have gradients of structure, composition, properties and other order parameters. Therefore, Tang et al. [13] introduced the term "complexion"[2] to denote an equilibrium interfacial state. A complexion, concisely defined, is interfacial material or strata that is in thermodynamic equilibrium with the abutting phase(s) and has a stable, finite thickness that is typically on the order of 0.2–2 nm [14]. A complexion cannot exist independently of the abutting phases and its average composition and structure need not be the same as the abutting phases.

com·plex·ion *noun* \kəm-ˈplek-shən\
Interfacial material or strata that is in thermodynamic equilibrium with its abutting phase(s)

The term "complexion" has been adopted by the authors of this overview [11,15–36], and has been recognized [37–41] and adopted [42–45] by others. Therefore, in this overview the term "grain boundary complexion" will be used rather than "grain boundary phase" to describe an equilibrium grain boundary state, even though the original "phase" terminology may have been used by the original author(s). Similarly, although the "surface phase" terminology is widely used in the surface science community, equilibrium interfacial states at free surfaces will be referred to here as "surface complexions".

Grain boundary complexion transitions are difficult to predict a priori and typically occur independently of bulk phase transformations, i.e. at different values of temperature, pressure or composition. Therefore, they often result in unexpected and seemingly inexplicable phenomena. In 1968, Hart postulated that grain boundary complexion transitions could be responsible for temper embrittlement in steel [3–5], although he recognized that insufficient experimental evidence existed at the time to support the hypothesis [4]. It was not until 20 years after Hart's first paper that the existence of grain boundary complexion transitions was deemed to be conclusive [8]. Since then, advances in transmission electron microscopy and other experimental techniques have provided strong evidence that grain boundary complexion transitions are responsible for materials phenomena as diverse as abnormal grain growth [17,46], solid-state activated sintering [47] and liquid–metal embrittlement [48].

Interfaces can be separated into two groups: external interfaces (e.g. surfaces) and internal interfaces (e.g. grain boundaries, heterophase boundaries, stacking faults and antiphase boundaries) [9]. All of these interfaces play an important role in materials science, and understanding their phase-like behavior has been identified as one of eight grand challenges in ceramic science [49]. In this overview, we will focus on grain boundary complexions and their impact on materials properties and processing. We will also occasionally discuss surface complexions and heterophase boundary complexions when appropriate to illustrate important concepts.

2. The fundamentals of grain boundary complexions

Seminal articles on the fundamentals of grain boundary transitions include those by Hart [3,5], Cahn [6] and Rottman [8,9]. Grain boundary transitions are also discussed in the textbook on crystalline interfaces by Sutton and Balluffi [1]. In this section, we will summarize the main points and conclusions of these thermodynamic treatments.

While the vast majority of research on grain boundary complexions has focused on non-pure systems in which grain boundary segregation plays a critical role, grain boundary complexion transitions may occur in even pure materials. We will first discuss grain boundary complexions in pure materials to illustrate their fundamental characteristics. Then we will discuss the more complicated complexion transitions in non-pure systems that can involve changes in grain boundary composition as well as structure.

2.1. Thermodynamic parameters of grain boundaries

The fundamental thermodynamic quantity that characterizes grain boundaries (and interfaces in general) is the energy per unit area, γ, which represents the amount of work required to create one unit of grain boundary area via a reversible process. In other words, γ represents the additional (excess) free energy per unit area that exists in the system due to the presence of the grain boundary. The value of γ is a function of both bulk and interfacial thermodynamic parameters. The usual bulk thermodynamic parameters are temperature (T), pressure (P) and/or chemical potential (μ_i) (or, alternatively, composition [6]). There are five interfacial thermodynamic parameters that describe the five macroscopic degrees of freedom of a grain boundary. Several different geometric conventions exist for describing these five parameters [50]. For ease of conceptual understanding, we use the simple convention followed by Rottman [9], in which three variables specify the misorientation vector $\boldsymbol{R}$ between the two crystals and two independent variables in the form of a unit vector, $\hat{\boldsymbol{n}}$, specify the average orientation of the grain boundary plane normal (i.e. the grain boundary plane inclination). The misorientation vector $\boldsymbol{R}$ is defined by a rotation of angle ω around a direction common to both grains specified by a unit vector $\hat{\boldsymbol{u}}$, i.e. $\boldsymbol{R} = \hat{\boldsymbol{u}}\omega$. Given a misorientation vector $\boldsymbol{R}$, the rotation angle and axis can be recovered using the relations $\omega = |\boldsymbol{R}|$ and $\hat{\boldsymbol{u}} = \boldsymbol{R}/\omega$.

The energy of a grain boundary defined using these parameters depends upon $6 + C$ independent variables,

[2] The term "complexion" was tentatively suggested by W.C. Carter and embraced by R.M. Cannon.

which includes the five geometric parameters of the grain boundary, where C is the number of components [6]. The grain boundary energy γ may also depend upon applied electric and magnetic fields, for example, but their influence on complexion stability and transitions has not been treated in detail and will not be discussed in this overview.

In addition to these $6 + C$ variables, there are three more geometric parameters that specify the relative translational displacement of the two crystals and an additional geometric parameter that specifies the translational displacement of the grain boundary plane along its normal direction with respect to the two crystal lattices [9]. However, in most analyses, the grain boundary is assumed to relax to equilibrium with respect to these four microscopic parameters, and thus they are typically ignored [6,9].

The grain boundary energy, γ, is always a continuous function of one of the thermodynamic parameters (e.g. T, P, μ_i, $\boldsymbol{R}$ or $\hat{\boldsymbol{n}}$) for a complexion transition that occurs under equilibrium conditions. This implies that two (or more) complexions may coexist at equilibrium in a manner analogous to the coexistence of bulk phases at solidus and liquidus lines on phase diagrams.

A first-order complexion transition occurs when there is a discontinuity in the first derivative of γ as a function of one of the thermodynamic parameters (T, P, μ_i, $\boldsymbol{R}$ or $\hat{\boldsymbol{n}}$). A second-order (or higher-order) complexion transition occurs when there is a discontinuity in a second (or higher-order) derivative of γ [8,9]. This thermodynamic definition of a complexion transition is fundamental and universal, and is directly analogous to the definition of a bulk phase transition [9]. It is the key to recognizing when one complexion is "thermodynamically distinct" from another complexion, in the same way that two bulk phases can be recognized as thermodynamically distinct from each other.

We emphasize that complexion transitions are not limited to changes in the atomic structure or thickness of the grain boundary core (which are sometimes called "structural transitions") but may also include transitions in composition, chemical bonding, roughening, atomic reconstructions of the grain boundary core even if they do not result in a thickness change, and, indeed, any physical change that results in a discontinuity of the first- or higher-order derivative of γ as a function of one of the thermodynamic parameters (T, P, μ_i, $\boldsymbol{R}$ or $\hat{\boldsymbol{n}}$).

Unfortunately, in real-world experiments, it is extraordinarily difficult to detect complexion transitions based on this thermodynamic definition, so approximations are made and observable features such as grain boundary thickness and solute adsorption are used as proxies to identify distinct complexions. The use of such proxies is not an infallible method and may sometimes lead to two complexions being identified as distinct from one another when they are in fact not thermodynamically distinct. Theoretical models and computer simulations are more amenable to applying the rigid thermodynamic definition of a complexion transition to identify distinct complexions.

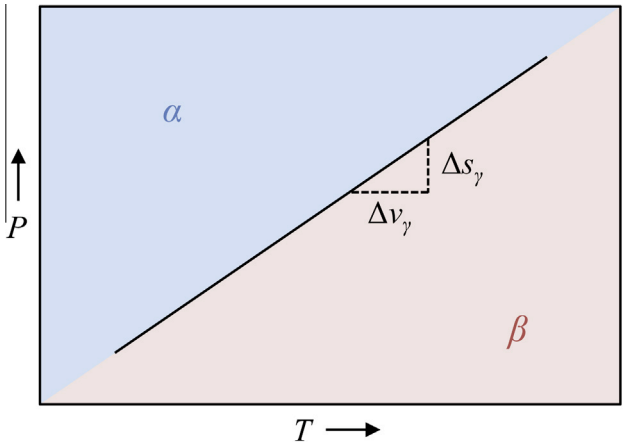

Fig. 1. An early theoretical grain boundary complexion diagram for a pure material showing the pressure–temperature (P–T) locus of a complexion transition between two hypothetical complexions, complexion α (blue region) and complexion β (red region). Hart [5] referred to β as the "high temperature grain boundary phase (H-phase)" and α was referred to as the "low temperature grain boundary phase (L-phase)". Adapted from Ref. [5] (For interpretation of the references to color in this figure legend, the reader is referred to the web version of this article.).

2.2. Grain boundary complexions in pure materials

Hart [5] conducted a theoretical thermodynamic analysis of a grain boundary with fixed geometry in a pure material and developed a Clausius–Clapeyron equation that defined the pressure–temperature locus of a grain boundary complexion transition. This analysis resulted in a grain boundary complexion diagram (Fig. 1) showing regions of complexion stability for two complexions in P–T space and the complexion transition line dividing these two regions. Hart further showed that, during a first-order complexion transition, the magnitude of the slope discontinuity in γ as a function of temperature or pressure can be directly related to a discontinuity in the specific excess volume Δv_γ and entropy Δs_γ of the grain boundary as follows (where Δv_γ and Δs_γ represent the difference in specific volume and entropy between the two complexions coexisting at equilibrium) [5]:

$$\Delta(\partial\gamma/\partial T)_P = -\Delta s_\gamma \quad (1)$$

$$\Delta(\partial\gamma/\partial P)_T = \Delta v_\gamma \quad (2)$$

In other words, the slope of γ–T and γ–P curves (at constant pressure and temperature, respectively) will be different above and below the complexion transition point, as shown schematically in Fig. 2.[3] There is no discontinuity in the value of γ itself at a complexion transition point, which follows from equilibrium thermodynamics [6]. As Hart points out, the type of first-order complexion transition shown in Fig. 2 is associated with a latent heat of transformation, $T\,\Delta s_\gamma$, which in principle can be measured

[3] An apparent drafting error led to a reversal of slopes in the original plot of γ vs. P in Ref. [5], which has been corrected in Fig. 2(a).

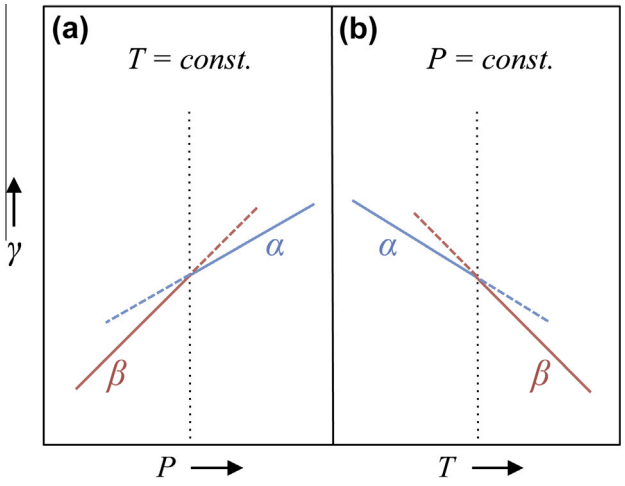

Fig. 2. A schematic illustration of grain boundary excess free energy γ in a pure material as a function of (a) pressure and (b) temperature for two "competing" complexions: α (blue line) and β (red line). Solid lines represent the stable complexion and dashed lines represent the metastable complexion. A first-order grain boundary complexion transition occurs at the vertical dotted black lines and is recognizable by the discontinuity in the slope of γ. (a) Complexion β has a larger excess specific volume than α (and hence a larger slope, $(\partial\gamma/\partial P)_T$), and is therefore the stable complexion at low pressure. (b) Complexion β has a larger excess specific entropy than α (and hence a larger negative slope, $(\partial\gamma/\partial T)_P$), and is therefore the stable complexion at high temperature. Hart referred to β, which has larger excess specific volume and larger excess specific entropy, as the "high temperature phase (H-phase)", and α was referred to as the "low temperature phase (L-phase)" [5]. Adapted from Hart [5]. (For interpretation of the references to color in this figure legend, the reader is referred to the web version of this article.)

experimentally, and in fact has been measured for complexion transitions at liquid–liquid interfaces [51,52]. It is also associated with a change in the specific excess volume of the grain boundary, Δv_γ, which in principle can be detected by sensitive dilatometry measurements [5].

Conceptually, we can understand the mathematical behavior of γ during a first-order complexion transition by envisioning that several different metastable grain boundary complexions could potentially exist at a given grain boundary. Each metastable complexion may have a different atomic structure (and, for multicomponent systems, may also have a different composition) and therefore a different value of γ. At thermodynamic equilibrium, the complexion with the smallest value of γ is the stable complexion and will be present in lieu of the other possible (metastable) complexions. As any given thermodynamic parameter is varied, the γ curve of a previously metastable complexion may cross that of the stable complexion, thereby forcing a complexion transition. This behavior is illustrated in Fig. 2 for complexions α and β. The α complexion is stable at low temperature and high pressure, while the β complexion is stable at high temperature and low pressure. There is a discontinuity in the first derivative of γ at the complexion transition point denoted by the vertical dotted lines, but γ is continuous at the complexion transition point.

The discussion thus far has focused on grain boundary complexion transitions in pure materials with fixed grain boundary shape and geometrical parameters $\boldsymbol{R}$ and $\hat{\boldsymbol{n}}$. Such complexion transitions are called "congruent" transitions [6] and are characterized by changes in atomic structure in the grain boundary core. At equilibrium, two complexions, α and β, may coexist, as shown schematically in Fig. 3(a). Grain boundary complexion transitions that result in a change in the geometrical parameters of the grain boundary (the "grain boundary character") are called "non-congruent" transitions [6] and can be categorized as either faceting transitions or dissociation transitions. In a faceting transition, the grain boundary plane normal $\hat{\boldsymbol{n}}$ decomposes into $\hat{\boldsymbol{n}}_1$ and $\hat{\boldsymbol{n}}_2$, the area-weighted average of which is equivalent to $\hat{\boldsymbol{n}}$. The coexistence of α and β during a faceting transition is shown schematically in Fig. 3(b). In a dissociation transition, a single grain boundary dissociates into two new interfaces, separated by a bulk phase, with misorientation $\boldsymbol{R}_1$ and $\boldsymbol{R}_2$, the combined misorientation of which is equal to the original misorientation $\boldsymbol{R}$ (Fig. 3(c)). The dissociation transition is more commonly known as a "wetting transition" and occurs when the sum of the energy of the two new grain boundaries is less than that of the original grain boundary. If the wetting phase is not crystalline, then $\boldsymbol{R}_1$ and $\boldsymbol{R}_2$ are undefined, but the original misorientation $\boldsymbol{R}$ is still maintained across the phase.

Cahn [6] discussed the geometry of grain boundary complexion transitions in great detail and reached several important conclusions, which we summarize here: (i) a smoothly curving grain boundary can be considered as a single grain boundary complexion; (ii) grain boundary complexion transitions usually occur at "singularities" in grain boundary geometry, e.g. at edges and facets; (iii) complexion coexistence and transitions are almost always non-congruent and thus involve discontinuities in grain boundary geometry (faceting or dissociation); (iv) congruent complexion transitions are possible but rare; (v) the observation of a congruent complexion transition might be an artifact of the transition occurring far from equilibrium conditions. For further details, the reader is referred to the original text [6]. However, recent experiments and simulations have shown that congruent complexion transitions are not as uncommon as Cahn suggested; some examples are discussed in the following paragraph. It should also be pointed out that Cahn made the above statements with pure systems in mind. On the other hand, essentially all materials contain impurities, and examples of congruent transitions are much more abundant in non-pure systems, such as the complexion transitions from a clean complexion to a monolayer, bilayer or trilayer complexion (see Section 2.3.3). Therefore, while faceting and dissociation are two important markers for grain boundary complexion transitions in pure materials, complexion transitions in general entail a rich variety of behaviors, including those that maintain the grain boundary geometry.

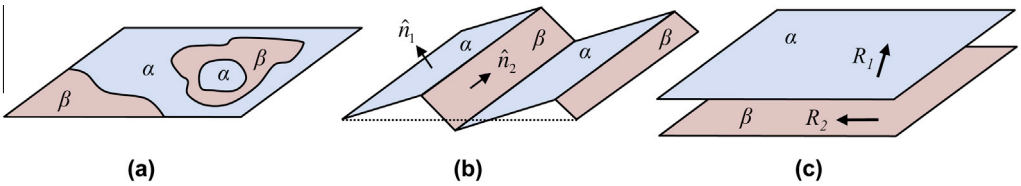

Fig. 3. Schematic illustration of the coexistence of two grain boundary complexions, α and β, at three different grain boundary geometries: (a) coexistence of two complexions (on the same macroscopic plane) at grain boundary with the same misorientation $\boldsymbol{R}$ and inclination $\hat{\boldsymbol{n}}$; (b) coexistence of two complexions with the same grain boundary misorientation $\boldsymbol{R}$ but different grain boundary inclinations, $\hat{\boldsymbol{n}}_1$ and $\hat{\boldsymbol{n}}_2$, resulting in a faceted structure; (c) coexistence of two complexions (separated by a bulk phase) with the same grain boundary inclination $\hat{\boldsymbol{n}}$ but different grain boundary misorientations $\boldsymbol{R}_1$ and $\boldsymbol{R}_2$, as might exist after a dissociation transition (i.e. a wetting transition). Complexion coarsening may occur in (a) and (b) to reduce the total length of the one-dimensional complexion boundaries. Adapted from Ref. [9].

Despite decades of research, efforts to identify grain boundary complexion transitions in pure metals via high-resolution transmission electron microscopy (HRTEM) and computer simulations have been largely unsuccessful. Nevertheless, experimental evidence suggesting grain boundary complexion transitions in pure metals has existed for decades. For example, researchers have reported anomalies and discontinuities in the activation energy as a function of temperature for grain boundary mobility in zone-refined lead [53], grain boundary diffusivity in pure copper [54] and grain boundary sliding in zinc bicrystals [55]. A fair criticism of these types of experimental studies is that they could be influenced by trace impurities. However, a recent molecular dynamics (MD) computer simulation employing an innovative methodology has successfully demonstrated a grain boundary complexion transition in pure Cu grain boundaries at temperatures well below the melting point, providing strong support for the existence of grain boundary transitions in pure materials [39]. The transition demonstrated by the MD simulation was a congruent transition, in which the atomic structure of the grain boundary core changed but the grain boundary geometry (character) remained invariant. The coexistence of these two intrinsic grain boundary complexions is shown in Fig. 4(a) and the atomic structure of each complexion is shown in Fig. 4(b and c). Furthermore, the complexion transition exhibited a discontinuity in grain boundary density, consistent with Hart's analysis [5]. The authors suggest that this type of grain boundary complexion transition may play a role in the healing of radiation damage, and that grain boundary complexion transitions in pure metals may be more common than previously thought [39].

2.3. Grain boundary complexions in non-pure materials

Grain boundary adsorption (segregation[4]) may occur in non-pure materials, causing the composition of grain boundaries to differ from the overall composition at equilibrium [2]. Differences in grain boundary composition may also arise from kinetic processes such as grain growth. Such non-equilibrium segregation is referred to as enrichment and will not be discussed in detail here.

Grain boundary adsorption plays a dominant role in complexion transitions in non-pure systems. Adsorption phenomena must also be considered when conducting experiments on nominally pure systems, which invariably contain impurities. When Hart first suggested the concept of grain boundary complexion transitions in 1968, he proposed that they might be responsible for temper embrittlement of steel via a first-order discontinuity in the grain boundary adsorption of solute elements [3]. Hart made this prediction based on an analogy to two-dimensional phase transitions on free surfaces, a concept already well known at the time from the work of Fowler and Guggenheim [56] and others [57,58].

Early theories of grain boundary adsorption were based on the McLean model, which assumes that segregation is constrained to a monolayer of atomic sites at the grain boundary [59]. Later models acknowledged that multilayer grain boundary segregation can occur and may be accompanied by structural changes in the grain boundary core [13,60,61]. When multilayer segregation occurs, entirely new structures may manifest at the grain boundary and induce a grain boundary complexion transition. Recent experimental work has demonstrated that such adsorption-based grain boundary complexion transitions are linked to phenomena such as abnormal grain growth in ceramics [17], activated sintering [47] and liquid metal embrittlement [48]. Various terms have been used to describe multilayer adsorption and structural transitions at grain boundaries. We will direct most of our focus on premelting and prewetting transitions, which are two of the most widely studied types of grain boundary complexion transitions.

In this section, we discuss the fundamentals of grain boundary complexion transitions in non-pure systems, with an emphasis on theoretical models for grain boundary adsorption. We first review the conditions necessary for a first-order complexion transition based on classical models of grain boundary adsorption, then move onto more modern models of premelting and prewetting transitions. Finally, we discuss the fundamentals of discrete complexions.

[4] The terminologies "grain boundary adsorption" and "grain boundary segregation" are used interchangeably to refer to the same phenomenon.

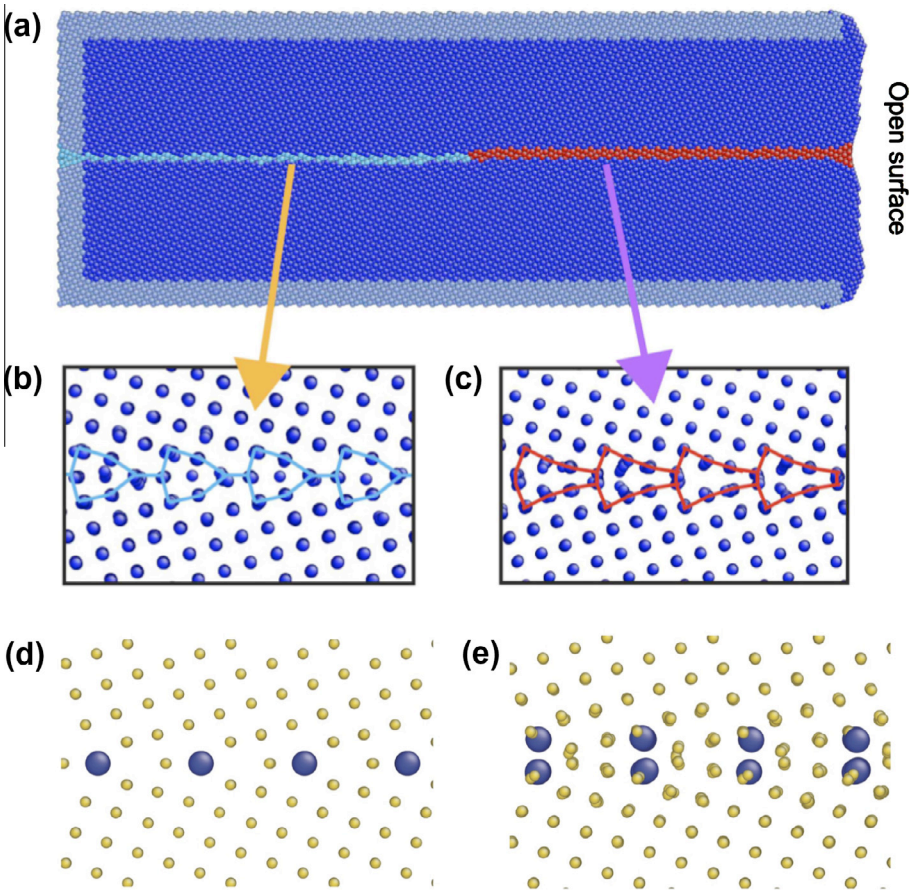

Fig. 4. MD and Monte Carlo simulation results that demonstrate intrinsic (a–c) and extrinsic (d, e) grain boundary complexion transitions at a Σ5(310) boundary in pure Cu (a–c) and Ag-doped Cu (d, e). A congruent complexion transition is shown in (a), in which the two intrinsic grain boundary complexions ("kites" and "split kites") coexist and meet at a one-dimensional complexion boundary. The atomic structure of the intrinsic "kites" complexion is shown in (b) and the atomic structure of the "split kites" complexion is shown in (c). When the Cu is doped with Ag, a similar complexion transition occurs from (d) "kites", with a monolayer complexion with Ag adsorption, to (d) "split-kites", with bilayer complexions with Ag adsorption. These two complexions can be considered as two different discrete Dillon–Harmer complexions (i.e. monolayer and bilayer complexions). The complexions in (b) and (c) are two manifestations of the clean complexion in the Dillon–Harmer scheme. Parts (a–c) reprinted from Ref. [39] with permission and parts (d, e) reprinted from Ref. [149] with permission.

We cannot hope to give a fully rigorous and complete account of all theories and models used to describe these phenomena, which are numerous and highly detailed. More complete accounts can be found in various textbooks [1,41,56,59,62] and review articles [2,15,22,23,32,63], and the original research articles referenced therein. Our aim here is to give an overview of grain boundary complexions and transitions in non-pure systems, with an emphasis on providing physical insight and understanding.

2.3.1. Classical grain boundary adsorption/segregation models

In 1957, McLean [59] proposed a classical grain boundary adsorption model via an analogy of the Langmuir surface adsorption model [64]. This Langmuir–McLean model can be derived with the following assumptions:

(1) There are a fixed number of (homogeneous) excess adsorption sites per unit area at a grain boundary.
(2) The grain boundary can be treated as a separate thermodynamic entity that is in equilibrium with the bulk phase (with a given fraction of solute of X_{bulk}).
(3) Both the bulk phase and the grain boundary can be treated as ideal solutions.

The grain boundary atomic fraction of solute X_{GB} is then given by the following Langmuir–McLean isotherm:

$$\frac{X_{GB}}{1-X_{GB}} = \frac{X_{bulk}}{1-X_{bulk}} e^{-\frac{\Delta G_{ads}}{RT}} \tag{3}$$

where R is the universal gas constant and ΔG_{ads} is the standard molar Gibbs free energy of adsorption, which is defined as a negative value for positive adsorption of solute at the grain boundary.

Great efforts have been made to refine and extend the Langmuir–McLean grain boundary adsorption model in various aspects; readers are referred to elegant articles by Hondros and Seah [65], Wynblatt and Chatain [66] and Lejček and Hofmann [67] for elaboration of these grain

boundary adsorption models. Perhaps the simplest way to illustrate the possible occurrence of a first-order grain boundary complexion transition is by analyzing the generalized Langmuir–McLean isotherm that was given in Ref. [67]:

$$\frac{a^I_{GB}}{a^M_{GB}} = \frac{a^I_{bulk}}{a^M_{bulk}} e^{-\frac{\Delta G^*_{ads}}{RT}} \tag{4}$$

where $a^I_{GB}, a^M_{GB}, a^I_{bulk}$ and a^M_{bulk} are the activities of the impurity (i.e. solute, I) and matrix (M) elements in the grain boundary (GB) and bulk phase, respectively. It is worth noting that this formulism [67] was derived by treating the grain boundary as a stand-alone "phase" instead of a complexion by ignoring the gradient energy term associated with the "cross" bonds between the grain boundary atoms and matrix atoms. A more rigorous treatment that considers the multilayer nature and compositional gradients is given by Wynblatt and Chatain [66]. Nonetheless, a special case of this less-rigorous generalized isotherm can illustrate the possible occurrence of a first-order grain boundary complexion transition as well as its origin. Here, we assume that the grain boundary can be represented as a regular solution (with an interaction parameter, Ω_{GB}) and the bulk phase is still an ideal solution (if the bulk phase is not an ideal solution, a similar result can still be obtained in the dilute-solution limit of the bulk phase, assuming Henry's law applies). The generalized Langmuir–McLean isotherm in Eq. (4) can then be simplified to:

$$\frac{X_{GB}}{1-X_{GB}} = \frac{X_{bulk}}{1-X_{bulk}} e^{-\frac{\Delta G^{(0)}_{ads} - 2\Omega_{GB} X_{GB}}{RT}} \tag{5}$$

where $\Delta G^{(0)}_{ads} (\equiv \Delta G^*_{ads} + \Omega_{GB})$. Eq. (5) is essentially equivalent to the Fowler–Guggenheim isotherm [56], which is commonly expressed as:

$$\frac{X_{GB}}{1-X_{GB}} = \frac{X_{bulk}}{1-X_{bulk}} e^{-\frac{\Delta G^{(0)}_{ads} + \alpha z X_{GB}}{RT}} \tag{6}$$

where z the coordination number and α ($\equiv -2\Omega_{GB}/z$) is a parameter characterizing adsorbate–adsorbate interactions. The Fowler–Guggenheim isotherm was also first proposed for surface adsorption and then adapted for grain boundary adsorption [3,65]. In a classic article in 1977, Hondros and Seah [65] pointed out that this Fowler–Guggenheim isotherm can produce a first-order grain boundary complexion transition if the adsorbate–adsorbate interaction is strongly attractive (under the condition that $2\Omega_{GB} \equiv -\alpha z > \sim 4RT$); this is illustrated in Fig. 5(a). It is interesting to note that this condition for the occurrence of a first-order complexion transition is identical to that for a phase separation of a regular solution ($\Omega > 2RT$), which provides a clear hint of the physical origin of this first-order grain boundary complexion transition.

We should further note that this first-order complexion transition as a result of an attractive adsorbate–adsorbate interaction occurs because of the same physical principle that produces the first-order gas-to-liquid bulk phase transition in the van der Waals isotherm for non-ideal gas with an attractive intermolecular interaction (Fig. 5(b)). In fact, in two original articles, published in 1968 and 1972 [3,5], Hart proposed that grain boundaries can undergo first-order complexion transitions, in part based on analogy to the three-dimensional gas–liquid bulk phase transformation, in addition to the analogy to surface phase transitions of the type described theoretically by Fowler and Guggenheim [56].

We point out that the Fowler–Guggenheim model, when applied to grain boundary adsorption, in essence demonstrates a first-order complexion transition within a grain boundary of fixed structural width (or, strictly speaking, of fixed number of adsorbate sites) in which there is a jump from low adsorbate content to high adsorbate content. With more advanced models, it is also possible to have similar complexion transitions between grain boundaries of different structural widths (and hence of different numbers of adsorbate sites), in which the thickness of the grain boundary core changes together with the amount of solute adsorption. The ability of a boundary to undergo structural and compositional transitions within a boundary core of fixed width or between boundaries of different fixed widths indicates that there could be many more or many fewer complexions in a given system than suggested by the discrete Dillon–Harmer complexion categories that are introduced later in Section 2.3.3.

The above discussion clearly demonstrates an analogy between the bulk phase transitions and interfacial complexion transitions. Although the Fowler–Guggenheim isotherm (i.e. a modified Langmuir–McLean model where the grain boundary behaves like a regular solution) can produce a first-order complexion transition, this model has several limitations, because it does not consider that:

- the grain boundary adsorption can occur in a multilayer fashion where the adsorption sites are not all equivalent [66];
- in addition to chemical adsorption, grain boundaries can undergo transitions in atomic structure that will change the adsorption free energies (i.e. an interfacial disordering transition can be coupled with an adsorption transition [16,60,61]); and
- rigorously, a grain boundary cannot be treated as a separate, homogeneous thermodynamic entity (e.g. even if we assume that adsorption only occurs within one monolayer at the grain boundary, there will be an extra gradient energy term that will depend on both bulk and grain boundary compositions) [66].

Thus, more realistic models should consider the spatial gradients in both composition and structure. These can be better treated in lattice-gas models [60,66,68] or diffuse-interface (phase-field) models [13,16,61,69], which will be discussed in the following sections.

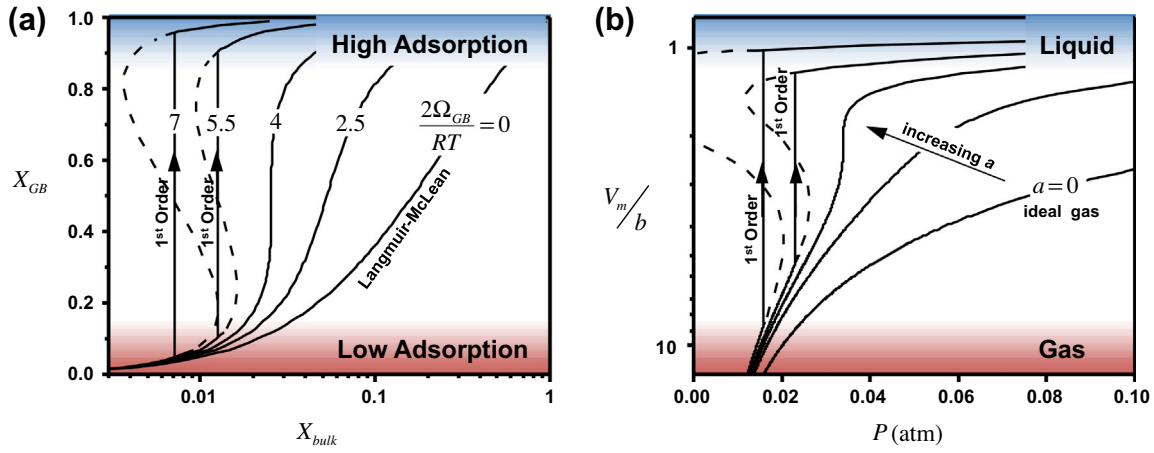

Fig. 5. Analogy between (a) a first-order complexion transition in which there is a discontinuous jump in adsorbed solute content and (b) a first-order bulk phase transition from gas to liquid. Both of these first-order transitions arise when the attractive interactions between particles (adsorbate atoms or gas molecules, respectively) reach a critical strength. (a) The Fowler–Guggenheim isotherm is plotted for increasing values of $2\Omega_{GB}/RT$ ($=-\alpha z/(RT)$). When this value is equal to zero, Langmuir–McLean behavior occurs. (b) The van der Waals equation of a non-ideal gas ($P = RT/(V_m - b) + a/V_m^2$) is plotted for increasing values of "a", where "a" is the strength of intermolecular attraction and "b" is the volume excluded by a mole of gas molecules. When "a" is equal to zero, the gas is ideal. First-order transitions in (a) and (b) are represented by vertical lines with arrows.

2.3.2. Prewetting and premelting complexion transitions

Prewetting and premelting transitions are two types of complexion transitions that have been studied extensively during the past few decades. Premelting refers to the formation of a disordered, liquid-like film on a crystalline surface (or at a grain boundary, phase boundary or free surface) at a temperature below the bulk melting temperature or solidus of the underlying crystal. Extensive discussions of premelting can be found in review articles [70,71]. Strictly speaking, premelting is defined only for unary systems in which there is a single melting temperature. However, premelting may also refer to high-temperature disordering of grain boundaries in multicomponent systems.

Prewetting is a type of complexion transition that occurs when a layer of material of fixed equilibrium thickness forms at the interface in the thermodynamic vicinity of a wetting transition, i.e. near the temperature or composition at which a wetting transition would occur. The discovery of the prewetting transition is attributed to Cahn [69] and Ebner and Saam [72]. As the term is commonly used, it refers to a first-order adsorption transition in which the "film" of material separating two phases undergoes a discontinuity in both adsorption and thickness. Premelting can be considered as a special case of prewetting in which there is a discontinuity in crystalline order and thickness but not necessarily in adsorption. These transitions are strongly related to wetting transitions and hence their analysis is rooted in a wetting analysis that compares relative interfacial energies between bulk phases. Therefore we will review the fundamentals of prewetting and premelting transitions – both of which are complexion transitions – in the context of wetting transitions.

When a liquid droplet is placed on top of a surface, it will partially wet the surface with a finite contact angle when $\gamma_{lv} + \gamma_{sl} > \gamma_{sv}$, where γ_{lv} (γ_{sv}) is the surface energy of the liquid (solid) phase and γ_{sl} is the liquid/solid interface energy. On the other hand, when the liquid will completely wet the surface by spreading on the surface to form a continuous film, which has an arbitrary thickness that is only determined by the volume of the liquid droplet, we have $\gamma_{sv} \equiv \gamma_{lv} + \gamma_{sl}$ thermodynamically (by definition). Prewetting refers to a transition that occurs between partial and complete wetting, in which a thin layer of material forms to cover the surface but has an equilibrium thickness that is controlled by thermodynamic state variables (e.g. temperature, pressure) and does not depend on the amount of liquid available. The prewetting transition was first predicted by Cahn in his seminal paper entitled "Critical Point Wetting" [69]. In this paper, Cahn considers a binary fluid with a miscibility gap that is in contact with a flat container surface. He applies a diffuse-interface model to describe the free energy of this system, which in one dimension is expressed as

$$F[c,T] = \Phi(c_s) + \int_0^\infty [f(c,T) + \kappa(dc/dx)^2]dx \qquad (7)$$

where Φ represents a short-range surface interaction energy that is a function of the liquid composition at the surface, $c_s = c(x=0)$, $f(c,T)$ is the homogeneous free energy density of the liquid and $\kappa(dc/dx)^2$ is the gradient energy term that penalizes the development of a composition gradient within the fluid. For the purpose of discussion, suppose that the surface energy with the container has a larger value for liquid phase α (rich in component A), $\gamma_{\alpha c}$, than for phase β (rich in component B), $\gamma_{\beta c}$. Mathematically, this is reflected by Φ being a decreasing function of c and having a minimum at $c = 1$ (pure B). For compositions within the miscibility gap (the two-phase coexistence region), Cahn uses a simple scaling argument to show that a first-order complete

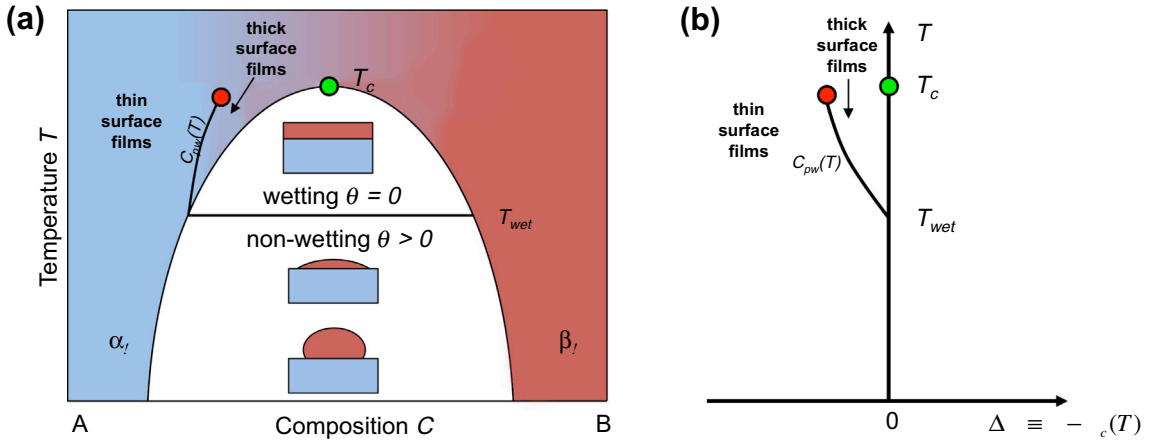

Fig. 6. Illustration of Cahn's surface wetting diagram in (a) the composition–temperature (c–T) space and (b) the excess chemical potential–temperature ($\Delta\mu$–T) space, where $\Delta\mu \equiv \mu - \mu_c(T)$ is the chemical potential of B (μ) relative to its value at two-phase coexistence (μ_c), which is a function of temperature. The prewetting line extends into the single-phase region from the two-phase region, beginning at T_{wet} (the bulk wetting temperature) and terminating at the surface critical point (marked by a red dot in (a) and (b)). The bulk critical temperature is T_c (green dot in (a) and (b)) and the two-phase coexistence condition is represented in (b) by a single vertical line, $\Delta\mu = 0$, in $\Delta\mu$–T space. Adapted from Ref. [15]. (For interpretation of the references to color in this figure legend, the reader is referred to the web version of this article.)

wetting transition will occur upon raising temperature towards the critical point of the bulk liquid. Above a transition temperature T_{wet}, $\gamma_{\beta c} + \gamma_{\alpha\beta} = \gamma_{\alpha c}$ and phase β will perfectly wet the container surface and separate phase α from the container, as illustrated in Fig. 6.

For compositions in the single α-phase region, the competition between the short-range surface interaction Φ, which favors β, and the homogeneous free energy $f(c, T)$, which prefers α, results in the formation of a thin, B-rich surface adsorption layer. When the bulk fluid composition reaches the solubility limit at $T > T_{wet}$, the adsorption layer will transform into bulk β phase and completely wet the surface. When gradually increasing the bulk liquid composition at $T > T_{wet}$, Cahn uses an elegant and general graphic analysis of Eq. (7) to show that a first-order prewetting transition can develop in the single-phase region before the adsorption layer becomes bulk β phase and perfectly wets the surface at the solubility limit. The conditions for the transition are represented by a prewetting line $c_{PW}(T)$ on the phase diagram, which is determined by solving the equilibrium equation of the system. As shown in Fig. 6(a), the prewetting line meets the solubility line at T_{wet} and terminates at a surface critical point on the other end. On $c_{PW}(T)$, two surface complexions coexist in equilibrium – a thicker complexion with more B segregation level and a thinner complexion with less B segregation. Both the B segregation amount and the layer thickness will undergo a discontinuous jump across this line (Fig. 6), which is characteristic of a first-order transition. The prewetting transition predicted by Cahn has been confirmed in liquid helium [73], organic [74] and liquid metal [75] systems.

The superposition of the prewetting line onto the bulk phase diagram represents perhaps the first example of a complexion diagram. Such diagrams supply information on the dependence of the equilibrium quantities of a microstructure defect (e.g. interface), such as width and composition on thermodynamic state variables, but these microstructural aspects do not produce additional degrees of freedom that would modify the rules governing the topology of bulk phase diagrams. We discuss the creation of grain boundary complexion diagrams later in Section 2.5.

Cahn's critical point wetting theory (CPWT) not only inspired substantial efforts in the experimental search of wetting transitions, it also laid the groundwork for many subsequent theoretical analyses of prewetting and related phenomena. As we shall show below, many of the models later proposed to explain analogous phenomena are in fact mathematically isomorphic to CPWT. CPWT can also be applied to model vapor adsorption on an inert substrate near the liquid–vapor critical point by simply replacing composition c with the density in Eq. (7) [63,76]. Here the prewetting transition gives rise to a dense, liquid-like[5] adsorption layer at the interface between the substrate and the bulk vapor phase, and the model predictions on the conditions for wetting transitions are identical to those given by Fig. 6.

Wetting transitions can also occur at interfaces in solid materials such as grain boundaries and phase boundaries. Furthermore, a grain boundary may be wetted by either a liquid or solid phase with a different composition from the bulk, with the former associated with the liquid metal embrittlement phenomenon [77,78] and evidence of the latter ("solid-state wetting") found in Al–Zn alloys [79]. Wynblatt and Chatain [80] modeled solid-state wetting

[5] In Cahn's model for a demixed liquid, the prewetting layer is liquid-like. However, in the general case, the prewetting layer does not necessarily have to be liquid-like (e.g. for prewetting in solids).

transitions in a binary alloy with a miscibility gap. Although their investigation is based on a regular solution lattice-gas model, it is essentially equivalent to CPWT, with all the energy terms in Eq. (7) represented by corresponding lattice interactions. The calculated wetting diagram (see Fig. 7) is qualitatively identical to Fig. 6. Like grain boundary energy, the wetting temperature at a grain boundary is found to be anisotropic and inversely related to grain boundary energy. Unlike wetting by a liquid phase, solid-state wetting transitions may incur additional strain energy due to the lattice mismatch between solid phases with different compositions, which is not included in the calculations of Wynblatt and Chatain. Cahn discussed the implications of such a difference on wetting transitions in a recent paper [81]. He pointed out that, when the two solid phases near the critical point of a miscibility gap form an incoherent interface or semi-coherent interface (i.e. lattice mismatch accommodated by interface dislocations), wetting transitions will not occur. A wetting transition is possible in the case of a coherent interface. However, because the misfit strain energy scales with the thickness of the wetting layer, the wetting film can only have a finite thickness and complete wetting is thus forbidden.

Surface or interface premelting offers another example of complexion transitions. Melting of a solid usually starts from its surface or interface. Free surfaces have been observed to start melting at a temperature T_{sm} below the bulk melting point T_m in various materials, including ice [70,71] and metals [82,83]. At $T_{sm} < T < T_m$, the equilibrium surface configuration switches from a "dry" surface state to a liquid-like surficial film. Such a film represents a specific complexion, and has an equilibrium thickness and a structure less ordered and less dense than the crystal phase. When raising temperature towards T_m, the structure of the surficial film approaches that of bulk liquid phase and its thickness diverges upon reaching T_m. The thermodynamic driving force underlying premelting is also related to minimization of surface energy. The liquid phase of a material usually has a lower surface energy (γ_{lv}) than its crystalline counterpart ($\gamma_{sv}^{(0)}$), where the superscript (0) denotes that it always represents a pristine "dry" surface without the premelting layer while the true γ_{sv} represents a premelted surface in cases where premelting does occur, and the inequality $\gamma_{sv}^{(0)} > \gamma_{lv} + \gamma_{sl}$ often holds for high energy surface orientations of the crystal. Therefore, it may become energetically favorable to form a liquid-like surficial film on top of the crystal phase provided that the molar free energy of the liquid phase is not much greater than that of the stable crystalline phase, i.e. near T_m (although we should recognize that the premelting layer should exhibit partial order and contain gradient energies that make its energy substantially different from that of a bulk liquid). Similarly, grain boundary premelting may also be expected when the grain boundary energy is larger than twice the liquid/solid interface energy.

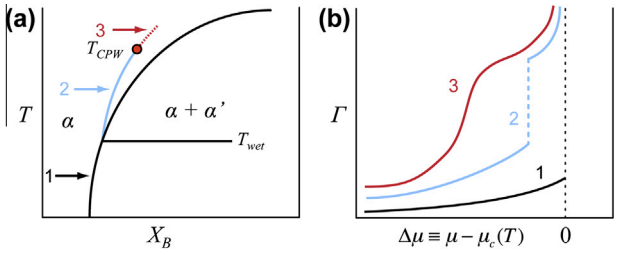

Fig. 7. (a) Prewetting line (solid blue) superimposed on the bulk phase diagram with a miscibility gap. Arrows indicate three paths of increasing composition, which correspond to (1) no prewetting transition, (2) first-order prewetting transition and (3) continuous prewetting transition that occurs above the prewetting critical temperature, T_{PWC}. (b) Adsorption vs. bulk composition diagram for three paths shown in (a); note the first-order discontinuous jump in adsorption for path 2. Adapted with from Ref. [80]. (For interpretation of the references to color in this figure legend, the reader is referred to the web version of this article.)

Surface (or interface) melting can be viewed as a special case of a wetting transition in which the interface between a crystal and a third phase is wetted by its own liquid phase of arbitrary thickness at the bulk melting point. Similar to the way that wetting and prewetting transitions are related, premelting transitions are the precursor to complete melting, and can be analyzed and predicted by CPWT-like mean-field models. Here we focus on models for grain boundary premelting transitions; analogous models for surface premelting have been reviewed in Refs. [78] and [23]. Lobkovsky and Warren [84] and Tang et al. [13,85] studied grain boundary premelting using a diffuse-interface model for polycrystalline materials developed by Kobayashi, Warren and Carter (KWC) [86,87]. In the KWC model for a single-component system, a two-dimensional polycrystalline structure is described by two field variables, i.e. a crystallinity field $\eta(x)$ and a crystallographic orientation field $\theta(x)$. η is a coarse-grained measure of local structural order [88,89]; $\eta = 1$ and 0 are defined as the perfect crystalline or disordered states, respectively. θ is a local measure of the "most likely" crystallographic orientation within fixed coordinates. The excess free energy of a planar grain boundary located at $x = 0$ is given by

$$F_{GB}[\eta, \theta; T] = \int_{-\infty}^{\infty} \left[\Delta f(\eta, T) + \frac{v^2}{2} \left(\frac{d\eta}{dx} \right)^2 + g(\eta) \left| \frac{d\theta}{dx} \right| \right] dx \tag{8}$$

which comprises the homogeneous free energy density Δf and energy terms related to the gradients of η and θ. The orientation gradient energy, $g(\eta)\left|\frac{d\theta}{dx}\right|$, characterizes the energy penalty associated with creating a misorientation across the grain boundary. Its prefactor, g, is required to be a monotonically increasing function of η and vanishes at $\eta = 0$. Such a requirement originates from a simple physical intuition: there should be no penalty for generating an orientation gradient in a completely disordered phase that has a randomly orientated structure and the penalty should increase with the increasing structural order of the material. It is shown that an additional quadratic term of the orientation gradient should be included in the free energy functional to model curvature-driven grain boundary

motion [90], but may be omitted for planar, stationary boundaries.

Kobayashi and Giga [91] proved that, for an equilibrium bicrystal which minimizes Eq. (8), the corresponding θ field must be a step function that localizes all of its change at the grain boundary core $x = 0$ where η has a minimum η_{GB}. Fig. 8(a) shows the schematic profiles of η and θ for a bicrystal that are admitted by the KWC model. With this knowledge, Tang, Carter and Cannon (TCC) [13,85] wrote Eq. (8) in another form:

$$F_{GB}[\eta;\Delta\theta,T] = g(\eta_{GB})\Delta\theta + 2 \times \int_0^{\infty}\left[\Delta f(\eta,T) + \frac{v^2}{2}\left(\frac{d\eta}{dx}\right)^2\right]dx \qquad (9)$$

where $\Delta\theta$ is the difference between the orientations of the two neighboring grains, i.e. the misorientation, and a symmetrical η profile about the grain boundary is assumed. Notably, Eq. (9) has the same form as the free energy expression in CPWT. The surface energy term $\Phi(c_s)$ in Eq. (7) favors a surface composition that is different from the bulk liquid composition preferred by the homogeneous free energy f. Similarly, the misorientation energy penalty $g(\eta_{GB})\Delta\theta$ in Eq. (9) favors a grain boundary more disordered ($\eta_{GB} = 0$) than the bulk crystalline phase stabilized by Δf. Inspired by such an analogy, a graphic construction method similar to Cahn's approach is employed in Ref. [13] to analyze the equilibrium grain boundary structure near T_m. As summarized in Fig. 8(b), the analysis predicts three types of grain boundary behavior near T_m that depend on the grain boundary misorientation value.

(i) For small misorientations ($\Delta\theta < \Delta\theta_{wet}$), the grain boundary energy is smaller than twice the liquid/solid interface energy, $\gamma_{GB} < 2\gamma_{sl}$. The boundary retains a relatively ordered structure up to the bulk melting point and can be superheated above T_m.

(ii) A first-order premelting transition can occur below T_m at intermediate misorientation values ($\Delta\theta_{wet} < \Delta\theta < \Delta\theta_{crit}$), which produces a discontinuous increase in the width and structural disorder of the grain boundary. The premelting line on the T–$\Delta\theta$ diagram starts at (T_m, $\Delta\theta_{wet}$) and terminates at a grain boundary critical point (T_{crit}, $\Delta\theta_{crit}$).

(iii) At large misorientations ($\Delta\theta > \Delta\theta_{crit}$), a grain boundary premelts continuously, i.e. the grain boundary crystallinity η_{GB} decreases to 0 and the grain boundary width diverges gradually without a discontinuity when approaching T_m.

Because the KWC model is isomorphic to CPWT, it is not surprising to see that the different types of predicted grain boundary premelting behavior have a parallel relation with Cahn's predictions of the prewetting phenomena. The grain boundary premelting diagram, Fig. 8(b), looks much like the prewetting diagram in the μ–T space (Fig. 6(b)).

Although grain boundary premelting in pure materials has been predicted by theory [13] and atomistic simulations (see Section 2.4) and suggested by some indirect experimental evidence, such as abrupt changes in grain boundary diffusivity and sliding [55,92,93], its direct observation (e.g. by HRTEM) in real material systems has been elusive [94]. In contrast, evidence of grain boundary premelting in non-pure systems is much more abundant. For example, nanometer-thick disordered interfacial films, known as "intergranular films" (IGFs), have been widely observed at grain boundaries in various ceramics that contain intentionally (e.g. as sintering aids) or unintentionally added impurities such as Si_3N_4–SiO_2 (impurity), ZnO–Bi_2O_3, $SrTiO_3$–TiO_2, etc. Similar nanoscale films have also been confirmed or deduced in metallic alloys (e.g. W–Ni, Mo–Ni, Cu–Bi, etc.). Comprehensive reviews of the IGF phenomenon can be found in Refs. [63,95]. Numerous

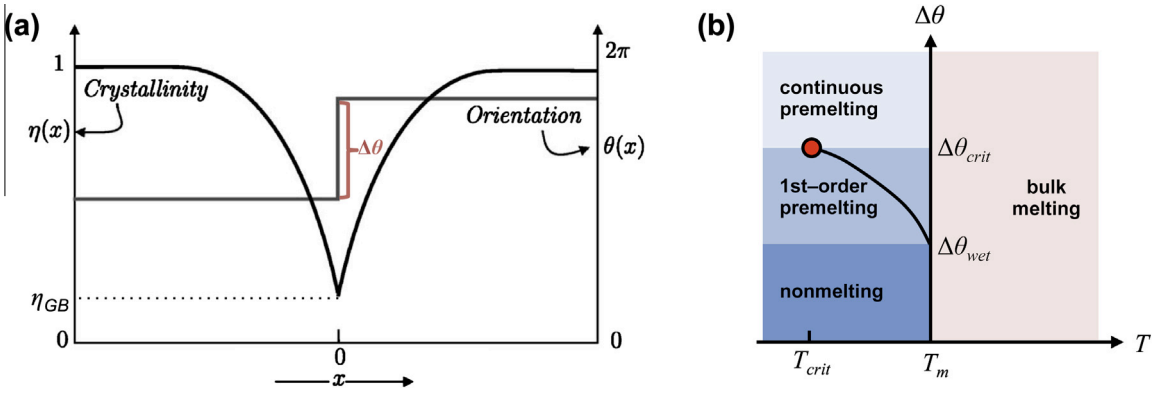

Fig. 8. (a) Schematic diagram of equilibrium profiles of η (degree of crystallinity) and θ (orientation) fields for a grain boundary at $x = 0$. $\Delta\theta$ is the misorientation between the two grains; its magnitude represents the grain boundary energy. The degree of crystallinity, η, reaches a minimum at the center of the grain boundary core ($x = 0$). (b) A schematic grain boundary premelting diagram for a pure system in temperature–misorientation (T–$\Delta\theta$) space. The premelting line terminates at a critical point marked by the red dot. Grain boundaries with large misorientation (i.e. high energy) above $\Delta\theta_{crit}$ continuously premelt as the bulk melting temperature T_m is approached, while grain boundaries with intermediate $\Delta\theta$ (energy) exhibit first-order premelting as the temperature is raised. Small $\Delta\theta$ (low energy) grain boundaries with misorientations smaller than the $\Delta\theta_{wet}$ do not undergo premelting. Adapted from Ref. [13].

experiments have confirmed that IGFs are in thermodynamic equilibrium with the bulk phase. They exhibit a liquid-like structure and equilibrium thickness, and exist under conditions off solid–liquid coexistence, which agree with the characteristics of premelting transitions. Compared to the abutting grains, IGFs are enriched in impurities; their formation causes the original grain boundary to develop multilayer solute adsorption, which is reminiscent of prewetting. IGFs can hence be viewed as products of coupled premelting/prewetting transitions.

To provide a thermodynamic description of premelting in non-pure materials, the TCC analysis for pure systems [13] was extended to binary systems [16], where the excess free energy of a grain boundary is given as

$$F_{GB}[\eta, c; \Delta\theta, T] = g(\eta_{GB})\Delta\theta + 2\int_0^\infty \left[\Delta f(c,\eta,T) + \frac{v^2}{2}\left(\frac{d\eta}{dx}\right)^2 + \frac{\kappa^2}{2}\left(\frac{dc}{dx}\right)^2\right]dx \qquad (10)$$

Compared to the free energy of pure systems (Eq. (9)), Δf is now also composition-dependent and an additional composition gradient energy term appears in Eq. (10). An analogous, but more involved, graphic construction was developed to determine the equilibrium grain boundary state that minimizes Eq. (10) [16]. While the binary model also predicts three categories of melting behavior (superheating, first-order and continuous premelting) in alloys, conditions for premelting display more intricate dependence on the thermodynamic state variables.

The TCC analysis of grain boundary premelting is based on simple model systems in which the grain boundary energy increases monotonically with misorientation. In real materials, the misorientation dependence of grain boundary energy is usually more complex, e.g. there exist low-energy cusps at large misorientations that correspond to special grain boundary geometries and low index interface planes. It is thus proper to view $\Delta\theta$ as a measure of grain boundary energy when interpreting the predicted grain boundary premelting behavior as a function of grain boundary misorientation. Mishin et al. [61] recently examined premelting transitions in Cu–Ag in a multi-phase-field model, using realistic bulk thermodynamic description of Cu–Ag alloys from the CALPHAD approach. Their calculations reveal several classes of melting behavior at boundaries of different energies that agree with the generic predictions of Ref. [16].

Fig. 9 illustrates a schematic grain boundary premelting diagram predicted by the TCC model for a eutectic alloy [13], to which many IGF-forming systems belong. It shows that, for states in the solid–liquid two-phase coexistence region, a grain boundary can be perfectly wetted by the equilibrium liquid phase with a composition on the liquidus above a complete wetting temperature T_{wet}. Similar to prewetting in binary liquid, a premelting/prewetting line

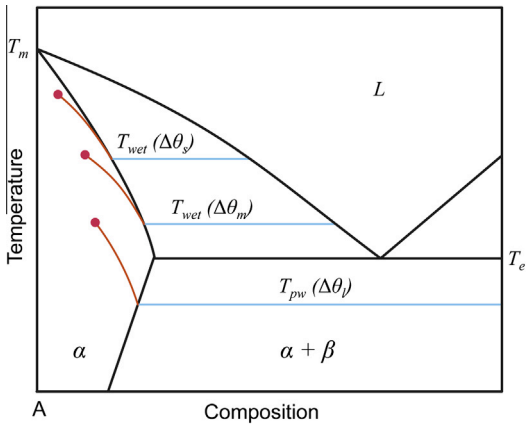

Fig. 9. A schematic grain boundary premelting diagram for an A–B binary system which has a eutectic transition at T_e. The prewetting lines (solid red) of three grain boundaries with different misorientation $\Delta\theta$ ($\Delta\theta_s < \Delta\theta_m < \Delta\theta_l$) are shown in the α single-phase region. Also shown are the complete wetting (T_{wet}) or premelting/prewetting (T_{pw}) temperatures (solid blue lines) for these boundaries in the α + liquid or α + β two-phase regions. (For interpretation of the references to color in this figure legend, the reader is referred to the web version of this article.)

extends into the single-phase region from T_{wet}. Upon crossing this line from low to high solute (B) saturation (or temperature), the grain boundary transforms to a more disordered structure with a higher solute segregation via a first-order transition. Importantly, there exists a distinct premelting/prewetting line for each grain boundary with a different misorientation (i.e. different grain boundary energy), and T_{wet} increases with decreasing misorientation $\Delta\theta$ (i.e. with decreasing grain boundary energy). When a boundary's T_{wet} is below the eutectic temperature T_e, the premelting/prewetting line intersects the solubility line of the solid–solid two-phase region at T_{pw}. In this case, complete wetting does not occur to the grain boundary in the two-phase region below T_e as the liquid phase is metastable there. Instead, the grain boundary will undergo a first-order premelting/prewetting transition in the two-phase region at T_{pw}, as shown in Fig. 9. The premelted intergranular film will thicken and completely wet the grain boundary when T reaches T_e, at which a stable liquid phase exists.

The predictions of the diffuse-interface model are in qualitative agreement with the experimental observations of IGFs. The model prediction that thicker, disordered grain boundaries can form in subeutectic and single-phase regions is consistent with the experimental conditions under which IGFs were found. The coupled premelting/prewetting transition leads not only to structural disordering but also to a higher segregation level of the minority species at the grain boundary. Nevertheless, the diffuse-interface model suggests that the equilibrium compositions of the premelted boundary differ from either solid or liquid bulk phase, which also agrees with experiments [96–100]. As shown in Fig. 9, a grain boundary's premelting/prewetting line may terminate at a grain boundary critical point and not extend to the end member A, which means that

the grain boundary can undergo a first-order premelting transition in alloys but not in the pure system. This demonstrates that the conditions for a first-order premelting transition could be less stringent in non-pure systems than in pure materials.

One limitation of Cahn's CPWT and similar diffuse-interface models for prewetting and premelting transitions is that only short-range interactions are considered in the free energy of the systems. On the other hand, long-range interactions, such as London dispersion and electrostatic forces, are known to influence the development and characteristics of interface wetting or melting transitions in significant ways [70,71,76], especially for inorganic materials. For example, the presence of an attractive dispersion force at a grain boundary could prevent it from being completely wetted by the liquid phase where a liquid and a solid coexist [101]. Bishop, Carter and Cannon developed a diffuse-interface model formulation that incorporates the electrostatic interaction between charged ion species in the system [15,102]. The model was used to numerically study the formation and stability of IGFs in Si_3N_4–SiO_2 [102]. Ebner and Saam [103] considered the effects of long-range dispersion force on wetting phenomena in a mean-field theory of an Ising lattice-gas system. They found that the inclusion of the long-range interaction significantly complicates the wetting behavior of an adsorbate on a substrate near the bulk critical point. Alternatively, the effects of long-range forces on IGFs can conveniently be taken into account in so-called force-balance models, which will be discussed in Section 2.4.

2.3.3. Discrete complexions

Grain boundary complexions often occur in discrete thicknesses and can be classified by their width in terms of the number of atomic layers. This complexion categorization scheme has its origin in a grain growth kinetics study on doped alumina, in which high-angle annular dark field scanning transmission electron microscopy (HAADF-STEM) imaging was used to observe the grain boundary complexions of specific grain boundaries with different mobility. As shown in Fig. 10 (a–f), the discrete complexions fall into six groups based on their thickness, as observed in either HAADF-STEM or HRTEM imaging. The physical origin of these different complexion thicknesses will vary from one materials system to the next; the categorization scheme is simply based on the approximate thickness. These six discrete complexions are referred to as Dillon–Harmer complexions [25], and include clean complexions (with no observable segregation of solute atoms), monolayer complexions, bilayer complexions, trilayer complexions, nanolayer complexions and wetting layers. These six complexion types were first discovered in Ref. [46] and formally categorized as complexions in Ref. [17]. Within the Dillon–Harmer complexion categorization framework, there is a general trend of increasing adsorption and structural and chemical disorder with increasing thickness. In practice, the Dillon–Harmer complexions are defined and categorized based on STEM observations of thickness and whether or not adsorbed solute is visible at the grain boundary.

We emphasize that the phrase "monolayer complexion" should not be confused with the surface science term "monolayer" (ML); the former phrase is a type of complexion within the Dillon–Harmer scheme, while the latter word is a quantity of adsorbate that can be defined in several different ways [104]. To avoid confusion, when discussing Dillon–Harmer complexions it is best to include the word complexion. In this work, we will use the abbreviation ML when referring to the concept of a specific quantity of adsorbate.

Nanolayer complexions are greater than three atomic layers in thickness but are not a bulk phase; these complexions are typically on the order of one or two nanometers thick. Historically, nanolayer complexions have been referred to as IGFs. The last category, wetting, is actually a bulk phase rather than a complexion. It has an arbitrary thickness while the other categories all have a fixed, finite thickness set by equilibrium thermodynamics. While the six discrete complexions are a useful method for categorizing complexions, it should not be inferred that all nanolayers, for example, have the same thickness, or that there can only be a single type of nanolayer complexion within a given system: there may be multiple types of nanolayers with different thicknesses within the same system.

The six discrete Dillon–Harmer complexions exhibit similarities to a simplified model where hard spheres are sandwiched between two hard walls (Fig. 11(b)). In such a case, well-known colloidal theories suggest that an oscillatory structural interaction will produce free energy minima that correspond to discrete thicknesses (at $D = n\sigma + 1/4\sigma$ for the case of hard spheres sandwiched between two hard walls, where D is the distance between two walls, σ is the diameter of the hard sphere and n is a positive integer ($n = 1, 2, 3, \ldots$); Fig. 11(c)) [105]. It was proposed, based on a phenomenological model [22,106], that a similar mechanism may produce a series of discrete Dillon–Harmer complexions (Fig. 11(a)). Since the statistical model suggests that the $(n+1)^{\text{th}}$ energy barrier should decay exponentially by a factor of $1/e$ as compared with the n^{th} energy barrier, the thickness of a complexion should be nearly continuous beyond the trilayer complexion (however, rigorously, it can still be discrete with smaller barriers). This will result in approximately six complexions, as shown in Fig. 11(a). It is also possible to have complexions with discrete thicknesses equivalent to four, five or more atomic layers; however, because the energy barriers between these thicker discrete complexions are small, they are considered to all be nanolayer complexions. Beyond the "roughening point",[6] the effective thickness of the complexion will be continuous, where nanolayers with continuous

[6] In this context, "roughening" refers to the changeover in behavior from discrete changes in thickness to continuous changes in thickness.

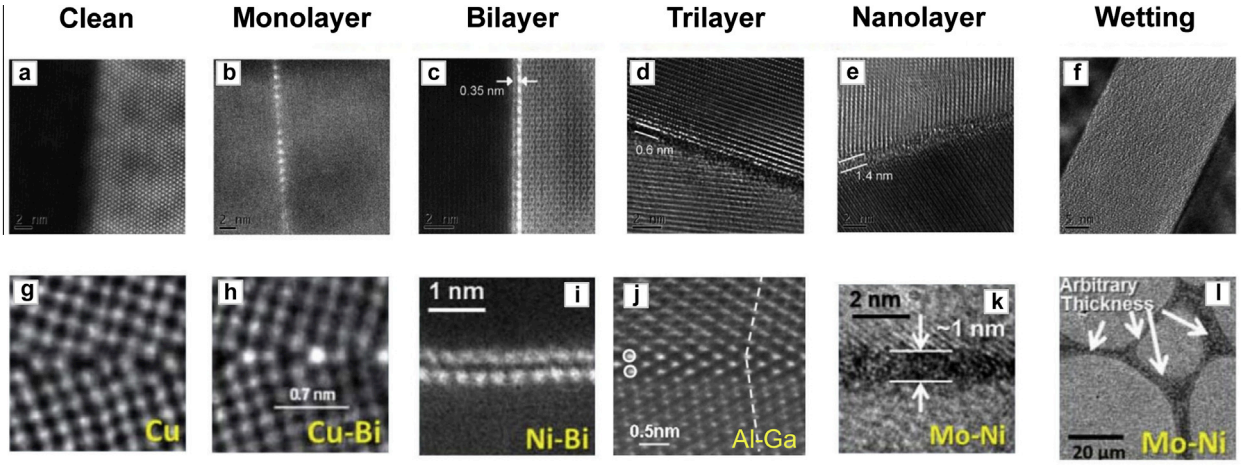

Fig. 10. The six discrete Dillon–Harmer complexions as originally discovered in undoped and doped (CaO, MgO, SiO_2, Nd_2O_3) Al_2O_3 (a–f) and analogous examples of discrete Dillon–Harmer complexions in metallic systems (g–l). The relationship between dopant type and grain boundary complexion type for the Al_2O_3 complexions can be seen in Fig. 21. Parts (a–f) reprinted from Ref. [17] with permission; parts (g, h) reprinted from Ref. [163] with permission; part (i) reprinted from Ref. [48] with permission; part (j) reprinted from Ref. [344] with permission; parts (k, l) reprinted from Ref. [205] with permission.

but finite "equilibrium" thickness are thermodynamically stable (Fig. 12). On the other hand, discrete complexions with a thickness of approximately zero, one, two or three atomic layers appear below the roughening points where the so-called stepwise "layering transitions" occur.

A seminal article by Pandit, Schick and Wortis provided further insight regarding the origin of discrete complexions [107]. Via a lattice-gas model for multilayer adsorption of inert gas molecules on an attractive substrate, Pandit et al. showed that layering transitions can occur below roughening transition points, producing discrete interfacial states with thicknesses of approximately a single atomic layer, two atomic layers, three atomic layers, etc. (Fig. 12(a)). A recently proposed model [25] further suggested that similar layering transitions can occur at grain boundaries to produce discrete Dillon–Harmer complexions (Fig. 12(b)). Semi-grand canonical Monte Carlo simulations have also recently demonstrated a transition between two different discrete Dillon–Harmer complexions (monolayer and bilayer complexions) at a Σ5(310) grain boundary in Ag-doped Cu, as shown in Fig. 4(d and e).

In reality, the adsorbates at grain boundaries are not "hard spheres". Thus, the ideal situation predicted by the simplified models shown in Figs. 11 and 12 is not typically observed in experiments. For example, a recent study [34] revealed a first-order grain boundary transition from a bilayer complexion to a clean complexion in Si–Au in the absence of the intermediate state of a monolayer complexion. Specifically, Fig. 13(a) shows the coexistence of a bilayer and a clean complexion at a low-symmetry (Σ43) twist grain boundary; the atomically abrupt transitions between the two complexions suggests that this complexion transition is likely to be a first-order transition, because it is associated with a discontinuity in the interfacial excess of the solute (Au) adsorption.

Fig. 13(b) schematically illustrates possible relative stabilities of a bilayer, a monolayer and a clean complexion. It was proposed that a bilayer complexion in Si–Au is stabilized because Au atoms bond strongly to the Si atoms on the adjacent Si grain surface (since the regular solution parameter for Au–Si amorphous alloy was estimated to be $\Omega \sim -8\ \mathrm{kJ\ mol^{-1}}$, Au–Si bonds are energetically favored to form) [34], similar to the case of Ni–Bi [48]. As illustrated in Fig. 13(b), it may be energetically more expensive to form an Au monolayer complexion at this low-symmetry boundary because the Au monolayer complexion cannot grow coherently with respect to both grain surfaces, i.e. some strong Au–Si bonds must be broken at (at least) one Si–Au interface. In other words, the monolayer complexion may represent a high energy state because both Si grain surfaces would tend to impose structural order onto the monolayer complexion and this structural ordering is incompatible, leading to a structural frustration that destabilizes the monolayer complexion [34].

In summary, the grain boundary complexion formation and transitions can be complex and material specific. For ceramic materials, directional bonds, the presence of both cations and anions, electrostatic space charges and van der Waals forces can make the interfacial interactions much more complicated. For example, an analogous surface complexion transition from the clean complexion to the nanolayer complexion (i.e. the free-surface counterpart to nanolayer complexions at grain boundaries [23]) was observed in V_2O_5 on TiO_2 [24,108]. In many ceramic systems, complete wetting may be inhibited by the presence of long-range attractive van der Waals interactions [63,109]. More realistic models that can predict the specific complexion stability and transitions in any (or a broad range of) real materials are yet to be developed.

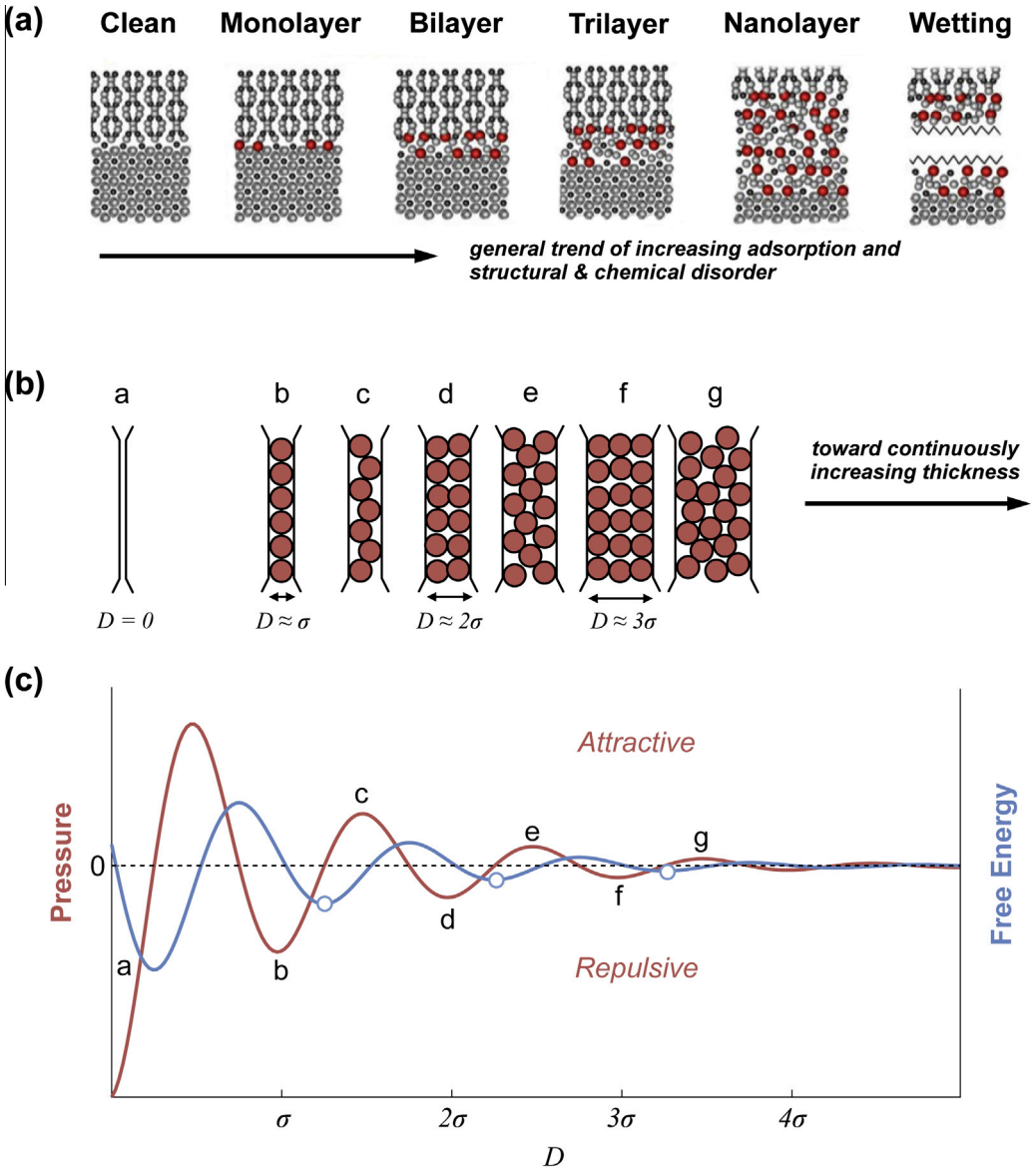

Fig. 11. The six discrete Dillon–Harmer complexions can be viewed as somewhat analogous to a simplified model where hard spheres are sandwiched between two hard walls. (a) Schematic depiction of the six discrete Dillon–Harmer complexions; (b) hard spheres of diameter σ sandwiched between hard walls of spacing D; (c) pressure (red line) and energy (blue line) as a function of wall spacing D. As D increases, there are periodic pressure and energy fluctuations. The equilibrium hard wall spacing D occurs at values of minimum energy, where $D = n\sigma + \frac{1}{4}\sigma$ (open circles on blue line). Parts (b, c) adapted from Ref. [105]. (For interpretation of the references to color in this figure legend, the reader is referred to the web version of this article.)

2.4. Other theories, models and important concepts

Historically, two types of models have been employed to describe wetting transitions: diffuse-interface and force-balance models. In Section 2.3, we discussed diffuse-interface models for interface prewetting and premelting complexion transitions, in which interfaces are considered to be intrinsically diffuse with a characteristic finite width. In contrast, a wetting (or melting) configuration in force-balance models is phenomenologically treated as a wetting (or melting) layer, i.e. a bulk phase, sandwiched by two sharp interfaces of zero thickness. The equilibrium thickness h of the wetting (or melting) film, and hence the wetting state ($h = 0$, $h = \infty$, $0 < h < \infty$), is determined by the balance of various forces between the two interfaces that are thickness-dependent.

A force-balance model was introduced by Clarke et al. [110,111] to explain the presence of stable IGFs at grain boundaries. A fundamental assumption of this model is that IGFs are quenched liquid films of the secondary phase confined by two grains of the primary phase. In the first paper [110], Clarke assumes that IGFs are mainly stabilized by an attractive long-range dispersion force Π_{disp} vs. a repulsive short-range steric force Π_{steric} with the following expressions:

$$\Pi_{disp} = \frac{A_{121}}{6\pi h^3} \tag{11}$$

$$\Pi_{steric} = -4\phi_0 \exp(-h/\xi) \tag{12}$$

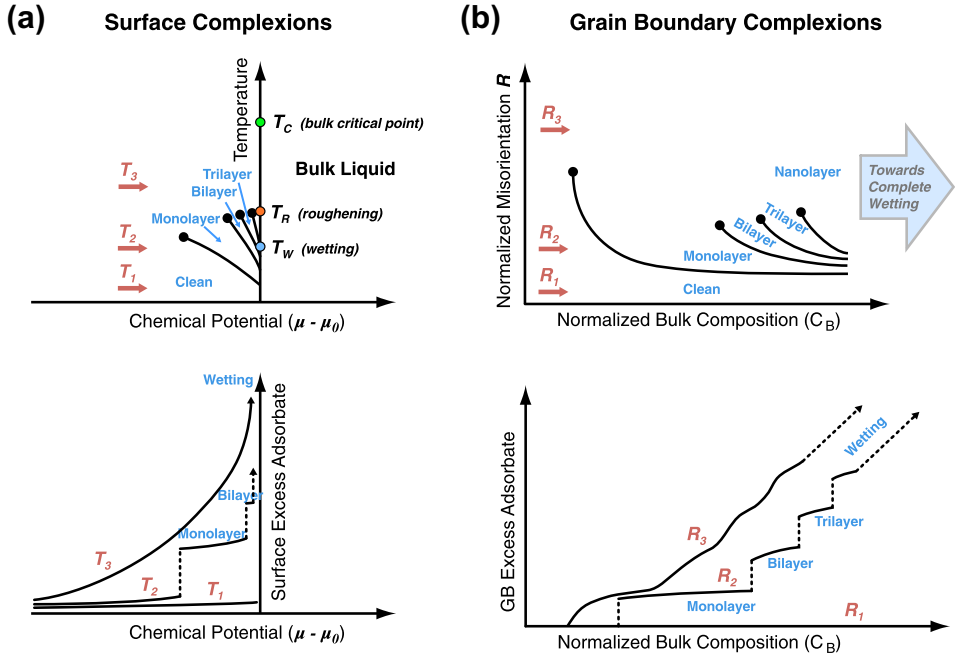

Fig. 12. (a) A schematic surface complexion diagram (top) and the corresponding surface excess adsorption vs. chemical potential curves (bottom) for multilayer surface adsorption of noble gas molecules on an attractive inert substrate. (b) A computed grain boundary complexion diagram (top) and the corresponding grain boundary excess adsorption vs. normalized bulk composition curves (bottom). Panel (a) is replotted from Ref. [107] with permission from APS and panel (b) is replotted from Ref. [25] with permission from AIP.

where h is the film thickness, A_{121} is the Hamaker constant of the grain/IGF/grain composite structure, ξ is the correlation length of the liquid phase and ϕ_0 is a strength constant. The repulsive steric force is also known as the structural disjoining pressure. The origin of such a force is related to the phenomenon that a liquid layer of microscopic thickness confined between two solid interfaces tends to have a more ordered structure and thus a higher free energy density than the bulk liquid; its structural order decreases with increasing interface separation, which is equivalent to an effective repulsive interaction between the two opposing interfaces. Interestingly, the expression of Π_{steric} was derived from a diffuse-interface model [110]. Under Clarke's simplifying assumption that steric and London dispersion forces dominate the equilibrium IGF thickness, the equilibrium thickness (which occurs at zero net force, F) can be found by setting Eqs. (11) and (12) equal to each other and solving for h. Using parameters estimated for the Al_2O_3–SiO_2 system, Clarke shows that the net force, $F = \Pi_{disp} + \Pi_{steric}$, vanishes at an IGF thickness of ~1 nm, which is in qualitative agreement with experimental observations. The possible contribution of the electric double-layer interaction to force balance was also considered by Clarke et al. later [111]. In contrast to IGFs at ceramic–ceramic interfaces in which dispersion forces are the primary attractive force, recent research on IGFs at metal–ceramic interfaces has shown that electrostatic image forces are the dominant attractive force at gold–sapphire interfaces [42].

Since the Clarke model was proposed more than two decades ago, there has been an ever increasing amount of evidence suggesting that IGFs are in thermodynamic equilibrium with the surrounding bulk phases rather than being a quenched liquid. There are also cases in which IGFs represent a metastable equilibration, e.g. as shown for SiO_2-based IGFs at TiO_2 grain boundaries by Ackler and Chiang [112]. This suggests that IGFs can also form under sub-eutectic or sub-solidus conditions, where bulk liquid is metastable; they are associated with an excess volumetric free energy $\Delta f_{vol}h$ relative to the stable bulk solid phase, which translates into a significant attractive force $\Pi_{vol} = -\Delta f_{vol}$ on the films and should be accounted for in the calculation. Such a modification has been applied to study the stability of IGFs and surficial amorphous films [63,113]. IGFs of an equilibrium thickness can also form above the solidus line, in equilibrium with a partial-wetting (non-wetting) bulk liquid phase. In such a case, the average composition of IGFs can differ markedly from the bulk liquid phase, despite a thermodynamic equilibrium between the liquid-like IGF complexion and the bulk liquid (see Refs. [23,63] and references therein).

In addition to continuum-level modeling, atomistic modeling has also been extensively used to study complexion transitions, which provides detailed insights into the atomic mechanisms of such transitions. There exists a large body of atomistic simulation studies of surface melting transitions in the literature (see e.g. the review in Ref. [114]). In an early modeling study of grain boundary

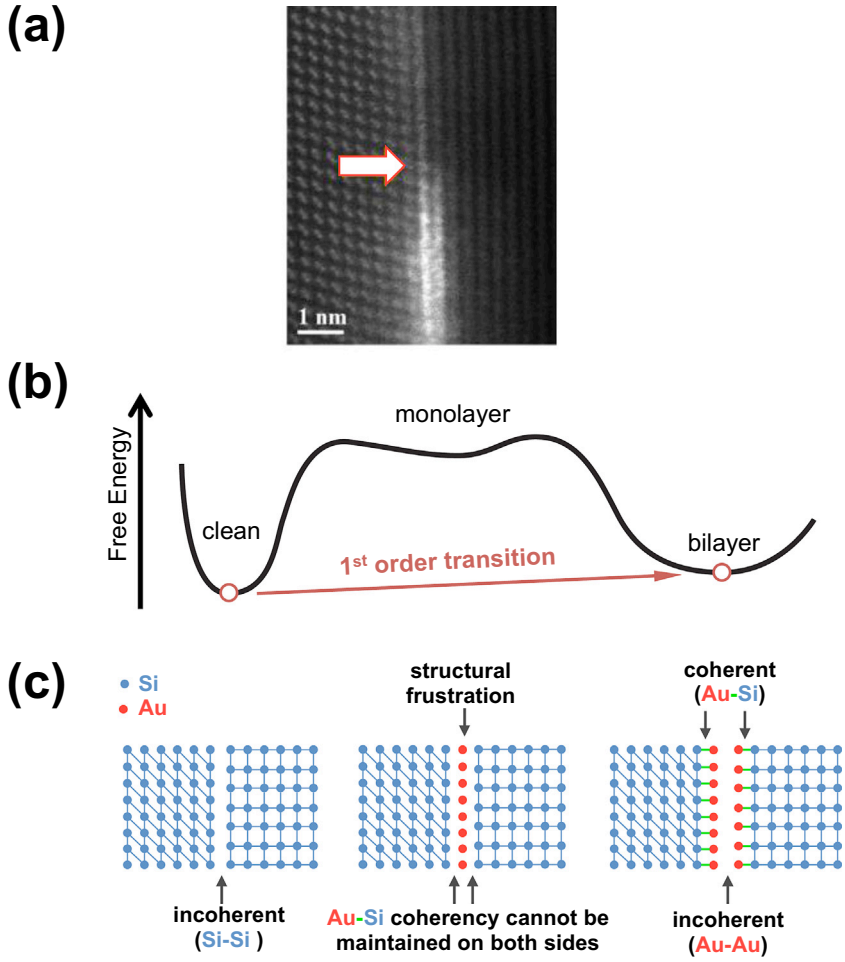

Fig. 13. (a) HAADF-STEM image of bicrystal boundary in Au-doped Si showing the abrupt transition region between the bilayer complexion and the clean complexion. The abrupt transition indicates the occurrence of a first-order complexion transition. The bicrystal is a (1 1 1) 15° twist boundary, i.e. Σ43. (b) Schematic illustration of the possible free energy states that may lead to this first-order transition. It was proposed that the monolayer complexion is a very shallow metastable state (and hence is essentially unstable) because it is energetically favorable to form strong Au–Si bonds. (c) Schematic diagrams of clean, monolayer and bilayer complexions showing that the Au-rich monolayer complexion is structurally metastable. Reprinted from Ref. [34] with permission.

premelting, Kikuchi and Cahn [68] analytically solved a lattice gas model with a simple interatomic potential and found that continuous premelting occurs at a tilt grain boundary that exhibits a logarithmic divergence in thickness when approaching the bulk melting point. A similar conclusion was obtained from Monte Carlo (MC) simulations of the same model [115].

Grain boundary melting behavior in elemental systems has been extensively investigated by molecular dynamics simulations using (semi-)empirical interatomic potentials [116–128], where grain boundary structural transitions are detected by measurement of changes in grain boundary structural order parameter(s) or other derived properties, such as grain boundary diffusivity [117,125] and sliding resistance [126]. The existence and nature of premelting transitions are not unequivocally resolved by these studies, which sometimes yield inconsistent results. A number of MD simulations show that high-angle grain boundaries tend to increase continuously in disorder with increasing temperature, indicating continuous premelting [116,118,128], while some simulations find that the grain boundaries still retain significant crystallinity at temperatures close to T_m [121–123]. Other simulations suggest that a first-order premelting transition occurs below T_m [119,120,124]. As pointed out by Tang et al. [13], such inconsistencies might originate from numerical artifacts, failure in accurate determination of bulk melting points, differences in atomic potentials used and challenges in obtaining ground state grain boundary structures [129,130]. Recently, von Alfthan et al. [128] examined the structures of several Si twist grain boundaries near T_m with improved simulation techniques. Among the three (0 0 1) twist grain boundaries (Σ25, Σ5 and Σ29, corresponding to twist angles of 16°, 37° and 44°) they studied, evidence of continuous premelting was found for high-angle/high-energy grain boundaries (Σ5 and Σ29), starting at 0.7–0.8T_m, but not at the low-energy Σ25 grain boundary. This finding reaffirms the dependence of the grain boundary

melting behavior on the "dry" grain boundary energy, as suggested by phenomenological models [13,61]. Nevertheless, no first-order grain boundary transition was observed in their simulations.

It is much more challenging to rigorously determine the existence and characteristics of premelting transitions in multicomponent systems from MD simulations because of the often impractically long simulation time required to establish equilibrated composition profiles in the systems. Existing MD studies of IGFs typically prepare intergranular films through simulated high-temperature equilibration and quenching processes. While the structures obtained may not necessarily correspond to the lowest energy states, they provide valuable insights on the detailed bonding structures and solute distributions within the films as well as their implications for various properties [131–138]. For example, Garofalini and co-workers [131–136] have systematically studied IGFs between silicon nitride and alumina grains using classical MD. Their work reveals the presence of structural order and composition gradients across the films and the segregation of impurity atoms at IGF/grain interfaces, which agree with experimental observations. Compared to MD, it is more feasible to obtain thermodynamically equilibrated structures through MC simulations. Williams and Mishin [139] recently applied the semi-grand canonical MC method with an embedded-atom potential to study grain boundary premelting in binary Cu–Ag alloys. They observed the formation of a thin disordered layer with a composition close to the liquid composition at a Σ5 grain boundary when the temperature nears the solidus line from below. However, the thickness of the liquid-like layer remains finite at the solidus and the grain boundary can be overheated or oversaturated above the solidus, which indicates nonmelting behavior.

Advances in computing power in the last few decades have enabled the application of first-principles calculations to almost every area of materials science including grain boundary complexions. Density functional theory has been employed to investigate various aspects of IGFs, including the bonding and electronic structures [140,141], the specific adsorption sites of rare-earth elements at IGF/grain interfaces [142–144], and the viscosity [145] and mechanical strength [146–148] of intergranular films. These calculations provide quantitative information on the atomistic structures and properties of IGFs, and facilitate the interpretation of experimental observations [144].

In addition to grain boundary premelting transitions, other types of grain boundary complexion transitions have also been studied and revealed by MD or MC simulations. A recent study predicted an extrinsic complexion transition in Σ5(310) boundaries in Ag-doped Cu as a function of temperature, from a monolayer to a bilayer complexion, as shown in Fig. 4(d and e) [149]. In this case, the bilayer complexion contained less total adsorbate (Ag) than the monolayer complexion, in contrast to the assumed general trend of increasing adsorbate content with increasing complexion thickness. Other examples include the roughening transition [150], the defaceting transition [151], a dislocation pairing transition at low-angle grain boundaries in body-centered cubic (bcc) Fe [152] and transitions between two ordered grain boundary structures [39,153]. A recent experimental study has revealed solid–solid interface reconstruction at an Ni–Al_2O_3 boundary [45]. Solid–solid interfacial reconstruction transitions at grain boundaries and heterophase boundaries could potentially be a very important type of complexion transition. As the study of these types of transitions is particularly difficult in a transmission electron microscope (because the images are a two-dimensional projection parallel to the interface), atomistic modeling will play a critical role in revealing the detailed structures and stability of such complexions.

A continuum field theory, referred to as the phase-field crystal model, was recently developed [154,155] to describe phenomena on atomic length and diffusive time scales. Unlike the diffuse-interface models introduced in Section 2.3.2, a phase-field crystal model constructs the free energy functional using the local-time-averaged atomic density as the order parameter and thus resolves the atomic structure of a crystalline material. At the same time, the mean-field approach allows it to cover time scales much larger than MD, which makes it computationally more efficient in obtaining equilibrium configurations of grain boundary structure. With such advantages, new insights on grain boundary complexion transitions have been obtained using this modeling approach. For example, Mellenthin et al. [156] performed a phase-field crystal study of grain boundary premelting in a two-dimensional single-component crystal with hexagonal ordering. A liquid film was found to form at high-angle grain boundaries and its thickness diverges logarithmically when the melting point is reached, which is consistent with the continuous premelting behavior depicted by diffuse-interface models. However, local melting only starts around dislocations at low-angle grain boundaries; the grain boundary structure consists of isolated liquid pools separated by solid bridges, which can be overheated. At intermediate misorientations, a first-order dislocation pairing transition occurs below the melting point, which is also observed in MD simulation [152]. Similar misorientation-dependent melting behavior was also found in a phase-field crystal study of a three-dimensional bcc crystal by Berry et al. [157].

2.5. Developing grain boundary complexion diagrams

The development of grain boundary complexion diagrams is a critical aspect of complexions research. Complexion diagrams have the potential to be as important and useful as bulk phase diagrams, which are indispensable for many aspects of materials science and engineering. Complexion diagrams can be developed based on experimental data and/or thermodynamic models and simulations, and we discuss both approaches in this section. In general, constructing complexion diagrams is very

challenging from a scientific perspective, but it can also be very technologically rewarding, given the important roles of grain boundaries in controlling both materials fabrication and properties. Thus, this section focuses on discussing the construction and potential applications of grain boundary complexion diagrams.

First, we comment on some general characteristics of complexion diagrams. Because grain boundary complexions have $6 + C$ degrees of thermodynamic freedom, a full complexion diagram, even for a single-component material ($C = 1$), cannot be plotted in two dimensions as is typically done for bulk phase diagrams, which have C degrees of freedom (hence, binary bulk phase diagrams can be plotted in two dimensions). However, two-dimensional complexion diagrams can be plotted in which the axes represent two of the five grain boundary geometrical parameters, as done, for example, in Ref. [9]. In such diagrams, the other three geometrical parameters and the bulk composition and temperature are held constant. Alternatively, if the five macroscopic geometric grain boundary parameters (and pressure) are held constant, then complexion diagrams will have C degrees of freedom and can therefore be overlaid onto bulk phase diagrams. For example, the premelting, prewetting and wetting lines shown in Fig. 9 are lines of complexion transition that represent the complexion transitions of three different grain boundaries, each with a fixed misorientation ($\Delta\theta_l$, $\Delta\theta_m$, and $\Delta\theta_s$). Additional lines of complexion transition could be drawn for other grain boundary misorientations, but such a complexion diagram would be overly complicated and hence not very useful.

When complexion diagrams are overlaid onto bulk phase diagrams, it is helpful to emphasize regions of complexion existence in addition to lines of complexion transition, the same way that regions of bulk phase coexistence are marked on phase diagrams in addition to the solvus, solidus and liquidus lines. Such complexion diagrams are overlaid onto a standard bulk phase diagram (Fig. 14(a)) by drawing lines of complexion transition and indicating regions of complexion stability (Fig. 14(b)). In the schematic example in Fig. 14(b), it is understood that, for a real sample with no restriction on allowed grain boundary geometry, not all grain boundaries in the bilayer region actually have a bilayer complexion; rather, some of the boundaries have the bilayer complexion (e.g. the grain boundaries with an initially higher energy), while the other grain boundaries have a monolayer complexion. Conversely, in the monolayer region, some grain boundaries might have the bilayer complexion. This somewhat imprecise situation necessarily results from the reduction of the $6 + C$ dimensional space of complexions into a subspace that can be plotted in two dimensions. We additionally point out that Fig. 14(b) is highly schematic and for purposes of illustration only; whether or not all features depicted in the diagram actually exist in a real materials system is an open question that has not been sufficiently explored experimentally. Furthermore, for simplicity, some features have been omitted; for example, the transition from a monolayer to a clean complexion as $X_B \rightarrow 0$ is not shown, although it is understood that for a material in which $X_B = 0$ and $X_A = 1$ (the far left side of Fig. 14(b)) there cannot be a monolayer complexion because there are no solute atoms.

2.5.1. Experimental approach

In practice, complexion diagrams can be constructed based on experimental data from bicrystals or polycrystals. As suggested by Hart [5], complexion transitions can be identified by discontinuous changes in properties such as adsorption, diffusivity, grain boundary mobility and mechanical properties. Additionally, electron microscopy can be used to identify the structure and chemistry of different complexions, as done, for example, in Ref. [17]. Thus, the construction of complexion diagrams can proceed in a manner analogous to the construction of bulk phase diagrams, in which properties and structure are studied as a function of thermodynamic parameters (usually temperature and bulk composition) and discontinuities represent transitions between regions of thermodynamic stability.

The solidus line on bulk phase diagrams (representing the line of solid–liquid bulk phase transition) has often been determined by the dramatic and discontinuous changes in properties between the solid and liquid phases [5]; mechanical properties testing is generally a reliable indicator of a bulk phase transition. However, since grain boundary complexion transitions can also cause dramatic changes in macroscopic properties, changes in mechanical properties do not always correspond to a bulk phase transition; sometimes they can correspond to a complexion transition. Where they do, the changes in mechanical properties (or other properties) can be used to create complexion diagrams.

To elucidate these ideas and give a concrete example of an experimentally derived complexion diagram, we will discuss the Cu–Bi system, a classic grain boundary embrittlement system. The bulk solubility of Bi in Cu is extremely low and the determination of the solidus line has been the subject of many experimental studies (see e.g. Ref. [158] and references therein). An early study using notched-bar mechanical testing concluded that the solid solubility of Bi in Cu is 30 ppm at 800 °C and 3 ppm at 600 °C; at lower Bi concentrations, embrittlement did not occur, presumably due to the absence of a bulk liquid phase [159]. It is now known that embrittlement in the Cu–Bi system, just as in the Ni–Bi system [48], is caused by a grain boundary complexion transition that results in a Bi-rich bilayer complexion at the grain boundary [35].

A more recent study in which Cu single crystals were annealed in the presence of a Bi vapor source, followed by mass spectrometry to measure the solid solubility of Bi, provides a more accurate and complete solidus line [160]. Studies have also measured Bi adsorption at Cu grain boundaries with Auger electron spectroscopy (AES) [161] and diffusivity of Cu and Bi in Bi-doped Cu [162] as a

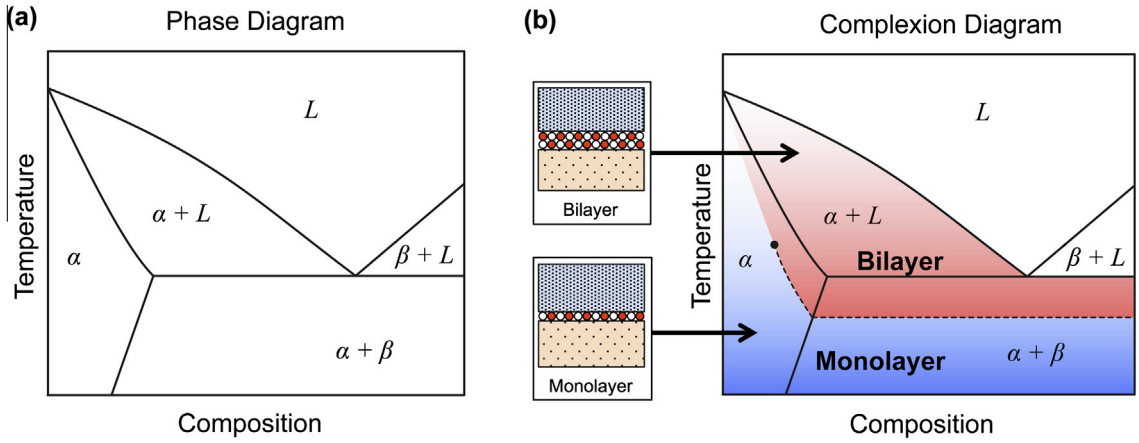

Fig. 14. (a) A schematic bulk phase diagram for a binary eutectic system; (b) a schematic complexion diagram overlaid onto the bulk phase diagram in (a), showing regions of monolayer and bilayer complexion existence. Such complexion diagrams represent an "average" grain boundary behavior (because they can only be strictly true for a single set of grain boundary geometrical parameters, $\boldsymbol{R}$ and $\hat{\boldsymbol{n}}$). It is understood that some grain boundaries in the bilayer region might actually have a monolayer complexion and vice versa. The complexion diagram here is for general illustration purposes only and not all features necessarily exist in a real materials system, and additional features that are not shown will be present in a real system. For example, as the composition tends toward $X_B = 0$ ($X_A = 1$), i.e. toward the left side of the diagram, the monolayer complexion will transition to a clean complexion. This transition may be of first or higher order, but for simplicity is not shown on the diagram.

function of temperature and bulk concentration. These experimental data can be used in conjunction with electron microscopy studies [35,163] to create a complexion diagram showing the regions of monolayer and bilayer complexion stability in the Cu–Bi system. Selected diffusion data are shown in Fig. 15(a and b), along with microscopy results (Fig. 15(c and d)) and a map showing the regions of ~1 ML and ~2 ML Bi adsorption based on AES data (Fig. 15(e)). In fact, Fig. 15(e) itself is a complexion diagram, but the adsorbate arrangement and atomic structure of the complexion was not known at the time. Taken together, these data can be used to plot the Cu–Bi complexion diagram shown in Fig. 15(f). Interestingly, the onset of embrittlement in the notched-bar mechanical test results discussed above [159] (indicated by two yellow dots on Fig. 15(e)) correlates better with the complexion transition line (monolayer-to-bilayer complexion transition) than it does with the bulk solidus line, consistent with the idea that the formation of a bilayer complexion in Bi-doped Cu is the root cause of embrittlement in this system.

There is an important caveat to note here: the STEM image in Fig. 15(c) shows a monolayer complexion at a high-symmetry grain boundary in a bicrystal. The grain boundary complexion at this bicrystal boundary (and in most bicrystals, unless special care is taken to form a general boundary) is a special case that may not be representative of general polycrystalline grain boundaries. In fact, general grain boundaries in Bi-doped Cu exhibit the clean complexion at low Bi content and the bilayer complexion at higher Bi content, but there is no evidence for a monolayer complexion at a general boundary in Bi-doped Cu [35]. This situation is similar to Bi-doped Ni, in which the clean and bilayer complexions were observed at general grain boundaries but a monolayer complexion was not observed [48]. The clean-to-bilayer complexion transition (with no observed monolayer complexion) was also observed in a low-symmetry bicrystal experiment in the Au-doped Si system, as shown in Fig. 13 [34]. Although there is not enough evidence to make a confident generalization, it is possible that the monolayer complexion rarely occurs at general grain boundaries in polycrystalline materials even though it is frequently observed in bicrystals and high-symmetry grain boundaries. More experimental work on this topic is needed, but the results at hand suggest that multilayer adsorption models (e.g. [164]) are substantially more physically relevant than monolayer adsorption models. Indeed, it is physically intuitive that each of the two atomic planes that terminate the adjacent crystals at a general grain boundary will contain adsorbed solute (as in a bilayer complexion) and that the solute would only be localized to a single atomic plane (as in a monolayer complexion) if the grain boundary is highly symmetrical and/or if the terminating planes are crystallographically similar or identical, as would occur in bicrystals or at special grain boundaries.

In Fig. 16, we present a complexion diagram for the Y_2O_3-doped Al_2O_3 system based on experimental results from grain growth studies. Although this diagram is in the initial stages of development and needs further work and more data for refinement, it illustrates the manner in which a complexion diagram for a ceramic material can be constructed. The foundation of this diagram is the idea that abnormal grain growth is caused by the coexistence of two (or more) grain boundary complexions with dramatically different grain boundary mobilities, as has been shown to exist in several different doped alumina systems [17].

There are three distinct regions of the complexion diagram in Fig. 16: a low-T complexion region with low grain boundary mobility (blue), a high-T complexion region with high mobility (red) and a region in which these two

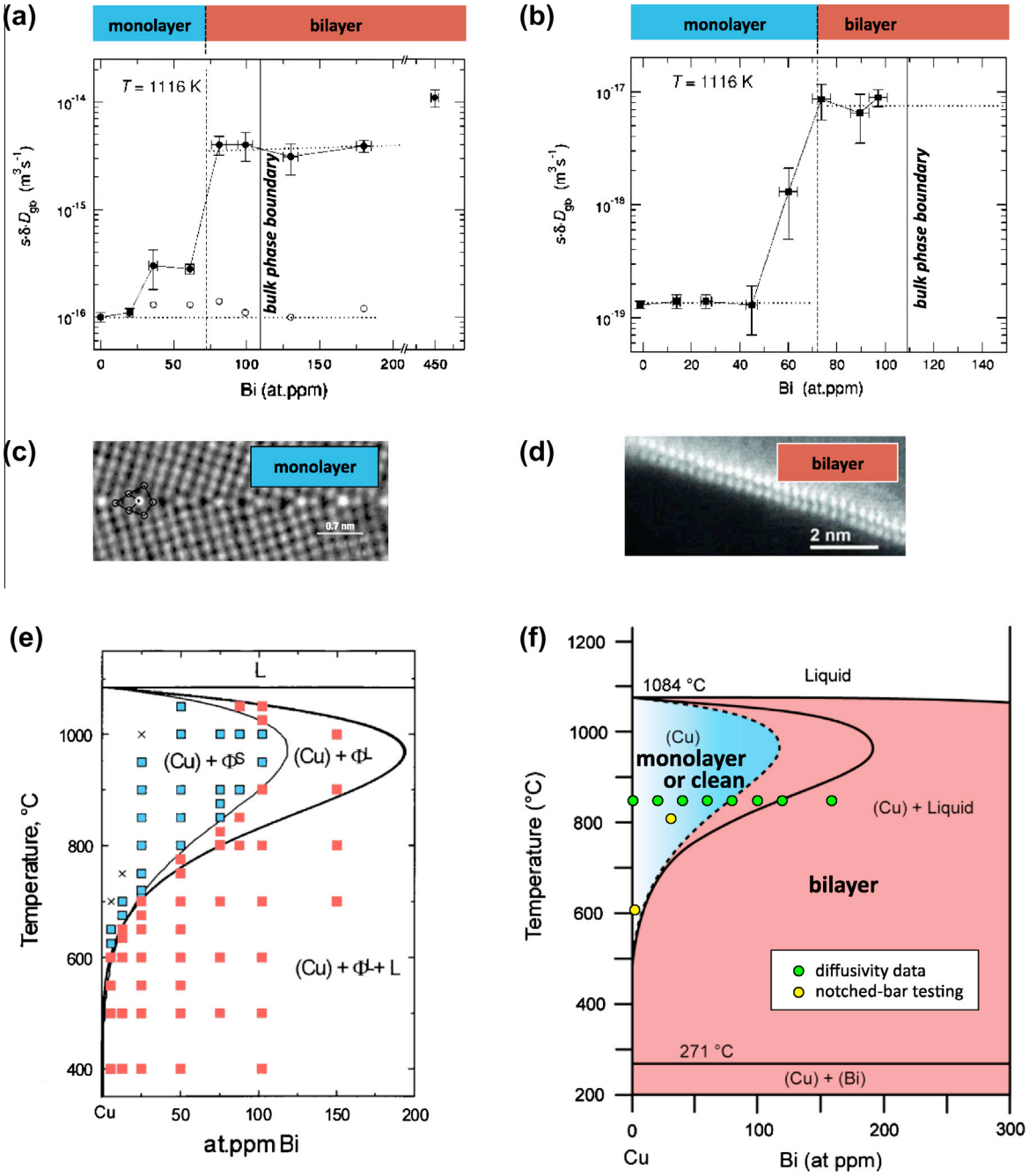

Fig. 15. By consideration of a collection of experimental data (a–e), a grain boundary complexion diagram can be constructed (e). (a, b) Grain boundary diffusivity for Cu and Bi radioisotopes in Bi-doped Cu as a function of Bi content at 1116 K (843 °C); there is a sharp jump in diffusivity at the complexion boundary shown by the dotted vertical line. (c, d) STEM-HAADF images of the Bi-rich monolayer complexion and bilayer complexion, which correspond to small and large overall Bi concentration, respectively. (e) A plot of AES results superimposed on the Cu–Bi phase diagram; blue squares represent approximately 1 ML of adsorbed Bi and red squares represent approximately 2 ML of Bi (color added). (f) A grain boundary complexion diagram showing regions of complexion stability (green dots correspond to diffusivity measurements shown in (a, b) and yellow dots correspond to embrittlement of notched-bar test specimens from Ref. [159]). The phrase "monolayer or clean" in the blue region means that there is conflicting information about which complexion is dominant in this region. A study employing STEM-HAADF images suggests that grain boundaries at very low Bi content typically have the clean complexion [35]. However, AES results show significant segregation in this region of approximately 1 ML [161], which would be consistent with the monolayer complexion shown in (c), although we note that the grain boundary in (c) is a high-symmetry bicrystal boundary and might not be representative of most general boundaries in a polycrystal. Parts (a, b) adapted from Ref. [162]; part (c) adapted from Ref. [163]; part (d) adapted from Ref. [35]; part (e) adapted from Ref. [161]. (For interpretation of the references to color in this figure legend, the reader is referred to the web version of this article.)

complexions coexist (purple). Experiment has shown that normal grain growth with a unimodal grain size distribution occurs in the low-T and high-T complexion regions, where a single complexion type dominates the grain growth behavior. In the region of complexion coexistence, abnormal grain growth occurs and the grain size distribution

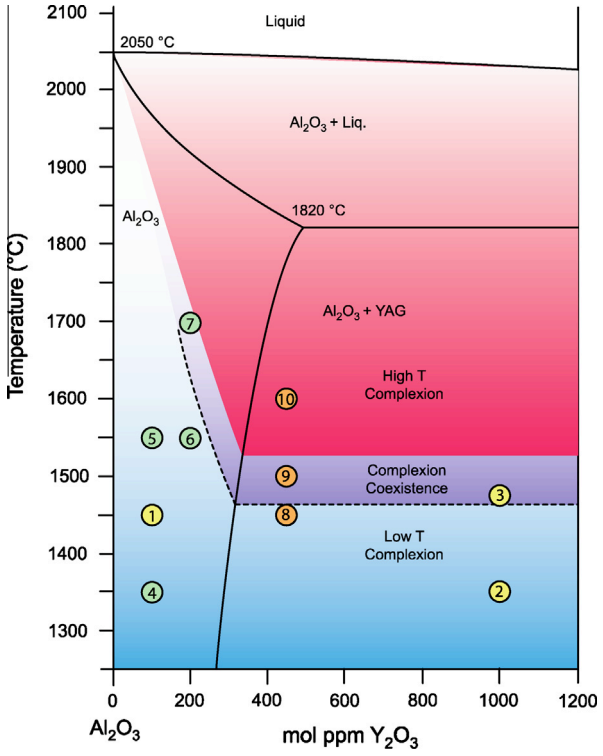

Fig. 16. Experimental complexion diagram for Y_2O_3–Al_2O_3 showing regions in which a low-temperature complexion with low grain boundary mobility (blue) and a high-temperature complexion with high mobility (red) are stable. Normal grain growth occurs in both regions. There is a region of overlap where it is believed that both complexions may coexist (purple). It is believed that abnormal grain growth occurs in this region because the high-T complexion has significantly higher grain boundary mobility than the low-T complexion. The diagram is still in the early stages of development and further experimental investigation is needed to refine it. It was constructed from a limited data set (10 points) compiled from various sources: data points 1–3 (yellow) are from Refs. [165–171], points 4–7 (green) are from Ref. [172] and points 8–10 (orange) are from Ref. [173]. (For interpretation of the references to color in this figure legend, the reader is referred to the web version of this article.)

becomes bimodal. The experimental data points in the figure (labeled 1–10) are gathered from several sources: data points 1–3 (yellow) are from Refs. [165–171], points 4–7 (green) are from Ref. [172] and points 8–10 (orange) are from Ref. [173].

The observations corresponding to these 10 data points are summarized in Table 1 and can be briefly described as follows. Data points 1, 4, 5 and 6 all demonstrate a unimodal grain size distribution and the absence of a second phase (YAG), indicating that they have a low-T complexion in the single-phase region of the bulk phase diagram. Data points 2 and 8 also have a unimodal grain size distribution, and data point 2 exhibits the presence of a second phase (YAG). No second phase was detected in the experiment represented by data point 8, though a second phase appeared at the same doping level at higher annealing temperatures (i.e. with increasing grain size), indicating that the solvus line may be grain size dependent. Abnormal grain growth occurred in the samples represented by data points 3, 7 and 9, suggesting that two complexions with dramatically different mobilities exist in this region. Of particular importance is data point 7, which contains no second phase and shows that a complexion transition may occur in the single-phase region of the phase diagram, leading to abnormal grain growth.

The two experimental complexion diagrams discussed in this section demonstrate a general approach to constructing experimental grain boundary complexion diagrams by combining results from several different types of studies, such as mechanical testing, grain growth studies, chemical analysis and electron microscopy. This approach is analogous to the method by which bulk phase diagrams are constructed, and can be applied to many other systems in which complexion transitions play a key role in materials processing and performance.

2.5.2. Thermodynamic calculation approach

In this section, we discuss efforts to calculate complexion diagrams. Since few prior studies have been conducted to compute rigorous grain boundary complexion diagrams for real systems that can be verified by experiment, we will discuss recent efforts to compute a type of diagram that is less rigorous but still practically useful, known as a "λ-diagram". The calculation of λ-diagrams can be viewed as a first step toward computing more rigorous grain boundary complexion diagrams for real systems.

We first note the existence of a vast literature [43,174–197] on constructing surface complexion diagrams, which are often called "surface phase diagrams" by the surface physics community. These include surface reconstructions for both pure, adsorbate-free surfaces and surfaces with adsorbed impurity atoms. However, the majority of this work has been done for either adsorbate-free surfaces or adsorbate amounts in the ML and sub-ML regime (yet with the observations of a rich variety of surface

Table 1
Experimental data used to construct the grain boundary complexion diagram for Y-doped Al_2O_3 (Fig. 16).

	1350 °C	1450 °C	1475 °C	1500 °C	1550 °C	1600 °C	1700 °C
100 ppm	NGG/1	NGG/1			NGG/1		
200 ppm					NGG/1		AGG/1
450 ppm		NGG/1		AGG/2		NGG/2	
1000 ppm	NGG/1		AGG/2				

The type of grain growth (normal – NGG or abnormal – AGG) and number of phases observed (1 or 2) are indicated for each level of Y dopant and temperature. These data points have been compiled from Refs. [165–173].

complexions). However, recent studies suggest the possibility of thicker complexions. A surface complexion diagram for nanoscale equilibrium-thickness "surface amorphous films" (i.e. the free-surface counterpart to the nanolayer complexion at grain boundaries) has been constructed experimentally for Bi_2O_3 on ZnO $(11\bar{2}0)$ surfaces [23,198–200], and a corresponding thermodynamic model (analogous to the grain boundary complexion model [13]) has been developed to construct surface complexion diagrams theoretically [113]. Complexion diagrams for heterophase interfaces have also been constructed by first-principles calculations, e.g. for V-doped WC–Co in a recent study [201]. Lines of grain boundary complexion transition have also been overlaid onto bulk phase diagrams based on experimental results [77,202].

A few prior studies have been conducted to compute rigorous grain boundary complexion diagrams (with transition lines and critical points) for simplified ideal systems, including regular solution alloys. These studies have computed a prewetting complexion diagram for a binary alloy that exhibits a solid-state miscibility gap (Fig. 7(a)) [80], a premelting complexion diagram for unary systems (Fig. 8(b)) [13], a coupled premelting and prewetting complexion diagram for a binary alloy with a eutectic reaction (Fig. 9) [16], and a complexion diagram for a system with a hard sphere type potential that leads to the formation of Dillon–Harmer complexions (Fig. 12(b)) [25]. A prior phase-field modeling study has computed a premelting-like complexion diagram for Cu–Ag [61], which has not yet been verified experimentally (see more discussion subsequently).

Since prior studies to compute rigorous grain boundary complexion diagrams that can be experimentally verified are lacking, some recent efforts have been made to develop λ-diagrams. These diagrams, which do not have well-defined transition lines, essentially treat the grain boundary as a nanoscale, liquid-like state of interfacial matter, similar to the nanolayer complexion shown in Fig. 10. Consequently, it has been proven that such computed λ-diagrams can effectively predict the thermodynamic tendency for general grain boundaries to disorder [22,31,32,105]. Although they are not rigorous complexion diagrams, the ability for λ-diagrams to predict some useful trends is demonstrated by the prior studies of solid-state activated sintering of oxide ceramics [47] and refractory metals [22,31,32,106,203–205].

Solid-state activated sintering refers to the enhancement of sintering rates due to solid-state additives (prior to the formation of a bulk liquid phase). After its discovery in the 1950s, the exact underlying mechanism for subeutectic activated sintering puzzled the materials community for decades. Recent studies showed that bulk phase diagrams are not adequate for designing optimal activated sintering protocols. This is because liquid-like complexions (nanolayer complexions) can form at thermodynamic equilibration well below the bulk solidus line and enhanced diffusion in these complexions can result in enhanced sintering rates, similar to the case of liquid-phase sintering but occurring under conditions where the bulk liquid is not stable. Specifically, formation of liquid-like grain boundary complexions and enhanced sintering can initiate below 60% of bulk solidus temperatures. Recent HRTEM studies have directly revealed the stabilization of liquid-like nanolayer complexions well below the bulk solidus line in both ceramic [23,47,63,206] and metallic [203,207] activated sintering systems.

To explain why liquid-like nanolayer complexions can form below the bulk solidus line, we should emphasize that these films should not follow the same thermodynamic relations as bulk phases in general. It is now well established that nanoparticles can often melt at hundreds of degrees below the corresponding bulk melting temperature (Fig. 17(b)) [208]. It is worth noting that the suppression of the melting point of the nanoparticles and surface premelting (which is a complexion transition; see Fig. 17(a) for an example) are two related, but not identical, phenomena. Following the same concept, Tanaka et al. [209–211] developed phase diagrams of binary nanoparticles showing that the solidus and liquidus lines are size dependent (Fig. 17(c)). As a first-order approximation, we can view the liquid-like nanolayer grain boundary complexions as interfacial films that are confined between two grains; it is thus not surprising that they can be stabilized at temperatures well below the bulk solidus line (Fig. 17(d)).

Pursuing along this line, grain boundary λ-diagrams have been calculated to forecast the stability of liquid-like grain boundary complexions via extending bulk CalPhaD (Calculation of Phase Diagram) methods to grain boundaries [22,31,32,106]. The basic idea is as follows. A nanometer-thick quasi-liquid complexion can be thermodynamically stabilized at an average general grain boundary if the excess free energy of this "dry" grain boundary ($\gamma_{GB}^{(0)}$; noting that γ_{GB} is reserved for the true, thermodynamically equilibrated, grain boundary energy that corresponds to the complexion that has the lowest energy, i.e. a complexion with the "equilibrium" thickness and a global minimum in $G^x(h)$ in this model) is greater than the sum of two solid–liquid interfacial energies ($2\gamma_{sl}$):

$$\Delta\gamma \equiv 2\gamma_{sl} - \gamma_{GB}^{(0)} < 0 \tag{13}$$

In the sharp-interface (or force-balance) model discussed in the prior section (extended from premelting models for unary systems [63,70,71,212]), the relative interfacial energy can be expressed as:

$$\begin{aligned} G^x(h) - \gamma_{GB}^{(0)} &= \Delta\gamma + \Delta G_{amorph}^{(vol)} \cdot h + \Delta G_{\eta,\nabla}(h) + \sigma_{int.}^{*}(h) \\ &\equiv \Delta\gamma \cdot f(h) + \Delta G_{amorph}^{(vol)} \cdot h \end{aligned} \tag{14}$$

where h is the film thickness and $\Delta G_{amorph}^{(vol)}$ is the volumetric free-energy penalty for forming an undercooled liquid (which can be quantified using bulk CalPhaD methods). It is important to recognize that this liquid-like complexion is not a true liquid as a partial order and a through-thickness gradient in the order parameter inevitably exist. Thus, the term $\Delta G_{\eta,\nabla}(h)$ can be introduced to represent the excess

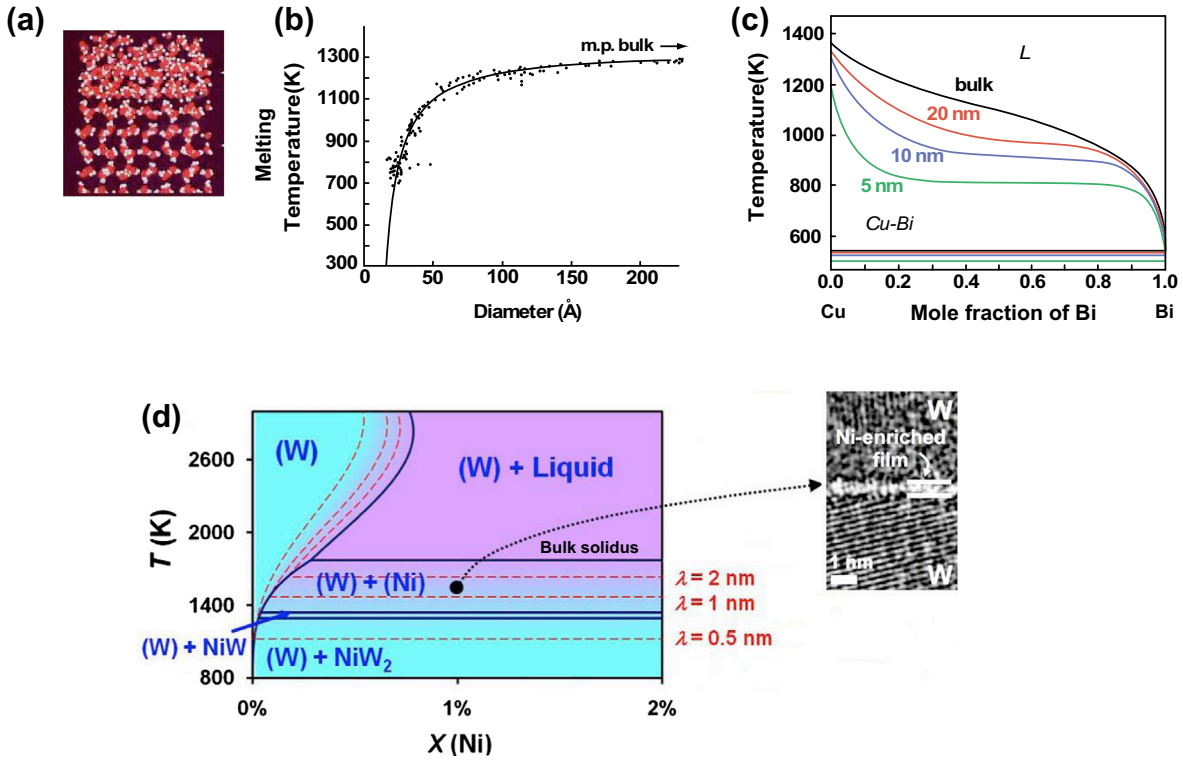

Fig. 17. (a) Premelting on the surface of an ice crystal (reprinted from Ref. [345] with permission) and (b) suppression of the melting temperature of nanoparticles (adapted from Ref. [346]) are two related, but different, interfacial phenomena. (c) Tanaka et al. [209–211] developed phase diagrams of binary nanoparticles, showing that the solidus and liquidus lines are size dependent; adapted from Ref. [210]. (d) Comparison between a grain boundary λ-diagram [22,31,32,106] for the Ni–W system and an experimental HRTEM image of a nanolayer complexion at a grain boundary in Ni-doped W; reprinted from Ref. [32] with permission.

free energies associated with partial order and gradient energies, such as those described by the integrals in Eqs. (9) and (10) in the diffuse-interface approach. The term $\sigma^*_{int.}$ represents all other interfacial interactions, such as the oscillatory structural solvation interaction that produces the Dillon–Harmer complexions, as discussed below, as well as dispersion and electrostatic interactions in ceramic systems – noting that $\Delta G_{\eta,\nabla}(h)$ also represents an interfacial interaction, even though it is listed separately here for clarity. The boundary conditions for the above equation dictate that (i) both $\Delta G_{\eta,\nabla}(h)$ and $\sigma^*_{int.}$ vanish as $h \to +\infty$ (noting that here we select $2\gamma_{sl}$, as our reference state and the excess free energies associated with partial order and gradient energy terms for the case of $h \to +\infty$ are already included in $2\gamma_{sl}$; thus, by definition, $\Delta G_{\eta,\nabla}(+\infty) \equiv 0$ [63]) and (ii) $G^x(0) = \gamma^{(0)}_{GB}$. Thus, we can define a dimensionless "interfacial coefficient", $f(h) \equiv 1 + [\Delta G_{\eta,\nabla}(h) + \sigma^*_{int.}(h)]/\Delta\gamma$, to describe the details of all interfacial interactions; by definition, it satisfies the boundary conditions $f(0) = 0$ and $f(+\infty) = 1$. A detailed discussion about the above formalism, partial order/gradient energies and other interfacial energy terms, as well as the appropriate reference states for writing the above equation consistently, can be found in Ref. [63] (noting that $\Delta G_{\eta,\nabla}(h)$ is one of interfacial interactions in Ref. [63], though this term is listed separately here to emphasize the importance of partial order and gradient terms).

A thermodynamic variable, λ, is then defined to represent the maximum thickness of a quasi-liquid IGF that can be stabilized at an average grain boundary (without consideration of the details of partial order, gradient terms, and other interfacial forces):

$$\lambda \equiv Max\{-\Delta\gamma/\Delta G_{amorph}\} \tag{15}$$

We argue that λ can be rigorously defined thermodynamically using a "reference" state of the true liquid; it explicitly represents the maximum thickness of an ideal liquid film that can be stabilized at the grain boundary under the conditions that the terms $\Delta G_{\eta,\nabla}(h)$ and $\sigma^*_{int.}(h)$ can be ignored, which is rigorously held at the limit of $h \to +\infty$. The actual interfacial width should correspond to the "equilibrium" thickness (h_{EQ}) that produces a minimum in the excess grain boundary energy. For simple (structureless) metallic alloys where an exponentially decaying interfacial force is dominant, liquid-like grain boundary complexions start to develop at $\lambda > \xi$ with an effective interfacial width of $h_{EQ} \approx \xi \cdot \ln(\lambda/\xi)$, where ξ is a coherence length. Moreover, an oscillatory structural interaction can produce discrete interfacial phases, as we have discussed above (Fig. 11). For ceramics, the existence of electrostatic space charges and London dispersion forces will further complicate the situation.

Nonetheless, the λ value represents the thermodynamic tendency to stabilize a liquid-like complexion at an average

general grain boundary, and it scales the actual interfacial width (although the predictability of grain boundary λ-diagrams will be less for thinner complexions with significant level of partial order and discrete thickness). Thus, we can quantify λ and plot lines of constant λ in bulk phase diagrams to construct grain boundary λ-diagrams – a (less rigorous but robustly useful) type of grain boundary complexion diagram. Examples are shown in Fig. 17(d) and Fig. 18(a). The correctness and usefulness of these grain boundary λ-diagrams in predicting general trends has been systematically validated by the following experiments:

- The model predictions were corroborated with direct HRTEM/Auger studies for several selected temperature/composition points in W–Ni and Mo–Ni, where the majority component, i.e. the solvent, is underlined [31,106,203,205,207].
- In a systematic model–experiment comparison study conducted for Mo–Ni, the estimated grain boundary diffusivities as a function of temperature and overall composition correlated well with the computed binary λ-diagram (Fig. 18) [31].
- The computed grain boundary λ-diagrams (with no free parameters) correctly predicted the onset of activated sintering temperatures for W–Ni, W–Fe, W–Co, W–Pd, W–Cu, and Mo–Ni [22,31,106]. These results, along with direct HRTEM observations, demonstrated that enhanced diffusion in nanolayer complexions is the root cause for solid-state activated sintering in refractory metals, thereby solving a greater than 50-year-old scientific mystery [22,203].
- The predicted grain boundary solidus temperature was consistent with a prior direct grain boundary diffusivity measurement for W–Co using radioactive tracers [106,213].
- Computed grain boundary λ-diagrams were used to rank the effectiveness of seven sintering aids (Ni, Co, Fe, Cr, Zr, Nb and Pd) on the densification of Mo–Si-B alloys [214].
- Most interestingly, a counterintuitive phenomenon of decreasing grain boundary diffusivity with increasing temperature predicted by the computed λ-diagram of the Mo–Ni system was subsequently corroborated experimentally for a Mo + 0.5 at.% Ni alloy [204].

It should be emphasized again that these grain boundary λ-diagrams are not yet rigorous grain boundary complexion diagrams, which should have well-defined grain boundary transition lines and critical points (similar to those shown in Fig. 12(b)). However, they have proven to be robustly

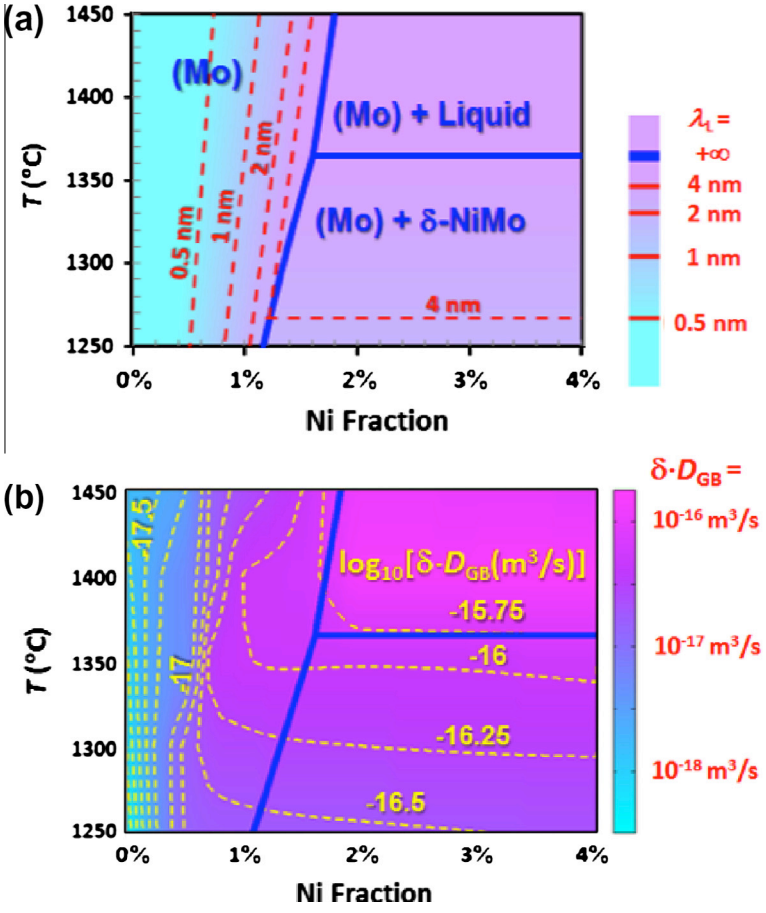

Fig. 18. (a) A computed grain boundary λ-diagram for Ni-doped Mo can predict the general trends of (b) the temperature- and composition-dependent grain boundary diffusivities estimated from sintering experiments. Reprinted from Ref. [31] with permission from APS.

useful in predicting some important trends. Recent studies on constructing binary λ-diagrams, along with efforts to develop other types of complexion diagrams, are reviewed by Luo [32]. Current efforts are in progress to compute such grain boundary λ-diagrams for multicomponent materials and to further consider boundary-to-boundary variations; these efforts will make grain boundary λ-diagrams a more practically useful materials design tool.

Future studies should also be conducted to further develop more rigorous grain boundary complexion diagrams with well-defined transition lines and critical points; in fact, a true grain boundary complexion diagram with a premelting transition line and critical point has already been calculated for Cu–Ag based on the CalPhaD data using a phase-field model [61]; however, the model has unknown fitting parameters and experimental validation has not yet been conducted. Nonetheless, this study signaled a good start to developing theoretical and modeling approaches to compute rigorous grain boundary complexion diagrams.

Bulk phase diagrams are arguably one of the most important materials design tools for guiding the devising of fabrication protocols and predicting materials properties. We believe that both rigorous grain boundary complexion diagrams and some simplified grain boundary diagrams (such as the λ-diagrams discussed above) can be equally useful materials design tools and make it possible to speed the development of new materials. Thus, developing such diagrams is consistent with the goals of the Materials Genome initiative [215].

3. Characterization of complexions

3.1. Overview

This section will describe techniques that can be used to characterize the structure and composition of grain boundary complexions. Broadly speaking, the techniques can be divided into direct characterization techniques, which permit visualization of the grain boundary structure and chemistry as well as quantification of compositional profiles across the grain boundary, and indirect characterization techniques, which measure changes in properties that depend upon grain boundary structure and chemistry, e.g. mobility, diffusivity, cohesive strength, and electrical and thermal properties. No single method, whether direct or indirect, can fully characterize a grain boundary complexion. The best approach to characterizing grain boundary complexion transitions is to use a combination of techniques.

3.2. Direct characterization of complexions

Direct characterization methods, such as Auger electron spectroscopy (AES), transmission electron microscopy (TEM) and atom probe tomography, can provide information about the structure and chemistry of grain boundaries. AES is a well-established technique capable of measuring the chemical composition of grain boundaries [216,217]. TEM is a versatile and powerful method for characterizing the structure and chemistry of grain boundaries, and can provide atomic-level image resolution as well as elemental and chemical analysis with the complementary techniques of energy-dispersive X-ray spectroscopy (EDS) and electron energy loss spectroscopy (EELS). The advent of aberration-corrected STEM in particular has enabled groundbreaking discoveries in grain boundary complexions, and atom probe tomography [218–220] is yet another powerful analytical technique which has been applied to study grain boundary chemistry and morphology.

If a grain boundary can be exposed by intergranular fracture, the composition of the exposed grain boundary region can be studied by AES [207,216]. AES can also be used to study the change in composition as a function of depth, and thereby determine the relative surface enrichment of an element that segregates to the grain boundary. Using sputtering, AES has been employed to demonstrate that multilayer adsorption exists at grain boundaries [216]. AES has also been used in combination with orientation imaging microscopy (OIM) in scanning electron microscopy (SEM) to study the anisotropy of grain boundary segregation [164,217]. However, because AES can only be applied to study grain boundaries that fail by brittle intergranular fracture, it is best suited to the study of materials systems that display some degree of grain boundary embrittlement of the type that occurs via grain boundary segregation of specific impurity elements. Thus AES is most useful for studying grain boundaries in multi-component systems and additionally has a selection bias for the weakest grain boundaries.

TEM enabled the first direct observations of grain boundary complexions and is still one of the most useful techniques for studying them. Referred to at the time as IGFs, the first grain boundary complexions identified by TEM were non-crystalline films of about 1 nm thickness found at grain boundaries in Si_3N_4 [221,222]. The discovery of IGFs was a seminal achievement in grain boundary research. The presence of the intergranular film was inferred from the lack of lattice fringes in a narrow region surrounding the boundary core. Determining the exact structure of this non-crystalline region remains an experimental challenge. The thickness of this grain boundary complexion was constant along the boundary, leading Clarke and Thomas [221] to conclude that it was in equilibrium with its surroundings. Furthermore, the IGFs were only observed at high-angle grain boundaries [221,222]. No IGFs were discovered at low-angle grain boundaries, and this absence is consistent with the idea that complexion transitions occur preferentially at high-energy grain boundaries. Although a correlation between the amount of segregated impurity and the grain boundary energy is not expected, the barrier for first-order complexion transitions could be lower at higher-energy boundaries. IGFs of about 1 nm thickness comprising mostly Co were also discovered at tungsten carbide grain boundaries in WC/Co composites

[223]. In this case, the carbide boundaries could be "dry", could have a 1 nm thick IGF or could have a much thicker wetting layer. IGFs have also been imaged in metals such as Ni-doped W [207]. In these early studies, little structural information could be extracted because the IGFs were non-crystalline. What could be extracted was the thickness of the layer and some composition information. For example, EDS and EELS can be used to determine the elemental constituents in the IGF [224,225,226].

Certain requirements must be met so that a grain boundary complexion can be imaged in the transmission electron microscope, and these requirements severely restrict the fraction of grain boundaries in a specimen that can be studied. The requirements vary depending upon whether image contrast arises predominantly from phase contrast, diffraction contrast or Z-contrast, for example. One requirement that applies to virtually all TEM imaging and contrast modes is that the grain boundary be in the "edge-on" condition, such that the grain boundary plane is parallel to the optical axis of the transmission electron microscope. As pointed out by Lou et al. [222], a grain boundary complexion of 2.5 nm width in a TEM sample of 50 nm thickness will be obscured by the adjacent grains if it is tilted more than 1.5° away from the exact edge-on condition. The edge-on condition is therefore rather stringent. It can be achieved by tilting the TEM sample in the microscope or by searching for a grain boundary that is already in the edge-on condition. Highly curved grain boundaries, i.e. boundaries that have atomic steps separated by tens of nanometers or less, may be impossible to image in the edge-on condition even if the TEM sample is extremely thin. Thus, the edge-on requirement introduces a selection bias that favors atomically flat grain boundaries. While the edge-on requirement generally applies to all S/TEM (where S/TEM refers to scanning and conventional TEM) imaging modes, it is possible to relax this requirement somewhat with the aid of computer simulations. For example, if at least one of the two adjacent grains can be aligned to a low-index zone axis, HAADF-STEM images of curved grain boundaries with through-thickness atomic steps may be interpreted with the aid of image simulations if adsorption of a high-Z element occurs on the grain boundary [227].

A second requirement that applies especially to phase contrast imaging of grain boundary complexions is that the adjacent grains must be aligned so that low-index atomic planes are parallel to the optical axis of the transmission electron microscope such that lattice fringes can be observed [222]. This orientation permits the identification of a thick, disordered grain boundary complexion (e.g. an IGF) due to the absence of lattice fringe contrast in the grain boundary core. Ideally, both grains should be aligned to low-index zone axis conditions, but alignment such that at least one set of lattice planes is visible in each grain is usually sufficient to recognize a thicker disordered complexion, such as an IGF. This combination of requirements is highly restrictive when one considers that the grain boundary itself must also be in the edge-on condition. These restrictions prohibit a large number of general, high-angle grain boundaries in a polycrystalline material from being analyzed, and thus introduce a selection bias towards special grain boundaries with a small population in the polycrystal. Since general high-angle grain boundaries tend to have the highest grain boundary energy and thus are most likely to exhibit complexion transitions, this selection bias against them may prohibit important grain boundary complexions from being identified even though they exist in the materials system.

The stringent requirements for high-resolution TEM imaging of grain boundaries has led to grain boundary studies being frequently done on carefully oriented bicrystals with relatively high symmetry. These bicrystals are often fabricated with symmetrical tilt boundaries so that the crystals have a common zone axis, making it possible to visualize atomic columns in both crystals. While these bicrystal studies are useful as model systems, such ideal grain boundaries represent only a small minority of grain boundaries in real polycrystalline materials. To characterize the structures of complexions, it is necessary to target the most general boundaries that are difficult to image in the S/TEM due to the inability to achieve the edge-on condition while simultaneously aligning the adjacent grains to low-index zone axes. Crystallographically "general" boundaries are most likely to have thicker, more disordered complexions, and these boundaries are rarely the subject of high-resolution TEM studies.

The recent availability of aberration correction for both TEM and STEM has made a dramatic impact on the study of grain boundary complexions. For example, with aberration-corrected STEM, it has been shown that some degree of order exists in IGFs in rare-earth-doped Si_3N_4 [144,228]. HAADF-STEM imaging (i.e. Z-contrast imaging) demonstrated that the dopants segregate preferentially and periodically to the interface between the IGF and the adjacent crystallite. Similarly, aberration-corrected TEM has demonstrated that a degree of order exists in IGFs at gold–sapphire interfaces [43]. Both of these electron microscopy studies were correlated with computer simulations that predicted the observed ordering within the IGF [43,144]. Atomistic computer simulations are becoming increasingly important in the context of high-resolution S/TEM because they can dramatically aid in image interpretation and can provide meaningful insight into the mechanisms governing grain boundary complexion formation.

It was very challenging, and in some cases impossible, to directly visualize the thinner multilayer grain boundary complexions (e.g. the bilayer complexion) until aberration-corrected STEM became available. For example, single- and multilayer complexions were imaged in doped alumina by Dillon and Harmer [229] (Fig. 10), in Bi-doped Ni by Luo et al. [48] (Fig. 10 and Fig. 19) and in Au-doped Si by Ma et al. [34] (Fig. 13). Dillon and Harmer could not readily distinguish between different amounts of multilayer

adsorption in the Al_2O_3 system with standard HRTEM (corresponding to a clean complexion, a monolayer complexion and a bilayer complexion) [17]. These complexions could only be distinguished – and their importance recognized – by the use of aberration-corrected HAADF-STEM imaging. Similarly, bilayer segregation of Bi at Ni grain boundaries was identified with aberration-corrected HAADF-STEM [48]. The segregation of Bi into a bilayer complexion and its role in liquid metal embrittlement in the Ni–Bi system had not been previously recognized because HRTEM imaging cannot show the Bi bilayer complexion. Furthermore, the Ni–Bi results highlight another major advantage of the aberration-corrected STEM method, which is the ability to study complexions at general, high-angle grain boundaries without the necessity of having the adjacent crystallites aligned to low-index zone axis conditions. This is possible because Z-contrast rather than phase contrast is the main contrast mechanism in HAADF-STEM imaging. Thus, grain boundary adsorption of higher-Z elements can be easily identified at grain boundaries even if the adjacent crystallites are not properly aligned for HRTEM imaging. The grain boundary, however, must still be aligned to the edge-on condition.

Despite the advances in aberration correction and other TEM technology, grain boundary complexions are almost always studied at room temperature, far away from the equilibrium conditions under which they formed. Many important grain boundary complexions are only stable at high temperatures, yet characterization is often carried out at room temperature. Thus, the specimen must be quenched to room temperature quickly enough to preserve the high-temperature complexion.

It is possible to study complexions under the conditions at which they are in equilibrium, e.g. at high temperatures in the TEM, if an in situ heating stage is employed. One such study demonstrated that the thickness of IGFs in Si_3N_4 changes as a function of temperature [230]. The width of the IGF was larger at 950 °C than at room temperature, and hysteresis was observed in the IGF width upon cooling. These interesting results demonstrate that in situ heating experiments are promising, and more efforts should be aimed at studying grain boundary complexions in the TEM at high temperatures.

Atom probe tomography combines a field ion microscope with a mass spectrometer to analyze composition and structure on the near-atomic scale [218–220]. As atoms are ionized and ejected from the sample, their trajectories are used to determine their original positions in the sample and their atomic masses are determined by mass spectroscopy. Technical advances have led to tremendous increases in the rate of data collection. With these latest advances, it is possible to image $\sim 10^8$ atoms in a period of hours, approximately 50% of all of the ionized atoms are analyzed, the composition sensitivity is in the parts per million range and spatial resolution is on the order of 1 nm. Atom probe tomography was used to measure the grain boundary segregation in nanocrystalline Ni–W alloys [231] and in Cu–Ni alloys [232]. In the Cu–Ni alloys, the grain boundary width (i.e. the width of the segregation zone in the grain boundary) increases monotonically as a function of annealing temperature, increasing from 0.7 nm at 563 K up to 2.5 nm at 643 K [232], with what appears to be an inflection point or perhaps a discontinuity in the plot of thickness vs. temperature at about 600 K. The increase in

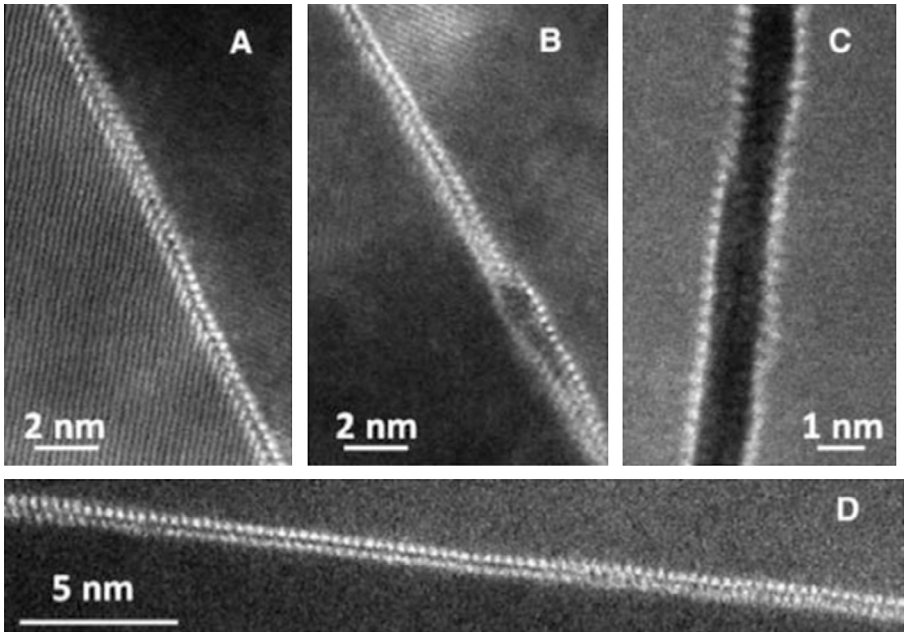

Fig. 19. HAADF-STEM images of a Bi-rich bilayer complexion on general grain boundaries in polycrystalline Ni. In (A) the grain boundary is still intact, but (B) and (C) show the initiation of brittle fracture. Reprinted from Ref. [48] with permission.

the thickness of the segregation zone with temperature is characteristic of a transition to a thicker complexion and counter to what is observed for conventional segregation. While it is not clear if these changes in grain boundary width represent a complexion transition, this study clearly highlights the unique capabilities of atom probe tomography and the promise it shows for studying grain boundary complexions.

It is often necessary to combine two or more direct characterization techniques to gain a better understanding of the structure and chemistry of grain boundary complexions. Each technique has benefits and drawbacks, and none can provide complete information about grain boundary structure and chemistry. For example, atom probe tomography has been combined with TEM imaging to study grain boundary segregation in Fe–Si alloys [233]. Furthermore, the combination of atomistic computer simulations with direct characterization techniques has become increasingly important in recent years for interpreting experimental results and understanding the mechanisms behind grain boundary complexion formation and stability [43,144]. The most fruitful studies of grain boundary complexions in the future will likely rely on a suite of characterization techniques combined with first-principles computer simulations.

3.3. Indirect characterization of complexions

When Hart predicted that grain boundaries may undergo complexion transitions, he suggested that the non-equilibrium grain boundary properties, such as grain boundary mobility, diffusivity, sliding resistance, and cohesive strength, would be most dramatically affected [3–5]. He pointed out that these properties are also much more easily accessible to experiment than the equilibrium properties, such as grain boundary energy, width and adsorbate content. Early studies by Aust [53] on grain boundary mobility in zone-refined Pb demonstrated a discontinuity in the activation energy of grain boundary mobility in carefully constructed bicrystals.

While bicrystal studies are useful as model systems, most engineering materials are polycrystals with a wide variety of general grain boundaries present. With the use of dual-beam focused ion beam (FIB)/SEM to prepare site-specific TEM samples, it is possible to correlate grain boundary mobility directly with atomic structure and chemistry of the grain boundary. The most well-known example of such a study was done on polycrystalline alumina, where boundaries with increasing mobilities have been associated with complexions that have increasing levels of disorder [17]. The appearance of large grains in annealed alumina has been used as an indicator of a complexion transition. For example, the fast-moving boundaries around the largest grains in Ca-doped Y_2O_3 have been associated with an IGF complexion [33]. Using this behavior to identify complexion transitions, Dillon and Harmer [19] found that the probability of complexion transitions increased with both temperature and grain boundary adsorbate concentration (which increases with grain size in a sample of constant bulk composition). In this way, abnormal grain growth in alumina was shown by Dillon et al. [17] to result from the coexistence of two or more grain boundary complexions with differing mobility. Fig. 20 shows schematically how a thicker, more disordered, higher mobility complexion exists at the grain boundaries of abnormal grains in alumina, whereas thinner, more ordered complexions exist at the grain boundaries of normal grains.

The changes in grain boundary mobility can be measured to characterize the grain boundary complexion transition. The mobility can be measured in a bimodal structure by characterizing the grain growth of both the normal and the unimpinged abnormal grains as a function of time [20,21]. The size of the normal grains is used to determine the driving force for the growth of the abnormal grains. If the grain size as a function of time obeys parabolic kinetics, then it is possible to determine the product of the grain boundary mobility and the grain boundary energy. The grain boundary energy term is assumed to be relatively constant compared to the variations in the mobility. Mobility measurements made using this technique, reported by Dillon and Harmer, were used to identify six different mobility classes for grain boundaries in alumina, as shown in Fig. 21 [17]. However, grain growth rates can be deceptive as they are sensitive to impurity drag, particle drag, pore drag and variations in driving force due to stored elastic energy.

Certain complexion transitions can also be detected by differential scanning calorimetry (DSC). For example, in Al–Zn [234] and Al–Mg [235] alloys, it has been shown that the grain boundaries and triple lines melt before the bulk solidus temperature is reached. The grain boundary premelting is detected by the DSC as an absorption of heat below the solidus temperature. The transition is only detected in fine-

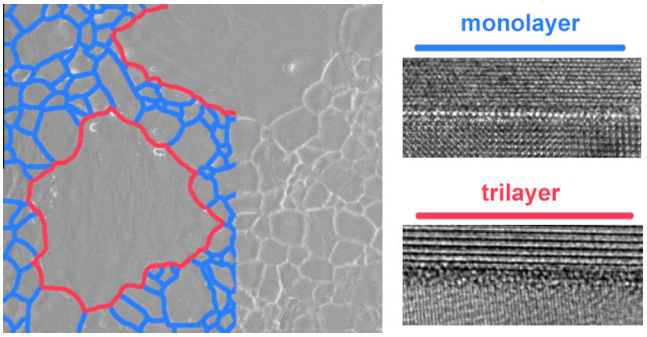

Fig. 20. A schematic diagram showing that abnormal grains are surrounded by thicker, more disordered complexions (e.g. the trilayer complexion) with higher mobility (red), whereas the normal grains have thinner, more ordered complexions (e.g. the monolayer complexion) with lower mobility grain boundaries (blue). In general, it is believed that AGG results from such coexistence of two or more grain boundary complexions with vastly different grain boundary mobilities. Adapted from Ref. [17]. (For interpretation of the references to color in this figure legend, the reader is referred to the web version of this article.)

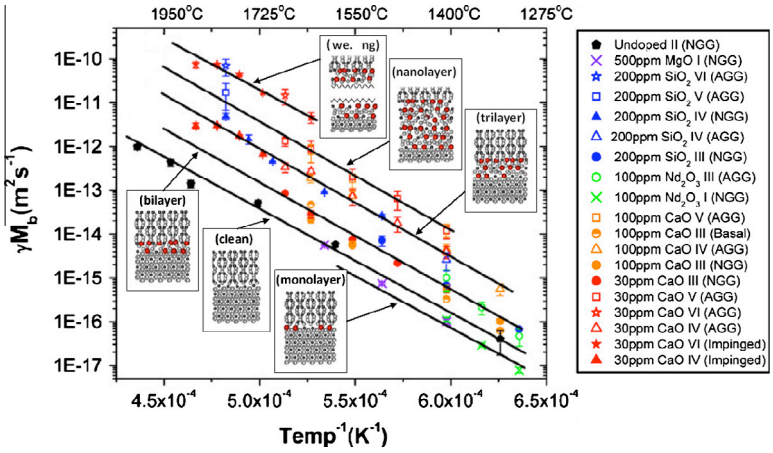

Fig. 21. Grain boundary mobility in doped and undoped alumina, showing six distinct regimes of mobility corresponding to the six discrete Dillon–Harmer complexions which are shown schematically. Adapted from Ref. [17].

grained samples (10–20 micron grain size, in this case) when there is enough grain boundary area to create a detectable heat signature [235]. Samples with large grains, produced in situ by melting and solidifying, do not have a detectable transition. The result on a phase diagram is that a separate grain boundary solidus appears at a temperature below the bulk solidus, e.g. as shown by the solid blue premelting/prewetting (T_{pw}) line in the solid two-phase region in Fig. 9 [236]. In principle, complexion transitions other than melting should be detectable by DSC. However, small enthalpy changes associated with the transition and the simultaneous occurrence of competitive enthalpic changes, such as grain growth, may mask the signal.

In several cases, it has been shown that complexion transitions are associated with reductions in the grain boundary energy [28,33,42]. Therefore, grain boundary energy measurements can be used to characterize complexion transitions. In practice, it is relatively simple to measure changes in the relative grain boundary energy, but much more difficult to measure absolute energies [237]. As a result, it is usually the relative energy that is measured. Thermal grooves form to balance the interfacial energies between the surfaces and the grain boundary. The relative energy of a grain boundary (γ_{gb}) to the adjacent grain surface (γ_s) can be expressed as a function of the dihedral angle (Ψ_s) at the groove according to Eq. (16).

$$\frac{\gamma_{gb}}{\gamma_s} = 2\cos\frac{\Psi_s}{2} \tag{16}$$

Using Mullins's [238] analysis, it is possible to measure the height and width of a thermal groove and solve for the relative interfacial energy of the grain boundary. However, this method includes a number of approximations and assumptions. For example, it is assumed that the two surface energies are the same, that the grain boundary is normal to the surface and that the interface energy anisotropy is small. While these assumptions will not hold for any single-grain boundary, it has been found that, for many measurements of grain boundary dihedral angles, the mean value and width of the distribution are reproducible and meaningful quantities [239–241]. In the last decade, atomic force microscopy (AFM) has greatly simplified these measurements and specific procedures have been established for making reliable grain boundary energy measurements using AFM [241].

As an example, the data in Fig. 22 shows the relative grain boundary energy distributions for two subsets of grain boundaries in the same 100 ppm Nd-doped alumina [30]. These measurements were derived from thermal grooves according to Eq. (16). In this case, the crystallographic characteristics of the junctions were not considered and we are concerned only with the distribution derived by averaging over more than 200 boundaries. The first subset of boundaries surrounds small grains growing normally (NGG) and the second subset surrounds grains growing abnormally (AGG). The grain boundaries growing normally are known, on average, to have a monolayer complexion with adsorbed Nd, whereas the grains growing abnormally have, on average, a bilayer complexion with adsorbed Nd and greater mobility. The results clearly show that the boundaries enriched with Nd have a lower average energy than those with less Nd. Similar changes have been observed in other systems [28,33,30]. Similarly, a study of IGFs that formed at gold–sapphire interfaces in contact with anorthite glass has shown that the IGF reduces the interfacial energy by about 190 mJ m^{-2} compared to the intrinsic gold–sapphire interfacial energy [42].

The changes in the grain boundary energy have an indirect influence on the distribution of grain boundaries in the sample. From comparative studies of the anisotropy of the grain boundary character distribution (GBCD, the relative areas of different types of grain boundaries) and the anisotropy of the grain boundary energy, it has been shown that there is an inverse relationship between the two quantities in polycrystals evolving by normal grain growth, which implies that there are relatively more low energy grain boundaries than there are high energy grain boundaries [237,242–245]. Therefore, if there is a transition in the kinds

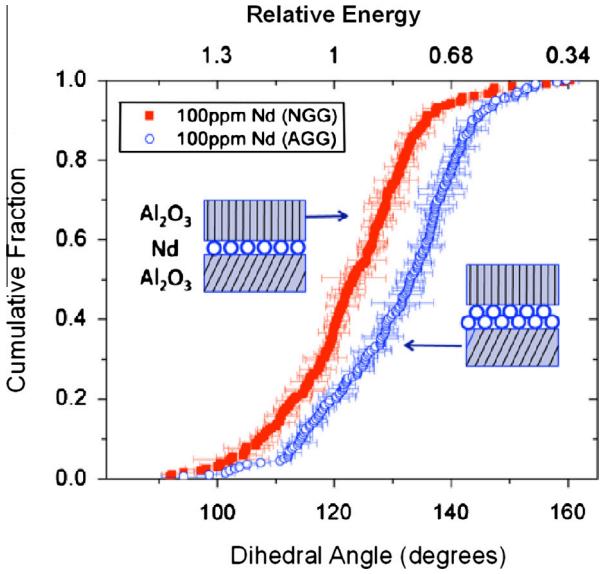

Fig. 22. Cumulative distribution of dihedral angles in neodymia-doped alumina annealed at 1400 °C with normal grain boundaries (monolayer complexion) and abnormal grain boundaries (bilayer complexion). Insets schematically illustrate the boundary structure of the two complexions. Reprinted from Ref. [30] with permission.

of complexions in a sample and this alters the grain boundary energies, it will also change the GBCD. This has been observed and measured in several cases [29,33]. For example, Fig. 23(a and b) compares the microstructure of a Ca-doped yttria sample before and after some of the boundaries have undergone a complexion transition. The abnormally large grains have an IGF complexion and the smaller ones have a bilayer complexion.

When the distributions of grain boundary planes are compared (Fig. 23(c and d)), the distribution in the sample with a normal grain size distribution is nearly isotropic, with a mild preference for grain boundaries with a (1 1 1) orientation, while in the sample after the complexion transition there is a strong preference for grain boundaries with (1 0 0) planes. This suggests that the energies of the (1 0 0) planes have been selectively reduced in energy compared to the other types of grain boundaries. Similar effects have been observed in doped aluminas [29].

4. Terminology and categorization of complexions

A wide variety of terminology has been used to describe grain boundary complexions and transitions between different complexions. The terminology can be confusing, and sometimes several terms are used in the literature to describe the same phenomenon. Furthermore, there is no generally accepted method of categorizing the many different types of complexion transitions that may occur. Now that it is possible to see more details of the structure and chemistry of grain boundary complexions using advanced electron microscopy, it is becoming increasingly important to develop a standardized nomenclature for describing and categorizing complexions. A categorization system will be especially important as grain boundary complexion diagrams are developed, so that lines of transition can be marked appropriately.

In this section, we will first give some examples of the various terms that have been used to describe grain boundary complexions and transitions between different complexions. Then we will discuss a categorization scheme for complexion transitions first proposed by Cahn [6]. Finally, we will suggest a method to categorize complexions based upon a combination of their physical characteristics and properties.

4.1. Common terminology used to describe grain boundary complexion transitions

Many descriptive terms have been used when discussing grain boundary complexion transitions, e.g. structural transitions, faceting transitions, defaceting transitions, roughening transitions, wetting transitions, prewetting transitions and premelting transitions. Countless variations of these terms exist in the literature, yet rigorous definitions are rarely given and therefore the terms can be confusing to non-experts. Complexion terminology that invokes the word "wetting" can be particularly misleading, because a wetting phase is a bulk phase (with arbitrary thickness) rather than an interfacial state (with a fixed equilibrium thickness). We will review some of these terms here.

As discussed in Section 2, a first-order complexion transition occurs when there is a discontinuity in the first derivative of γ as a function of one of the thermodynamic parameters (T, P, μ_i, $\boldsymbol{R}$, or $\hat{\boldsymbol{n}}$), or in a higher-order derivative for a second or higher-order transition [8,9]. Thus, cusps in grain boundary energy as a function of grain boundary misorientation $\boldsymbol{R}$ or inclination $\hat{\boldsymbol{n}}$ represent complexion transitions, as do the disappearance of the cusps as a bulk thermodynamic parameter is varied (e.g. as temperature is raised) [8].

A structural transition is defined as a complexion transition that occurs when a bulk thermodynamic parameter is varied (T, P, μ_i, etc.) while all five interfacial thermodynamic parameters ($\hat{\boldsymbol{n}}$, $\boldsymbol{R}$) are held constant [8]. Despite the name, structural transitions can involve changes in the chemical composition of the grain boundary in addition to structural rearrangement of atoms within the grain boundary core. A structural transition can be first-order if it results from the crossing of two or more "competing" grain boundary free energy curves (as shown schematically in Fig. 2), or it can be second-order, for example, if the transition involves the gradual replacement of one type of grain boundary repeating structural unit for another [8]. By definition, all structural transitions are congruent transitions and vice versa (congruent transitions are discussed in Section 4.2).

A faceting transition is a complexion transition that involves the restructuring of an initially singular or curved grain boundary into a hill-and-valley structure [246] with at least two different boundary inclinations, $\hat{\boldsymbol{n}}_1$ and $\hat{\boldsymbol{n}}_2$, as a

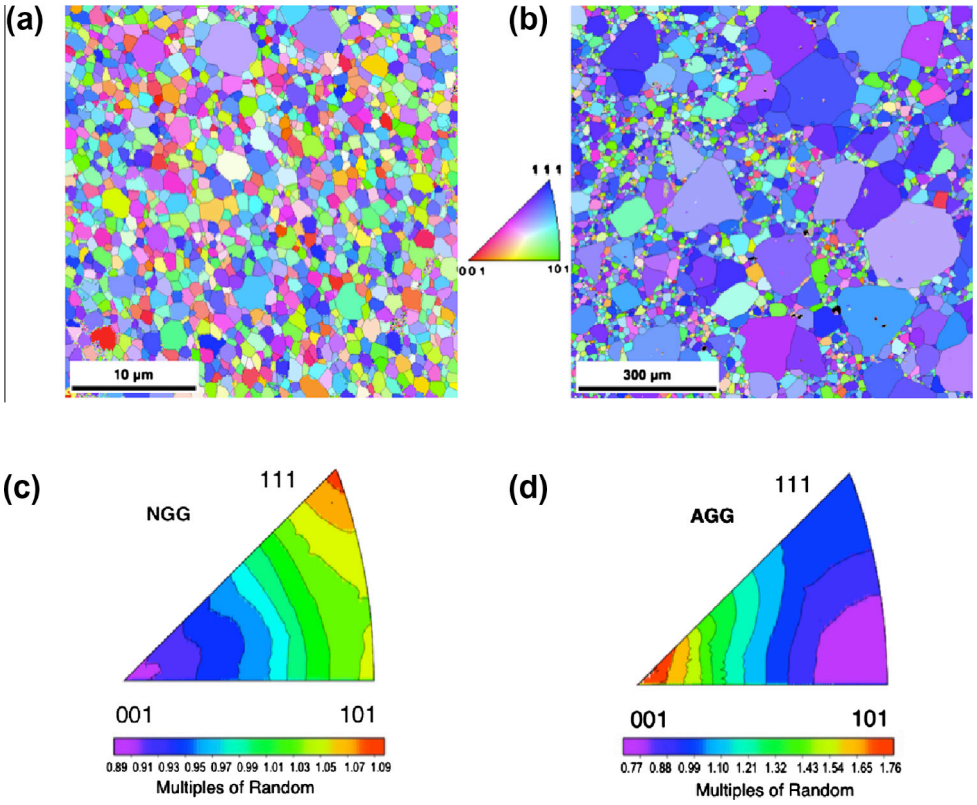

Fig. 23. EBSD data for a Ca-doped yttria sample with superimposed reconstructed grain boundaries for (a) an NGG sample, which exhibits a homogeneous grain size distribution before some boundaries undergo a complexion transition, and (b) an AGG sample, displaying a bimodal grain size distribution (as a result of some boundaries undergoing a complexion transition to a higher mobility complexion) and an apparent change in texture. The grain boundary plane distributions, independent of misorientation, for the (c) NGG sample and (d) AGG sample plotted in the standard stereographic triangle. Reprinted from Ref. [33] with permission.

bulk or interfacial thermodynamic variable is varied (T, P, μ_i, or $\boldsymbol{R}$, for example) [8]. The reverse transition, from faceted to planar grain boundary, is referred to as a defaceting transition. Reversible faceting/defaceting transitions induced by changes in composition have been demonstrated in the Cu–Bi system [247]. Each facet represents a complexion and is associated with a specific free energy. The coexistence of two such facets is shown in Fig. 3(b). These facets, initially present on a fine scale as microfacets, may coarsen into macrofacets to eliminate the energy associated with the one-dimensional complexion boundary between each pair of facets. Microfacets may only be visible by transmission electron microscopy (e.g. as shown in Fig. 24(a)) and therefore this type of complexion transition can be easily overlooked. By definition, all faceting transitions are non-congruent transitions and vice versa (non-congruent transitions are discussed in Section 4.2).

Recent experimental evidence in Bi-doped Cu has demonstrated that faceting transitions may be associated with changes in the structure and chemistry of the grain boundary core [35]. In this study, a Bi-rich bilayer complexion was observed on one of the two facet inclinations (see Fig. 24). However, it is not known if the grain boundary faceting transition occurred simultaneously with formation of the Bi-rich bilayer complexion. It is possible that the Bi-rich bilayer complexion formed before grain boundary faceting, in which case the bilayer complexion formation would be a structural transition, which was then followed by a faceting transition. We can simply say that a complexion transition has occurred and then describe its characteristic features, rather than attempt to categorize the transition as a faceting transition or structural transition, which could be misleading because faceting and structural transitions are mutually exclusive by definition.

A grain boundary roughening transition is a complexion transition that occurs when an initially smooth grain boundary becomes disordered and rough on an atomic scale. Roughening transitions are well known and have been extensively studied [150,248–251]. They occur at a critical temperature (which may vary as a function of $\hat{\boldsymbol{n}}$ and $\boldsymbol{R}$). The high-temperature rough grain boundary is predicted to have a significantly larger mobility than the low-temperature smooth grain boundary [150]. Different grain boundaries roughen at different temperatures and not all grain boundaries may undergo a roughening transition, even at temperatures as high as the melting temperature. Computer simulations predict that grain boundaries which remain smooth at high homologous temperatures, and hence are low mobility boundaries, are responsible for grain growth stagnation in pure materials [248]; such

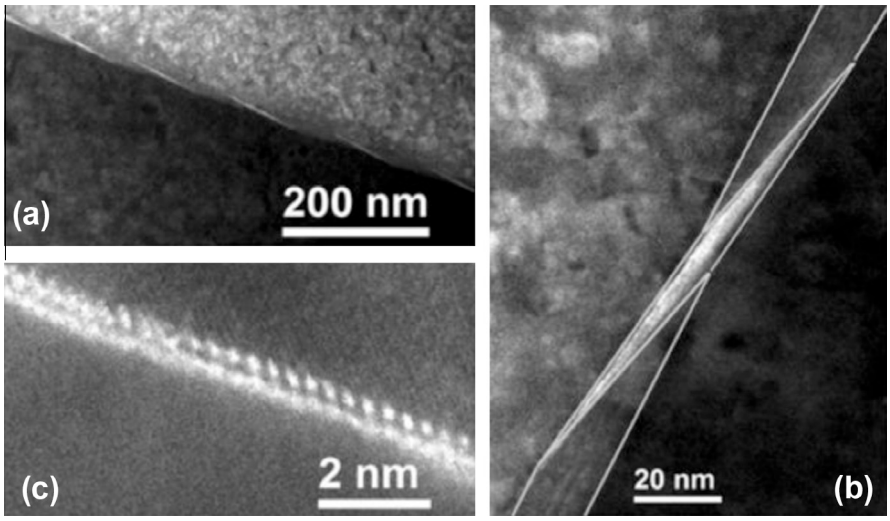

Fig. 24. HAADF-STEM images of faceted grain boundary in Bi-doped Cu, exhibiting the coexistence of two complexions on different inclinations of a faceted grain boundary. There is a Bi-rich bilayer complexion on one of the two facet inclinations and a clean complexion on the other facet. This type of complexion coexistence is represented schematically in Fig. 3(b) and Fig. 26. Reprinted from Ref. [35] with permission.

stagnation at high temperatures cannot otherwise be explained by solute drag or other mechanisms.

Grain boundary roughening has long been presumed to be a second-order transition, but a recent simulation suggests that roughening transitions can also be first-order [150]. Although roughening and faceting are distinct phenomena [248], it is possible to have combined roughening/defaceting transitions in which an initially faceted boundary (with two smooth facets) decomposes upon heating into an undulating, rough boundary [1,94]. It is also possible that one or both of the two orientations in a hill-and-valley structure can be rough rather than smoothly faceted [251].

Wetting, prewetting and premelting transitions are closely related phenomena. The prototypical wetting transition involves three bulk phases – a liquid drop, l, a solid substrate, s, and a vapor phase, v, as shown schematically in Fig. 25(a). Equilibrium between the three phases can be described by a balance of three interfacial energies, γ_{sl}, γ_{sv} and γ_{lv}. The contact angle, ϕ, defines the degree of wetting. Poor wetting occurs if $\phi > 90°$, good wetting if $\phi < 90°$ and non-wetting if $\phi = 180°$ [252]. Complete wetting occurs if $\phi = 0°$, as shown in Fig. 25(b). A wetting transition occurs when the interface energies change such that the wetting phase with an initial wetting angle $\phi > 0°$ flattens out and covers the entire surface of the substrate with a wetting angle of $\phi = 0°$. Wetting transitions need not involve a liquid phase, and can occur even if all three of the phases are solid. This situation is shown schematically in Fig. 25(c and d), which depicts a solid δ phase existing at a ε–ε grain boundary with a finite contact angle (Fig. 25(c)) and then undergoing a wetting transition such that the δ phase covers the entire grain boundary, as shown in Fig. 25(d). Although it can be defined in terms of bulk phases, this solid-state wetting transition can also be viewed as a dissociation complexion transition in which the initial ε–ε grain boundary complexion dissociates into two different ε–δ grain boundary complexions. A dissociation transition is shown schematically in Fig. 3(c), and occurs when the grain boundary inclination $\hat{\boldsymbol{n}}$ remains constant while the misorientation $\boldsymbol{R}$ changes as a single grain boundary complexion decomposes into two complexions.

Some authors use the convention that the wetting phase described above is non-wetting if $\phi > 90°$ [252]. Confusingly, the phrase "non-wetting film" has been used to refer to nanolayer complexions (historically referred to as IGFs) [253]. The rationale behind this terminology is that a wetting film (which may have an arbitrary thickness) is a bulk phase because wetting is a bulk phenomenon, and therefore a non-wetting film (which has a fixed, finite thickness) is a non-bulk phase and is thus an interfacial phase – what we call a complexion. This terminology is especially confusing in light of the convention that a non-wetting phase is defined based on a non-zero contact angle as discussed above ($\phi > 90°$ or $\phi = 180°$, depending on the convention). The phrase "non-wetting film" therefore implies a non-zero contact angle and suggests that the complexion does not cover the entire grain boundary, which is misleading. Rather, it is understood that a complexion completely covers the entire interface at the grain boundary, because it is the interface. If two complexions coexist at equilibrium (as shown in Fig. 3(a), for example), then each one does not cover the entire interface but there is no notion of a contact angle between them. The complexion boundary that separates these two complexions is essentially one-dimensional, so the notion of a contact angle implied by the term "non-wetting" does not apply to complexions.

Prewetting and premelting transitions are both complexion transitions whose names allude to the related bulk phenomena (wetting and melting). Prewetting describes a first-order complexion transition in which the interfacial thickness and the adsorbed solute increase discontinuously.

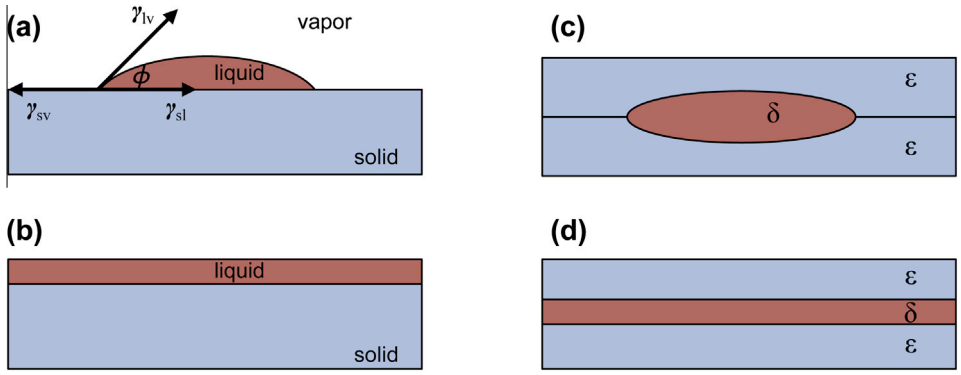

Fig. 25. Schematic wetting diagrams: (a) the prototypical three-phase wetting geometry when a liquid drop is on a solid substrate in contact with a vapor; (b) the geometry after a wetting transition, when the contact angle goes to zero; (c, d) analogous solid–solid wetting phenomena at a grain boundary in a two-phase solid, with the δ phase (c) partially wetting the ε–ε grain boundary and (d) completely wetting the ε–ε grain boundary.

Prewetting is often described as a "thin to thick film transition" [23]. Both the "thin" and the "thick" film are complexions rather than bulk films. Prewetting transitions are adsorption transitions, and thus typically occur in multicomponent systems, but they may occur in either one- or two-phase regions on the bulk phase diagram, as shown in Fig. 9. The prewetting terminology derives from Cahn's critical point wetting theory for fluids [69]. Prewetting does not necessarily imply any type of atomic rearrangement or restructuring in the grain boundary core, but rather simply refers to an abrupt jump in adsorbate content of the grain boundary and an associated discrete increase in the thickness. It typically occurs under thermodynamic conditions near a bulk wetting transition, when the phase that would be involved in the wetting transition is not yet a thermodynamically stable bulk phase.

On the other hand, premelting is a complexion transition in which the grain boundary inclination remains invariant and the core becomes disordered and liquid-like at high temperatures near the melting temperature (in contrast, roughening transitions result in local changes in grain boundary inclination and may occur at much lower homologous temperatures). Premelting can be considered as a special case of prewetting. For grain boundaries in binary or multicomponent systems, the term "premelting" is used to emphasize the structural disorder, while the term "prewetting" is used to emphasize the compositional variation (particularly adsorption). Complexion transitions tend to have elements of both prewetting (adsorption transitions) and premelting (disordering transitions), which has led some researchers to use the phrase "coupled prewetting/premelting transition" to refer to a complexion transition which has discontinuities in both adsorption and structure [13].

4.2. Congruent, non-congruent and dissociation transitions

Cahn suggested classifying grain boundary complexion transitions into two types, congruent and non-congruent [1,6]. During a congruent transition, the structure and/or chemistry of the grain boundary core changes while the morphology of the grain boundary remains invariant, so that flat boundaries remain flat and curved boundaries remain curved. Non-congruent transitions involve different grain boundary inclinations, $\hat{\boldsymbol{n}}$, and occur when a grain boundary facets to a new orientation or otherwise undergoes a change in $\hat{\boldsymbol{n}}$. A third type of transition described by Cahn is the dissociation transition, in which one grain boundary separates into two boundaries by the insertion of a new bulk phase [6]. The two new boundaries have a total free energy less than the original boundary, and the combined misorientation $\boldsymbol{R}$ is conserved. This transition is commonly referred to as a wetting transition. Cahn concluded that congruent complexion transitions are exceedingly rare, saying "The search for congruent transformations has all the aspects of a search for a needle in a $6 + C$ dimensional haystack" [6]. This was a rather remarkable conclusion, because most reports of grain boundary transitions implicitly assume that a congruent transition has occurred.

The coexistence of two complexions at equilibrium within the three categories of transitions discussed by Cahn can be visualized according to Fig. 3: (a) congruent transition, (b) non-congruent transition and (c) dissociation transition. As discussed by Rottman [9], coarsening of the complexions in Fig. 3(a) and (b) may occur to minimize the energy associated with the one-dimensional α–β complexion boundaries. If the two facets in Fig. 3(b) have different specific free energies, there would be an additional driving force for the elimination of the higher-energy facet and the growth of the lower-energy facet. If this coarsening and growth occurred quickly enough, evidence of a non-congruent (faceting) transition could essentially disappear for a grain boundary in a polycrystal and the complexion transition might appear to have been congruent because the boundary is not faceted. This possibility complicates experimental analysis: if a grain boundary is examined ex situ in a scanning/transmission electron microscope and there is evidence of a grain boundary complexion transition (e.g. multilayer adsorption) but no observable faceting, can

it be concluded that a congruent transition has occurred rather than a non-congruent transition? In light of Cahn's comments on the rarity of congruent transitions, it seems presumptuous to classify complexion transitions as congruent without strong evidence that the transition did indeed occur congruently, without a change in grain boundary inclination. Therefore, while categorization based on the scheme of congruent vs. non-congruent transitions is attractive in principle, in practice it is rather impractical because it is not always apparent which type of transition has occurred by studying the grain boundary ex situ. We therefore recommend a more empirical categorization scheme that is based on linking the structure and chemistry of complexions to their properties.

4.3. Other methods for categorizing complexions

An ideal grain boundary complexion categorization scheme would be simple enough to be used as an engineering tool but robust enough to be applicable to all types of complexions in all materials systems. Unfortunately, any categorization scheme will necessarily be a simplification that does not capture every detail and nuance of every possible complexion or transition. A method of categorizing complexion transitions can be very useful, especially with regard to developing practical complexion transition diagrams. Despite the inherent shortcomings of categorization, we can make some generalizations regarding various types of grain boundary complexions, and it is possible in some instances to develop a categorization scheme based on structure–properties relationships within a given materials system.

Grain boundary complexion transitions can be categorized broadly into two groups, intrinsic and extrinsic. Intrinsic transitions occur in pure materials, including unary systems and stoichiometric or non-stoichiometric compounds, and may include structural and roughening transitions. Extrinsic transitions occur in non-pure materials and usually involve the adsorption of impurity or dopant elements. Due to the ubiquitous presence of impurities in real materials, intrinsic complexion transitions are extraordinarily difficult to study experimentally. The minimum concentration of impurities that can induce an extrinsic complexion transition varies depending on the materials system, but as little as 30 ppm CaO has been shown to induce extrinsic complexion transitions in Al_2O_3, for example [17].

One of the earliest studies on grain boundary complexion transitions identified a discontinuity in the activation energy of the grain boundary migration rate in high-purity, zone-refined Pb [53]. The study was done on Pb bicrystals, and the discontinuity was assumed to be evidence of an intrinsic transition between a low-temperature and high-temperature grain boundary structure. However, impurities may have contributed to this transition, i.e. it may not have been an intrinsic transition. Modern computer simulations can offer more insight into intrinsic transitions. For example, as discussed earlier, a recent MD simulation of Σ5 grain boundaries in pure copper demonstrated a first-order grain boundary structural transition at elevated temperatures, as well as the coexistence of two complexions on a single grain boundary separated by a one-dimensional complexion boundary [39].

Intrinsic grain boundary roughening transitions have also been predicted in pure metals by computer simulations, and these transitions are associated with abrupt discontinuities in grain boundary mobility [150]. Some grain boundaries do not roughen even at high temperatures near the melting point, and this is believed to be responsible for grain growth stagnation [248]. Such roughening transitions would be difficult or impossible to study by standard room-temperature TEM, which is the predominant mode of grain boundary complexion analysis today. In-situ heating experiments in the transmission electron microscope could conceivably demonstrate defaceting/roughening transitions, and indeed this has been done for multicomponent systems previously [247]. However, such experiments invariably contain impurities, which is not the case for computer simulations, and therefore would not be very useful for studying intrinsic complexion transitions. Impurities will typically be present in TEM samples prepared using a FIB microscope, due to Ga implantation from the ion beam.

There has not been enough work done on intrinsic complexion transitions to suggest a useful categorization scheme. Work is ongoing in this area, and useful advances are likely to be dominated by computer simulations, which can be impurity-free.

Significantly more research has been done on extrinsic complexion transitions. Since most engineering materials are multi-component systems, extrinsic complexion transitions are generally of greater engineering interest than intrinsic complexion transitions. A useful categorization scheme for extrinsic grain boundary complexion transitions will likely be empirical, system-specific and simple enough so that complexion transitions can be overlaid on a bulk phase diagram, but not so simple that critical information relevant to changes in materials properties is omitted.

To develop a categorization scheme, the structure and chemistry of grain boundaries in a given materials system must be studied experimentally, typically by electron microscopy, and correlated to grain boundary properties of interest. Such a direct correlation between grain boundary structure and properties was carried out in doped Al_2O_3 by Dillon and Harmer [17]. TEM samples of high-mobility grain boundaries from fast-growing abnormal grains and normal grain boundaries with lower mobility were prepared via the in situ FIB lift-out method so that grain boundary structure and chemistry were directly correlated to grain boundary mobility. Six distinct mobility regimes were discovered, as shown in Fig. 21, and these regimes correlate to six categories of grain boundary complexions shown in Fig. 10. Of course, by simplifying a vast, multi-dimensional phase space into only six categories,

some information is necessarily lost. Nevertheless, there is strong experimental evidence that this Dillon–Harmer categorization scheme works very well for understanding how complexion transitions influence grain boundary mobility in doped Al_2O_3 [17,20,21].

All six complexion categories will not necessarily exist in other materials systems, but many of them have been shown to exist in several other materials. Likewise, six distinct structures are not sufficient to describe the types of complexions in any arbitrary system. In a system such as Bi-doped Ni, for example, only two major types of grain boundary complexions were identified (a clean complexion with no observable Bi adsorption, and a bilayer complexion rich in adsorbed Bi). These two types of complexions correlate strongly to grain boundary cohesive strength [48]. Although other complexion categorization schemes might make sense for Ni–Bi or doped Al_2O_3 if grain boundary properties other than cohesive strength and mobility are studied, these two examples illustrate how grain boundary structure and chemistry can be correlated with grain boundary properties to develop an empirical, system-specific complexion categorization scheme.

Another categorization scheme for grain boundary complexions has been previously proposed in which three categories exist: dry, moist and wet, as defined by Cannon et al. [254–256]. Despite the terminology that implies liquid phases are involved, these three categories usually refer to grain boundaries and other solid–solid interfaces. The dry category corresponds to the clean complexion in the Dillon–Harmer categorization scheme, in which the grain boundary is free of solute adsorption or contains a very small amount of solute. The moist category encompasses complexions that display multilayer adsorption, which corresponds to the Dillon–Harmer bilayer, trilayer and nanolayer complexions. The wet category describes the case where a bulk wetting film exists at the boundary, and this corresponds directly to the Dillon–Harmer wetting category.

The terms and definitions discussed in this section are summarized in Table 2. This table is designed as a quick reference guide for terms that have been used to describe complexions and complexion transitions. In an effort to unify terminology in grain boundary complexions research, we recommend using a subset of these terms to describe grain boundary complexions and transitions between different complexions. The recommended terminology is summarized in Fig. 26: complexion transitions are shown schematically in the top section of the figure along with the preferred terms, while methods of categorizing complexions are shown schematically in the lower section. While the terminology in Fig. 26 is not necessarily sufficient to describe all possible complexion phenomena, it provides a framework within which specific complexion behavior and phenomena may be discussed. For example, the roughening complexion transition is not explicitly shown, but there could be a "congruent, intrinsic roughening complexion transition" in a pure material in which the macroscopic grain boundary geometry (character) does not change but the boundary becomes disordered and rough on the atomic (microscopic) scale upon heating to a critical temperature. Similarly, one can imagine other types of complexion phenomena that can be described in greater detail within this framework.

Some of the terms are specific to grain boundary complexions, while other terms can be used for any type of complexion, whether it is a surface complexion, a grain boundary complexion or a phase boundary complexion.

5. The effect of complexions on properties, processing and microstructure

Efforts to better understand anomalous microstructural development and materials properties have motivated much of the development of the science of grain boundary complexions [17,47,203,222,257]. Grain boundaries may undergo complexion transitions independently of bulk phase transformations, and thus grain boundary related properties may change unexpectedly and unpredictably as temperature, pressure or chemical potential is varied. A complexion transition can affect equilibrium properties such as grain boundary energy, entropy, enthalpy, defect density and adsorbate concentration. Complexion transitions may also induce discontinuous changes in the non-equilibrium properties of grain boundaries, such as mobility, cohesive strength and sliding resistance. It is the discontinuity in properties that is the hallmark of a complexion transition, and is the reason why such transitions play a large role in the properties, processing and microstructure development of materials [5]. The effect of a grain boundary transition on these properties is not easy to predict and may be difficult to rationalize on the basis of classical models for grain boundary structure–property relationships. For example, a grain boundary complexion transition in Ga-doped Al increased grain boundary mobility by approximately an order of magnitude [258], in stark contrast to the classical impurity drag theory, which predicts that grain boundary segregation will always reduce grain boundary mobility [259].

Despite their relatively small volume fraction, grain boundaries often play a dominant role in materials properties. Grain boundary engineering was first proposed by Watanabe in 1984 [260], and has since been considered by others. While grain boundary engineering recognizes the effects of grain boundary solute segregation, the emphasis is usually on the geometric structure of grain boundaries and a categorization scheme based on the coincident site lattice model that compares "low-angle" and "high-angle" boundaries, or "special" to "general" boundaries. Clearly, grain boundary complexion transitions deserve attention in the context of grain boundary engineering, especially given the non-classical behavior induced by some grain boundary complexion transitions. In particular, grain boundary complexion engineering may provide

new opportunities to engineer nano- and microstructures, control mass transport dependent properties and tailor mechanical properties. In this section we will discuss the effect of complexion transitions on grain boundary properties, bulk properties, and materials processing.

5.1. Grain boundary properties

During a complexion transition, the slope of the grain boundary energy (as a function of temperature, pressure, chemical potential, etc.) will exhibit special behavior such that a discontinuity may appear in the first derivative (or a higher order derivative) of the grain boundary energy curve. This discontinuity in the derivative of the grain boundary energy is the defining characteristic of a complexion transition. However, it is difficult and time consuming to measure the grain boundary energy curves. Therefore, discontinuities in grain boundary properties, structure and chemistry can serve as excellent proxies for identifying grain boundary complexion transitions.

One early such study measured the grain boundary energy in Pb by observing the dihedral angles of a tricrystal as a function of temperature [261]. Based on these measurements, which showed a discontinuous change in dihedral angle at a specific temperature, it was claimed that a grain boundary transition had occurred and was accompanied by a discontinuous change in grain boundary energy. Because grain boundary energy must be continuous even at transition points, this work has been criticized by others [5,6,262]. Cahn discussed the controversy of discontinuities in dihedral angles and pointed out that Gleiter's work showed evidence of a grain boundary faceting transition, which is itself evidence of a grain boundary complexion transition, and furthermore that a discontinuity in the dihedral angle (which was incorrectly assumed to prove a discontinuity in energy) accompanying such a faceting transition is not inconsistent with thermodynamic principles [6]. This early study in Pb tricrystals and the subsequent criticism and analysis demonstrates the difficulty involved in properly identifying grain boundary complexion transitions by experimentally measuring the grain boundary energy. A number of studies have observed hysteresis in complexion transitions upon heating and cooling [28,108,112]. Such hysteresis results from a complexion transition occurring under non-equilibrium conditions (e.g. at a higher or lower temperature) and can lead to the measurement of a discontinuous change in energy.

A more recent study of grain boundary energy in Bi-doped Cu demonstrated that a grain boundary complexion transition can be identified by measuring the dihedral angle of a grain boundary groove using AFM [263]. The dihedral angle measurements in the Cu–Bi bicrystals showed two discontinuities in the slope of the grain boundary energy as a function of Bi content. Based on the transition from approximately ~1 ML of Bi adsorption to ~2 ML of Bi adsorption, which was measured with AES, it was concluded that the second slope discontinuity was associated with a grain boundary complexion transition, whereas the first slope discontinuity was an artifact arising from a surface complexion transition that changed the dihedral angle of the grain boundary groove. Grain boundary energy measurements using dihedral angles are relative measurements that compare surface energy to grain boundary energy. Therefore, surface complexion transitions can create discontinuities in the slope of the (relative) grain boundary energy graphs derived from these measurements. This study on Cu–Bi bicrystals [263] highlights the problem of relying exclusively on dihedral angle measurements of grain boundary grooves to identify grain boundary complexion transitions. Concurrent measurements of at least one additional grain boundary property are typically needed to confirm the results of such studies.

The difficulty in experimentally measuring grain boundary energy has led researchers to measure other properties that are strongly correlated with grain boundary complexion transitions, such as grain boundary mobility and diffusivity. Discontinuities in these properties are indirect indicators of complexion transitions in which an increase in mass transport kinetics accompanies increases in the structural or chemical width of the grain boundary [17,22,47,106,203,214]. Grain boundary diffusivity measurements in polycrystalline Cu–Bi alloys demonstrated an abrupt increase in diffusivity by two orders of magnitude at a Bi concentration less than the bulk solidus concentration [162]. This Bi concentration was in agreement with the concentration at which a discontinuity in the slope of grain boundary energy was measured in a previous experiment [263]. These results provide confirmation of Hart's [5] prediction that grain boundary complexion transitions can induce large discontinuities in non-equilibrium grain boundary properties. Although discontinuities in the grain boundary structure and chemical width in the Cu–Bi alloys were not confirmed directly by TEM in these studies, the observed discontinuity in diffusivity as a function of composition is likely associated with a complexion transition that has been identified by STEM in another study [35].

Grain boundary mobility measurements can also be used to identify complexion transitions. To carry out a mobility measurement on a single grain boundary, a special bicrystal geometry is typically used to control the driving force throughout the experiment [264]. This type of bicrystal measurement was used to show that small (10 ppm) additions of Ga to Al increased the grain boundary mobility by about an order of magnitude [258]. The activation enthalpy and the preexponential factor both changed with Ga doping as well, suggesting a change in the mechanism of grain boundary motion due to a grain boundary complexion transition. Grain boundary mobility can also be deduced using grain growth studies on polycrystalline samples, as was done with doped Al_2O_3 [17]. In this study, grain boundary mobility spanning more than three orders of magnitude was directly correlated with six types of grain boundary complexions in polycrystalline Al_2O_3 by S/TEM studies of individual grain boundaries (Fig. 21).

Table 2
Terminology related to complexion transitions and methods of categorizing complexions.

Complexion transitions	*Defined by geometry*	Congruent transition	A complexion transition that occurs without a change in grain boundary character ($\boldsymbol{R}$ and $\hat{\boldsymbol{n}}$ remain invariant); typically involves changes in atomic structure and composition of the grain boundary core
		Non-congruent transition	A complexion transition that results in a change in grain boundary character ($\boldsymbol{R}$ and/or $\hat{\boldsymbol{n}}$ change)
		Structural transition	A complexion transition that occurs when a bulk thermodynamic parameter is varied (T, P, μ_i, etc.) while all five interfacial thermodynamic parameters ($\hat{\boldsymbol{n}}$, $\boldsymbol{R}$) are held constant [8]
		Faceting transition	A complexion transition in which a single complexion decomposes into two complexions: during a faceting transition, the grain boundary plane normal $\hat{\boldsymbol{n}}$ decomposes into $\hat{\boldsymbol{n}}_1$ and $\hat{\boldsymbol{n}}_2$, the area-weighted average of which is equivalent to $\hat{\boldsymbol{n}}$
		Dissociation transition	A complexion transition in which a single complexion decomposes into two complexions: during a dissociation transition, a single grain boundary dissociates into two new interfaces, separated by a new bulk phase, with misorientation $\boldsymbol{R}_1$ and $\boldsymbol{R}_2$, whose combined misorientation is equal to the original misorientation $\boldsymbol{R}$. Also known as a "wetting transition"
	Defined by structure and/or composition	Premelting transition	The formation of a disordered, liquid-like film on a crystalline surface (or at a grain boundary or phase boundary) at a temperature below the melting temperature (or solidus) of the bulk crystalline phase
		Prewetting transition	Occurs when a nanolayer complexion of fixed equilibrium thickness forms at the interface in the thermodynamic vicinity of a wetting transition, i.e. near the temperature or composition at which a wetting transition would occur
		Adsorption transition	A dramatic change (usually a first-order transition) in the composition of an interface in which the relative amount of solute increases or decreases significantly
Complexion categories	*Defined by composition*	Intrinsic	Any complexion that exists in pure systems such as an elemental metal; the composition of the complexion is identical to the bulk composition (although the density may be different)
		Extrinsic	Any complexion that exists in a non-pure system, e.g. in a system that is intentionally doped with additional elements or a system that contains unintentional impurities, such that the complexion composition is in general not equal to the bulk composition
	Defined by thickness and composition	Dry	A complexion with no adsorbed solute or very little adsorption (corresponds to the monolayer complexion in the Dillon–Harmer scheme)
		Moist	A complexion with multilayer solute adsorption (corresponds to the bilayer, trilayer and nanolayer complexions in the Dillon–Harmer scheme)
		Wet	Refers to the existence of a bulk wetting film (solid or liquid) at a boundary (corresponds to the wetting category in the Dillon–Harmer scheme)
	Dillon–Harmer complexions, defined by thickness and composition	Clean complexion	A complexion that is structurally abrupt with a core thickness that is not detectably widened by solute segregation. Solute segregation is not necessarily entirely absent, but is minimal or is not observed at all, and does not lead to an increase in thickness of the grain boundary core, phase boundary core or surface
		Monolayer complexion	A complexion in which adsorbed solute is observed and the majority of the solute is confined to a thickness of a single atomic layer
		Bilayer complexion	A complexion in which most of the adsorbed solute occupies a thickness equal to two atomic layers
		Trilayer complexion	A complexion in which most of the adsorbed solute occupies a thickness equal to three atomic layers
		Nanolayer complexion	A complexion in which the adsorbed solute occupies a thickness greater than three atomic layers, but which is still finite, fixed and governed by equilibrium thermodynamics. Equivalent to IGF
		Wetting	Refers to the existence of a bulk wetting film (solid or liquid) at a grain boundary or interface. There are two complexions (one on each side of the wetting film)
	Defined by degree of periodicity	Ordered	A complexion which has a recognizable degree of long-range structural or chemical periodicity

(*continued on next page*)

Table 2 (*continued*)

	Disordered	A complexion with no recognizable long-range periodicity in either structure or composition
Related terminology	Monolayer	The term "monolayer" is used in surface science to quantify the coverage of a surface by atoms or molecules arranged in a two-dimensional layer. There are several different conventions for defining monolayer. A common convention is that a monolayer is "a number density equal to that of the atoms in a single atomic layer of the substrate material parallel to the surface" [104]. This particular definition breaks down for general grain boundaries, which have two different atomic planes or layers parallel to the boundary plane, and thus another convention must be used. The lone word "monolayer" should not be confused with the phrase "monolayer complexion", which is one of the Dillon–Harmer complexions
	Segregation	An equilibrium phenomenon that occurs in multicomponent materials, causing the composition of grain boundaries to differ from the overall composition at equilibrium
	Adsorption	The term "adsorption" is often used to refer to specific interfacial excess, Γ, which appears in Gibbs adsorption isotherm: $d\gamma = -\sum_i \Gamma_i d\mu_i$ [252]. "Adsorption" is also used descriptively to refer to the phenomenon of the interfacial composition being different than the bulk composition. Although it is sometimes used interchangeably with "segregation" when speaking of grain boundaries, "adsorption" was originally used to discuss this phenomenon when it occurs at surfaces
	Intergranular film (IGF)	A film of material at a grain or phase boundary that is approximately 1–2 nm thick; IGFs have been widely observed in various ceramics that contain impurities such as Si_3N_4 with SiO_2 impurities, ZnO with Bi_2O_3 impurities, and $SrTiO_3$ with TiO_2 impurities. An IGF is referred to as a nanolayer complexion under the Dillon–Harmer categorization scheme

The work of adhesion, $\boldsymbol{W}_{ad}$, of a grain boundary is the reversible work necessary to convert a grain boundary into two free surfaces. For brittle fracture, it may be described by the relationship

$$\boldsymbol{W}_{ad} = 2\gamma_s - \gamma_{gb} \tag{17}$$

Here, γ_s and γ_{gb} are the surface and grain boundary energies, respectively. The reduction in grain boundary energy associated with disordering complexion transitions suggests that the work of adhesion, and therefore the grain boundary strength, should increase. However, in many systems studied experimentally, such complexion transitions have been associated with grain boundary embrittlement [48,265]. Local configurational considerations could outweigh classical thermodynamic considerations in such a case. For example, high enthalpy bonds forming with the adjacent lattice could primarily contribute to lowering the boundary energy, while percolating low enthalpy bonds in the interface could induce embrittlement. This mechanism has been proposed by Luo et al. [48] to explain embrittlement in Ni–Bi. Alternatively, the grain boundary energy may be reduced by an increase in entropy. An entropy increase may result from an increase in the free volume of the boundary, point defects or site disorder, for example, which could also decrease the strength of the boundary. The effect of complexions on strength and toughness is difficult to generally rationalize on the basis of Eq. (17) because the energies of the two resultant surfaces are difficult to predict.

The grain boundary self-diffusion coefficient, D_{GB}, may be described in a manner analogous to the bulk self-diffusion coefficient in terms of the atomic jump frequency, υ, the lattice parameter, a_o, the free energy of vacancy formation, $\Delta G_{f,b}$, the activation energy barrier to atomic migration, $\Delta G_{m,b}$, and a geometric term, g, as follows:

$$D_{GB} = g\upsilon a_o^2 \exp(-\Delta G_{f,b}/RT)\exp(-\Delta G_{m,b}/RT) \tag{18}$$

Borisov et al. [266] first postulated that the free energy of activation for grain boundary diffusion, $\Delta G_b (=\Delta G_{f,b} + \Delta G_{m,b})$, is proportional to the corresponding free energy of activation for diffusion in the lattice, ΔG_l, minus the Gibb's free energy of the grain boundary, γ.

Although this rule is empirical, it provides reasonable predictability in alloys [267]. A reduction in grain boundary energy dominated by enthalpy should increase the activation energy and reduce the grain boundary diffusivity. However, a decrease in energy dominated by increasing entropy should result in enhanced diffusivity. This was recently demonstrated in the Ni–Bi and Cu–Bi systems, where an increase in the entropy of vacancy formation, of 32 and 71 J mol^{-1} K^{-1}, respectively, was associated with thermally induced complexion transitions [268].

A chemically induced transition in segregation level and an associated transition in diffusivity have been also reported in Cu–Bi alloys [162]. The observed discontinuous enhancement in diffusivity as a function of composition is likely associated with a complexion transition [35]. Indirect

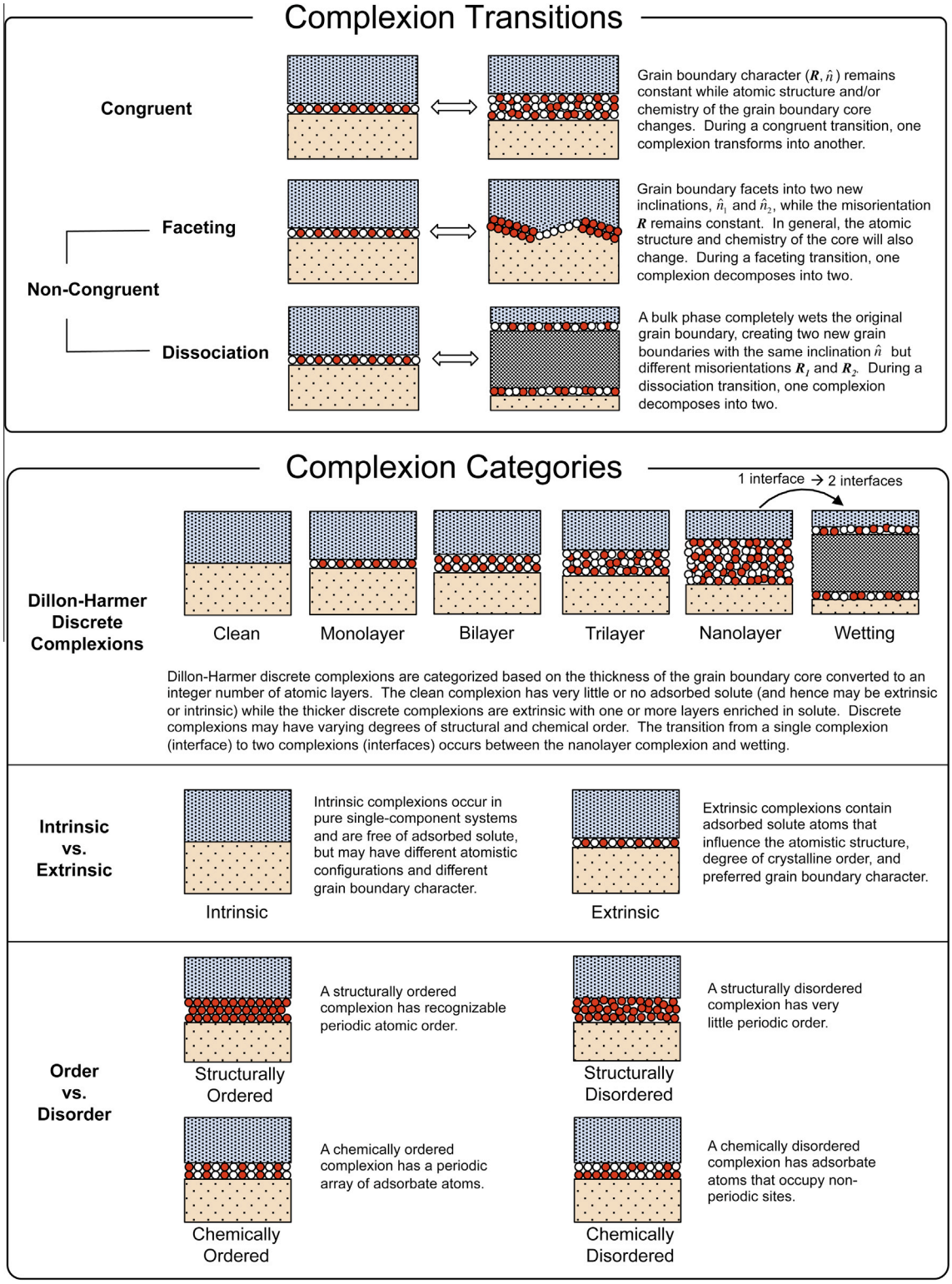

Fig. 26. Schematic diagrams showing different types of complexion transitions and different ways of categorizing complexions. The terminology used in these diagrams is the recommended and preferred terminology for describing complexions and transitions. Terms not shown in these diagrams to describe complexion phenomena in more detail (e.g. "roughening") can be used within the framework of terminology presented here.

indicators, such as sintering rate or grain boundary mobility, have also indicated an enhancement in mass transport kinetics associated with complexion transitions that increase the structural or chemical width of the grain boundary [17,22,47,106,203,214]. The simultaneous decrease in grain boundary energy and increase in diffusion-dependent mass transport kinetics suggests that these complexion transitions primarily impact the entropic con-

tribution to diffusivity. For ionic crystals, the response of the anion and cation sublattices have not been isolated in any given system. It remains unclear how anion and cation doping might affect each sublattice, either together or separately.

In principle, grain boundary complexion transitions may impact many other grain boundary properties as well, including electrical, thermal, optical, chemical and magnetic properties. The role of complexions in affecting these various properties has not been thoroughly investigated, although there is some evidence that complexion transitions are correlated with marked changes in these properties. For example, intergranular films in ZnO introduce barriers to electrical conductivity that produces a non-linear I–V response [269,270]. The electrical properties of individual grain boundaries in MnZn ferrites containing no solute segregation, CaO segregation and intergranular films have been characterized [271,272]. The grain boundaries with no solute segregation displayed the highest conductivity, while the segregated boundaries exhibited the lowest conductivity. The resistance of $X_2Ru_2O_7$ (X = Pb or Bi) samples containing intergranular films is highly sensitive (three orders of magnitude) to the chemistry of those intergranular films [273]. Low-temperature electrical resistivity measurements in Cu–Bi, annealed at high temperatures and then quenched, demonstrated special behavior under conditions in which a dramatic change in Bi adsorption at the grain boundary occurred [274], suggesting that grain boundary complexion transitions in metallic systems may also produce measurable changes in electrical properties. One might envision that higher conductivity complexions may exist in certain materials that could enhance bulk conductivity. Grain boundary complexion transitions occur often in doped titanates, such as $BaTiO_3$ and $SrTiO_3$, and have been utilized to tailor microstructural development [275,276]. $SrTiO_3$ grain boundaries with intergranular films may display varistor behavior [277]. However, their effects on the ferroelectric and dielectric response of the grain boundary have not been studied in detail.

The thermal conductivity of grain boundaries is also affected by complexion transitions. A decrease in the thickness of a Y_2O_3-based intergranular film in AlN was correlated with an increase in bulk thermal conductivity (24%) [278]. However, these results were not completely isolated from the influence of second phase and grain size. Intergranular films have also been associated with a similar decrease in the thermal conductivity of SiC [279,280]. Complexion transitions should affect color centers at grain boundaries as they influence the average coordination and bond distances of atoms at the interface. The effect on local bonding has been demonstrated through X-ray absorption fine spectra characterization [167,281]. Optical mapping of complexions could be an ideal approach to characterizing their distributions in bulk microstructures. Related techniques have been utilized to map grain boundary networks in three dimensions [282,283]. With the proliferation of nanostructured materials containing larger interfacial volume fractions, the need to understand the effect of complexion transitions on interfacial properties will continue to grow. Investigating interfacial structure–property relationships in the context of complexions provides ample future research opportunities.

5.2. Microstructural development

Grain boundary complexion transitions have received the most attention as a result of their influence on microstructural development. In fact, the first direct observation of intergranular films was motivated by their role in dramatically influencing the sintering behavior of Si_3N_4 [221,222]. Subsequently, complexion transitions were implicated in activated sintering, activated grain growth or abnormal grain growth in Al_2O_3 [17,257,284–286], $BaTiO_3$ [276,287], Mo [204,205], SiC [288,289], $SrTiO_3$ [275,290], W[106,207], Y_2O_3 [33,291] and ZnO [47,292,293]. Higher entropy complexions (i.e. complexions that are thermodynamically stable at higher temperatures at fixed T, P and composition) are known to exist in systems such as Al [265], AlN [278,294], Cu [35,295–297], Ni [48], Si [34], TiO_2 [36], $X_2Ru_2O_7$ (X = Pb or Bi) [273], ZnMn ferrite [271,272] and ZrO_2 [298]. In general, higher entropy complexions are associated with increased rates of mass transport and high diffusivity, and therefore are likely to affect abnormal grain growth, activated grain growth or activated sintering exhibited by those systems.

While high diffusivity complexions will generally reduce the characteristic temperature at which sintering becomes practical, in general they will not necessarily enhance densification because similar surface complexions – which may also have increased diffusivity – have been observed in most systems exhibiting higher entropy grain boundary complexions (e.g. Al_2O_3, TiO_2 and ZnO) [24,42,109,198,299]. The classic competition between surface diffusion and grain boundary diffusion in promoting coarsening and densification, respectively, complicates a simple prediction of how interfacial complexions will influence the early stages of sintering in a particular system [300–302]. In the final stages of sintering, the grain boundary complexion will also significantly impact the competition between grain growth and densification. The influence of the complexion transitions on the thermodynamic driving forces (γ_{gb} and γ_s) must be considered along with their distribution amongst grain boundaries and surfaces [29].

Abnormal grain growth results from a difference in the average grain boundary velocities of the boundaries surrounding a particular grain and the rest of the neighboring population [303]. The difference in velocity between normal and abnormal grain boundaries is typically at least a factor of two. This velocity difference may result from a variety of factors related to the local driving force (e.g. strain energy or a non-linear driving force associated with interface-controlled processes) or the grain boundary mobility (e.g. localized complexion transitions or a persistent mobility advantage for a specific misorientated grain in a crystallo-

graphically textured material) [304–307]. Here we distinguish between abnormal grain growth, in which a small subset of the population experiences rapid growth, and activated grain growth, in which a large portion of the population exhibits a discontinuous change in the average grain growth rate as a function of annealing time or temperature. Systems exhibiting normal grain growth have self-similar grain size distributions, systems growing abnormally are never self-similar and systems undergoing activated grain growth are not self-similar for a transient period.

Complexions promote abnormal grain growth when the grain boundaries adjacent to a small fraction of the grains (typically $< 10^{-3}$–10^{-5}) undergo a transition that dramatically increases their mobility relative to the average surrounding population [19,303,304,307]. This phenomenon results in a bimodal (or multimodal) grain size distribution that characterizes abnormal grain growth. The specific boundaries at which these transitions occur will be influenced by chemical heterogeneities and, more importantly, anisotropy in grain boundary energy and structure. While this transition decreases the interfacial energy, and therefore the thermodynamic driving force for growth, the increase in mobility typically dominates the grain growth rate [17,19,29]. These rapidly growing grains become abnormally large with increasing time. For a chemically induced complexion transition, the growing grain will continuously accumulate solute at the grain boundary. This excess solute might precipitate in the lattice behind the moving boundary, partition to neighboring boundaries, precipitate on the boundary or thicken the grain boundary complexion. In $BaTiO_3$, continued abnormal grain growth has been associated with thickening of intergranular films, but not to an extent that can account for all of the excess solute [276]. In Al_2O_3, precipitation of excess solute has been observed behind rapidly migrating abnormal grain boundaries. However, when large abnormal grains impinge in this system, grain boundary-precipitate depinning becomes more difficult and precipitates can persist at the boundaries [21]. Investigations of solute redistribution to neighboring grain boundaries have been limited. Such redistribution is necessary for the observation that a particular complexion type can seemingly surround an entire grain, in spite of the fact that it likely nucleated at an individual boundary, triple line or quad junction [28]. Continued accumulation of solute may partially explain why abnormal grain growth persists even as the misorientation of the boundary varies during grain growth. However, hysteresis associated with complexion transitions may play a role in stabilizing either or both the normal grain population and the abnormal grain population [108,308].

When grain boundary complexion transitions occur at a larger fraction of grain boundaries (typically $> 10^{-3}$–10^{-2}), almost the entire population rapidly re-establishes a unimodal grain size distribution [20,33]. During this transition, the size distribution may deviate significantly from log-normal behavior, but may re-establish such a distribution with continued annealing. Such behavior has been observed in Y_2O_3, where a 10 °C change in annealing temperature changes the average grain size of a log-normal distribution by an order of magnitude [33]. This transition may also be captured as a function of annealing time. These complexion transitions may not be obvious absent a detailed investigation over a broad range of annealing times and temperatures, with data collected at reasonably small time and temperature intervals. Similar activated grain growth behavior has been observed in SiO_2-doped Al_2O_3 [20]. It has also been observed in Al_2O_3 that, when abnormal grains impinge in the presence of high dopant concentration, bulk second-phase pinning will reduce the growth rate of these boundaries [21]. This effect previously suggested that inconsistent results existed with regard to whether intergranular films enhance or suppress grain boundary mobility.

The above discussion highlights the importance of understanding how complexion transitions occur spatially, temporally and as a function of temperature. In Al_2O_3, the number density of abnormal grains increases linearly with grain size at a fixed temperature and exponentially with increasing temperature [19]. A qualitative correlation exists between the relative grain boundary anisotropy in the system and the temperature dependence of the complexion transition rate [29]. The grain size dependence may result from the fact that new grain boundaries are formed randomly during grain growth [19].

Grain growth suppression has attracted significant interest in recent years for applications in nanostructure stabilization [309–313]. Complexion transitions should be considered as important microstructural phenomena in this context. Preventing complexion transitions that enhance diffusivity might be an effective method of suppressing diffusion-controlled grain growth processes. However, the reduction in grain boundary energy associated with complexion transitions may also reduce the driving force for grain growth. In fact, a reduced driving force for grain growth achieved by lowering the grain boundary energy via judicious selection of dopants is currently believed to be the primary contributor to nanocrystalline thermal stability. The concept that grain growth is suppressed by the stabilization of complexions with dramatically low mobility (rather than low grain boundary energy) is a competing explanation that remains to be explored.

Strategies to drive the grain boundary energy toward zero have produced some success in suppressing grain growth. Recently, a significant discontinuous decrease in grain boundary mobility was observed with increasing temperature in $SrTiO_3$ [314]. The exact mechanism remains controversial, although the experimental results indicate that the phenomenon relates to a grain boundary complexion transition in which the atomic structure and chemistry of the grain boundary changes. Abnormal grain growth in $SrTiO_3$ and $BaTiO_3$ without intergranular films is difficult

to explain, but may still relate to transformations in the local structure and chemistry [27,314].

Activated sintering, a process associated with significant sub-eutectic enhancement in sintering rate, was poorly understood for decades [315–317]. Three decades ago, the process became associated with grain boundary complexion transitions that enhance diffusivity in ceramics [221,292]. The existence of intergranular films enables the practical pressureless sintering of refractory non-oxides such as AlN, SiC and Si_3N_4 [278,292,318]. Activated sintering promoted by complexions, specifically intergranular films, has been noted in various oxides [47,273,319]. The concept has recently been extended to explain activated sintering in alloys [22,32,203,320]. Complexions might be related to other anomalous sintering behavior that has been reported in the literature, where intergranular films are not observed (e.g. $MgAl_2O_4$ [321,322] or $Y_3Al_5O_{12}$ [323–325]), but more investigation is required. Recently, it was observed in systems with retrograde solubility that disordered complexions become less stable with increasing temperature [204]. This effect reduces the diffusivity and sintering rate with increasing temperature. The result highlights the role of the thermodynamic stability of interfacial complexions in introducing complex microstructural evolution and response.

Grain boundary complexions will also likely affect other grain-boundary-related processing phenomena, such as grain boundary sliding, superplastic deformation and wetting [298,326,327]. The role of complexions in affecting these processes has not been thoroughly explored. The stability of complexions may be sensitive to process variables such as pressure [296,328], electric field or magnetic field that have not been investigated in detail.

5.3. Bulk properties and behavior

Thermodynamically induced grain boundary complexions may alter fundamental grain boundary properties, which ultimately affects the performance of a bulk polycrystalline aggregate. While the role of complexions in affecting diffusional transport during materials processing is reasonably well studied, their impact on diffusion-dependent properties such as oxidation, creep and ionic conductivity remains somewhat unexplored. Creep in systems containing intergranular films such as oxide-doped silicon nitride has been linked to enhanced transport in these films [298,329,330]. The creep and oxidation rates in alumina are known to vary by several orders of magnitude at a single temperature as a function of dopant type, dopant concentration and processing history [37]. The system also displays various complexions as a function of these same parameters, but the phenomena have not been directly correlated. The published literature often focuses on conditions that produce desirable properties (e.g. low oxidation rate or low creep rate), which may explain the limited investigation of complexion-enhanced oxidation rate or creep rate. In order to identify the complexion transitions responsible for improved properties such as low oxidation and creep rates, regimes of both good and bad properties must be explored, with special attention paid to the dividing line between these regimes.

Silica-rich intergranular films have been observed in zirconia utilized as ion conducting electrolytes [298,331]. These films have been demonstrated to reduce anion conduction [331]. However, similar films may also enhance cation conduction. For example, intergranular films enhance proton conduction in $LaPO_4$ [332]. Similarly, lithium phosphate-based surficial films on lithium ion battery cathode particles have been shown to enhance battery discharge rate [299,333,334]. Enhanced surface diffusion has been invoked as a possible explanation, although other theories have also been proposed [334].

Complexion transitions have been linked to embrittlement in Al–Ga [265], Ni–Bi [48], SiC [335,336] and Si_3N_4 [337–339], and complexion transitions likely explain the anomalous embrittlement observed in Al_2O_3 [340]. Chemically and thermally induced transitions, analogous to complexion transitions, in the structure of dislocations, triple lines and four-grain junctions may also occur. Such transitions have not been well explored, but could play an important role in affecting the nucleation and propagation of cracks. In many systems, avoiding transitions to disordered complexions may be a critical feature of effectively processing materials with desired properties. However, embrittling complexions have been exploited to control crack propagation around large abnormal grains in a scheme that utilizes those grains as toughening fibers [336,338]. This can introduce *r*-curve toughening behavior into intrinsically brittle materials. Cermets such as WC–Co contain intergranular films at grain boundaries [223,341]. However, their impact on the relative strength and toughness of these materials is not fully understood.

6. Conclusion

The term “complexion” has been introduced to differentiate thermodynamically stable interfacial states of matter from bulk phases [13]. Although the concept of grain boundary complexion transitions was proposed in the late 1960s [3], sufficient experimental evidence that conclusively demonstrated the existence of such transitions did not exist until the 1980s [8]. In recent years, complexion transitions have been shown to dramatically affect microstructure development and properties of polycrystalline materials. Grain boundary complexion transitions offer mechanistic explanations for many materials phenomena, such as abnormal grain growth [17], activated sintering [47] and liquid metal embrittlement [48]. Many other properties, such as thermal, electrical, optical and magnetic properties, may also be affected by grain boundary complexion transitions, and these properties should be explored in future studies.

Much of the progress in the study of grain boundary complexions can be attributed to the dramatic enhance-

ment in atomic resolution capability of modern S/TEMs that occurred with the commercial introduction and wide availability of spherical aberration correction during the past decade. Nevertheless, despite the enormous progress that has been made in the field, several outstanding challenges in the study of grain boundary complexions remain. In closing, we will highlight a few of these challenges and suggest avenues for future research.

From a materials engineering perspective, one of the most important tasks is the development of grain boundary complexion diagrams for technologically relevant materials systems. Efforts in this area are already underway. Lines of complexion transition have been determined by theory and experiment, and overlaid onto phase diagrams [22,31,32,106,161,342]. The majority of this work has been carried out on binary systems, although some results for ternary systems exist [342]. Grain boundary transitions in multi-component systems remain largely unexplored, even though they represent the majority of engineering materials. Future research should focus on determining complexion transition lines in model binary and ternary systems as well as in multi-component engineering materials, and should be done in parallel with experiments that determine the direct relationship between each type of complexion and its properties. Such experiments are time-consuming and challenging, but grain boundary complexion diagrams overlaid onto bulk phase diagrams will be most useful if it is known how each complexion transition affects grain boundary properties of interest, such as diffusivity, conductivity and mechanical strength.

Many important grain boundary complexions are only stable at elevated temperatures, but most experimental studies to date have relied on room-temperature observations of grain boundary complexions. The structure and chemistry of the high-temperature complexions is presumably "frozen" in place by rapid quenching of the specimen to room temperature. However, in almost every case explored to date it is unknown whether important changes have occurred in the structure and chemistry of the grain boundary complexion during cooling. In situ heating experiments in the S/TEM are the next frontier in complexions research, and may prove to be one of the best experimental methods for constructing complexion diagrams. In situ experiments allow the observation of grain boundary complexions under nominally equilibrium conditions. Some in situ observations of complexions at elevated temperatures have already been made [230], but this area of study remains largely unexplored. Issues that could complicate the analysis of in situ heating TEM experiments include contamination from TEM specimen preparation (especially Ga contamination from TEM specimen preparation with the FIB), the close proximity of free surfaces on each side of the thin TEM specimen, and electron beam–specimen interaction effects. The relative importance of each of these effects in disturbing the complexion under observation is not clear and must be determined by careful experimentation. Furthermore, the magnitude and influence of each effect will depend upon the properties of the material and the complexion under study.

It is believed that complexion transitions occur via a nucleation and growth process. However, the mechanism and kinetics of the process are not yet known. Some studies have explored the kinetics of wetting transitions [343], but analogous experimental studies on complexion transitions have not yet been done. A recent computer simulation of a Cu $\Sigma5(310)$ grain boundary showed that a structural complexion transition nucleates at the intersection of the grain boundary and the free surface then grows inward along the boundary away from the surface [39]. Research into the nucleation and growth mechanisms of complexions could potentially explain the spatial inhomogeneity of complexion transitions and may also provide novel insight into methods of inhibiting complexion transitions, which could be useful, for example, in the thermal stabilization of nanocrystalline materials.

A great deal of progress has been made during the past few decades in understanding grain boundary complexion transitions. These transitions can strongly influence the properties of polycrystalline materials and should be taken into account when anomalous or unexpected materials behavior occurs. The advent of aberration-corrected S/TEM and other advanced characterization techniques, combined with ever more powerful and realistic computer simulations, offers great promise for the advancement of grain boundary complexions research. By better understanding and controlling grain boundary complexion transitions, it will be possible to advance the science of grain boundary complexion engineering and develop new materials with novel behavior and dramatically improved properties.

Acknowledgements

The authors would like to gratefully acknowledge W. Craig Carter (MIT) for the refined definition of complexions used in this overview, and to thank Paul Wynblatt (Carnegie Mellon University), Jeffrey M. Rickman (Lehigh University), and Andrea J. Harmer (Kutztown University) for helpful discussions, suggestions, and edits. Naixie Zhou (UCSD) drew an initial version of Fig. 5. The authors are indebted to the reviewer, who carefully analyzed the manuscript and offered many insightful and beneficial comments. Financial support from the ONR-MURI under the grant no. N00014-11-1-0678 monitored by David Shifler is gratefully acknowledged by PRC, SJD, JL, GSR, and MPH. MT acknowledges support by the Office of Basic Energy Sciences (OBES), Materials Science Division (MSD), under the auspices of the U.S. Department of Energy by Lawrence Livermore National Laboratory under Contract DE-AC52-07NA27344.

References

[1] Sutton AP, Balluffi RW. Interfaces in crystalline materials. Oxford: Oxford Scientific Publications; 1995.

[2] Lejcek P, Hofmann S. Crit Rev Solid State Mater Sci 1995;20:1.
[3] Hart EW. Scripta Metall 1968;2:179.
[4] Hart EW. In: Burke JJ, Weiss V, editors. Ultrafine-grain metals. Syracuse (NY): Syracuse University Press; 1970. p. 247.
[5] Hart EW. In: Hu H, editor. The nature and behavior of grain boundaries. New York: Plenum; 1972. p. 155.
[6] Cahn JW. J Phys Colloques 1982;43:C6–199.
[7] Pontikis V. J Phys Colloques 1988;49:C5–327.
[8] Rottman C. J Phys Colloques 1988;49:C5–313.
[9] Rottman C. MRS Proc 1991;238:191.
[10] Rabkin EI, Shvindlerman LS, Straumal BB. Int J Mod Phys B 1991;5:2989.
[11] Harmer MP. Science 2011;332:182.
[12] Gottstein G, Shvindlerman LS. Grain boundary migration in metals: thermodynamics, kinetics, applications. Boca Raton (FL): CRC Press; 2010.
[13] Tang M, Carter WC, Cannon RM. Phys Rev B 2006;73:024102.
[14] Carter WC. Personal communication, 2012.
[15] Bishop CM, Tang M, Cannon RM, Carter WC. Mater Sci Eng, A 2006;422:102.
[16] Tang M, Carter WC, Cannon RM. Phys Rev Lett 2006;97:075502.
[17] Dillon SJ, Tang M, Carter WC, Harmer MP. Acta Mater 2007;55:6208.
[18] Dillon SJ, Behera SK, Harmer MP. Acta Mater 2008;56:1374.
[19] Dillon SJ, Harmer MP. J Eur Ceram Soc 2008;28:1485.
[20] Dillon SJ, Harmer MP. J Am Ceram Soc 2008;91:2314.
[21] Dillon SJ, Harmer MP. J Am Ceram Soc 2008;91:2304.
[22] Luo J. Curr Opin Solid State Mater Sci 2008;12:81.
[23] Luo J, Chiang Y-M. Annu Rev Mater Res 2008;38:227.
[24] Qian H, Luo J. Acta Mater 2008;56:4702.
[25] Luo J. Appl Phys Lett 2009;95:071911.
[26] Dillon SJ, Harmer MP, Luo J. JOM 2009;61:38.
[27] Baeurer M, Shih SJ, Bishop C, Harmer MP, Cockayne D, Hoffmann MJ. Acta Mater 2009;58:290.
[28] Dillon SJ, Harmer MP, Rohrer GS. J Am Ceram Soc 2010;93:1796.
[29] Dillon SJ, Miller H, Harmer MP, Rohrer GS. Int J Mater Res 2010;101:50.
[30] Dillon SJ, Harmer MP, Rohrer GS. Acta Mater 2010;58:5097.
[31] Shi X, Luo J. Phys Rev B 2011;84:014105.
[32] Luo J. J Am Ceram Soc 2012;95:2358.
[33] Bojarski SA, Ma S, Lenthe W, Harmer MP, Rohrer GS. Metall Mater Trans A 2012;43A:3532.
[34] Ma S, Meshinchi Asl K, Tansarawiput C, Cantwell PR, Qi M, Harmer MP, et al. Scripta Mater 2012;66:203.
[35] Kundu A, Asl KM, Luo J, Harmer MP. Scripta Mater 2013;68:146.
[36] Ma S, Cantwell PR, Pennycook TJ, Zhou N, Oxley MP, Leonard DN, et al. Acta Mater 2013;61:1691.
[37] Heuer AH. J Eur Ceram Soc 2008;28:1495.
[38] Straumal BB, Baretzky B, Kogtenkova OA, Straumal AB, Sidorenko AS. J Mater Sci 2010;45:2057.
[39] Frolov T, Olmsted DL, Asta M, Mishin Y. Nat Commun 2013;4:1899.
[40] Nussbaum E, Meltzman H, Kaplan WD. J Mater Sci 2012;47:1647.
[41] Priester L. Grain boundaries: from theory to engineering. Berlin: Springer; 2013.
[42] Baram M, Chatain D, Kaplan WD. Science 2011;332:206.
[43] Baram M, Garofalini SH, Kaplan WD. Acta Mater 2011;59:5710.
[44] Kaptay G. J Mater Sci 2012;47:8320.
[45] Meltzman H, Mordehai D, Kaplan WD. Acta Mater 2012;60:4359.
[46] Dillon SJ, Harmer MP. Acta Mater 2007;55:5247.
[47] Luo J, Wang H, Chiang Y-M. J Am Ceram Soc 1999;82:916.
[48] Luo J, Cheng HK, Asl KM, Kiely CJ, Harmer MP. Science 2011;333:1730.
[49] Rohrer GS, Affatigato M, Backhaus M, Bordia RK, Chan HM, Curtarolo S, et al. J Am Ceram Soc 2012;95:3699.
[50] Frank FC. Metall Trans A 1988;19A:403.
[51] Benedetti L, Camurri G, Fontanesi C, Ferrarini P, Giovanardi R. Electrochim Acta 2004;49:1655.
[52] Fontanesi C. Entropy 2010;12:570.
[53] Aust KT. Can Metall Quart 1969;2:173.
[54] Budke E, Surholt T, Prokofjev SI, Shvindlerman LS, Herzig C. Acta Mater 1999;47:385.
[55] Watanabe T, Kimura S-I, Karashima S. Philos Mag A 1984;49:845.
[56] Fowler RH, Guggenheim EA. Stastistical thermodynamics. Cambridge: Cambridge University Press; 1939.
[57] Hill TL. Statistical mechanics. New York: McGraw-Hill; 1956.
[58] de Boer JH. The dynamical character of adsorption. London: Oxford University Press; 1953.
[59] McLean D. Grain boundaries in metals. Oxford: Oxford University Press; 1957.
[60] Kikuchi R, Cahn JW. Phys Rev B 1987;36:418.
[61] Mishin Y, Boettinger WJ, Warren JA, McFadden GB. Acta Mater 2009;57:3771.
[62] Lejcek P. Grain boundary segregation in metals. Berlin: Springer; 2010.
[63] Luo J. Crit Rev Solid State Mater Sci 2007;32:67.
[64] Langmuir I. J Am Chem Soc 1918;40:1361.
[65] Hondros ED, Seah MP. Metall Trans 1977;8A:1363.
[66] Wynblatt P, Chatain D. Metall Mater Trans A 2006;37A:2595.
[67] Lejcek P, Hofmann S. Crit Rev Solid State Mater Sci 2008;33:133.
[68] Kikuchi R, Cahn JW. Phys Rev B 1980;21:1893.
[69] Cahn JW. J Chem Phys 1977;66:3667.
[70] Dash JG, Fu H, Wettlaufer JS. Rep Prog Phys 1995;58:115.
[71] Dash JG, Rempel AM, Wettlaufer JS. Rev Mod Phys 2006;78:695.
[72] Ebner C, Saam WF. Phys Rev Lett 1977;38:1486.
[73] Rutledge JE, Taborek P. Phys Rev Lett 1992;69:937.
[74] Kellay H, Bonn D, Meunier J. Phys Rev Lett 1993;71:2607.
[75] Chatain D, Wynblatt P. Surf Sci 1996;345:85.
[76] Bonn D, Ross D. Rep Prog Phys 2001;64:1085.
[77] Straumal B, Baretzky B. Interf Sci 2004;12:147.
[78] Chatain D, Rabkin E, Derenne J, Bernardini J. Acta Mater 2001;49:1123.
[79] Lopez GA, Mittemeijer EJ, Straumal BB. Acta Mater 2004;52:4537.
[80] Wynblatt P, Chatain D. Mater Sci Eng, A 2008;495:119.
[81] Cahn JW. Physica A 2000;279:195.
[82] Frenken JWM, van der Veen JF. Phys Rev Lett 1985;54:134.
[83] Frenken JWM, Maree PMJ, van der Veen JF. Phys Rev B 1986;34:7506.
[84] Lobkovsky AE, Warren JA. Physica D 2002;164:202.
[85] Tang M, Carter WC, Cannon RM. J Mater Sci 2006;41:7691.
[86] Kobayashi R, Warren JA, Carter WC. Physica D 2000;140:141.
[87] Warren JA, Kobayashi R, Lobkovsky AE, Carter WC. Acta Mater 2003;51:6035.
[88] Bishop CM, Carter WC. Comput Mater Sci 2002;25:378.
[89] Pruessner G, Sutton AP. Phys Rev B 2008;77:054101.
[90] Lobkovsky AE, Warren JA. Phys Rev E 2001;63:051605.
[91] Kobayashi R, Giga Y. J Stat Phys 1999;95:1187.
[92] Demianczuk DW, Aust KT. Acta Metall 1975;23:1149.
[93] Maksimova EL, Shvindlerman LS, Straumal BB. Acta Metall 1988;36:1573.
[94] Hsieh TE, Balluffi RW. Acta Metall 1989;37:1637.
[95] Subramaniam A, Koch CT, Cannon RM, Rühle M. Mater Sci Eng, A 2006;422:3.
[96] Gu H, Cannon RM, Rühle M. J Mater Res 1998;13:376.
[97] Gu H, Pan XQ, Cannon RM, Rühle M. J Am Ceram Soc 1998;81:3125.
[98] Wang HF, Chiang YM. J Am Ceram Soc 1998;81:89.
[99] Chiang YM, Wang H, Lee JR. J Microsc 1998;191:275.
[100] Gu H, Cannon RM, Tanaka I, Rühle M. Mater Sci Eng, A 2006;422:51.
[101] Lipowsky R. Phys Rev Lett 1986;57:2876.
[102] Bishop CM, Cannon RM, Carter WC. Acta Mater 2005;53:4755.
[103] Ebner C, Saam WF. Phys Rev Lett 1987;58:587.
[104] Woodruff DP, Delchar TA. Modern techniques of surface science. Cambridge: Cambridge University Press; 1994.

[105] Israelachvili JN. Intermolecular and surface forces. London: Academic Press; 1994.
[106] Luo J, Shi XM. Appl Phys Lett 2008;92:101901.
[107] Pandit R, Schick M, Wortis M. Phys Rev B 1982;26:5112.
[108] Qian HJ, Luo J. Appl Phys Lett 2007;91:061909.
[109] Qian HJ, Luo J, Chiang YM. Acta Mater 2008;56:862.
[110] Clarke DR. J Am Ceram Soc 1987;70:15.
[111] Clarke DR, Shaw TM, Philipse AP, Horn RG. J Am Ceram Soc 1993;76:1201.
[112] Ackler HD, Chiang Y-M. J Am Ceram Soc 1999;82:183.
[113] Luo J, Tang M, Cannon RM, Carter WC, Chiang Y-M. Mater Sci Eng, A 2006;422:19.
[114] Tartaglino U, Zykova–Timan T, Ercolessi F, Tosatti E. Phys Rep 2005;411:291.
[115] Besold G, Mouritsen OG. Phys Rev B 1994;50:6573.
[116] Ciccotti G, Guillope M, Pontikis V. Phys Rev B 1983;27:5576.
[117] Guillope M, Ciccotti G, Pontikis V. Surf Sci 1984;144:67.
[118] Broughton JQ, Gilmer GH. Phys Rev Lett 1986;56:2692.
[119] Nguyen T, Ho PS, Kwok T, Nitta C, Yip S. Phys Rev Lett 1986;57:1919.
[120] Deymier P, Taiwo A, Kalonji G. Acta Metall 1987;35:2719.
[121] Phillpot SR, Lutsko JF, Wolf D, Yip S. Phys Rev B 1989;40:2831.
[122] Lutsko JF, Wolf D, Phillpot SR, Yip S. Phys Rev B 1989;40:2841.
[123] Nguyen T, Ho PS, Kwok T, Nitta C, Yip S. Phys Rev B 1992;46:6050.
[124] Keblinski P, Phillpot SR, Wolf D, Gleiter H. Phys Rev Lett 1996;77:2965.
[125] Keblinski P, Wolf D, Phillpot SR, Gleiter H. Philos Mag A 1999;79:2735.
[126] Broughton JQ, Gilmer GH. Model Simul Mater Sci Eng 1998;6:87.
[127] Suzuki A, Mishin Y. J Mater Sci 2005;40:3155.
[128] von Alfthan S, Kaski K, Sutton AP. Phys Rev B 2007;76:245317.
[129] von Alfthan S, Haynes PD, Kaski K, Sutton AP. Phys Rev Lett 2006;96:055505.
[130] von Alfthan S, Kaski K, Sutton AP. Phys Rev B 2006;74:134101.
[131] Garofalini SH. Mater Sci Eng, A 2006;422:115.
[132] Blonski S, Garofalini SH. J Am Ceram Soc 1997;80:1997.
[133] Litton DA, Garofalini SH. J Mater Res 1999;14:1418.
[134] Garofalini SH, Luo WW. J Am Ceram Soc 2003;86:1741.
[135] Su XT, Garofalini SH. J Mater Res 2004;19:752.
[136] Jiang Y, Garofalini SH. Acta Mater 2011;59:5368.
[137] Yoshiya M, Tatsumi K, Tanaka I, Adachi H. J Am Ceram Soc 2002;85:109.
[138] Yoshiya M, Tanaka I, Adachi H. J Eur Ceram Soc 2012;32:1301.
[139] Williams PL, Mishin Y. Acta Mater 2009;57:3786.
[140] Painter GS, Becher PF, Sun EY. J Am Ceram Soc 2002;85:65.
[141] Rulis P, Chen J, Ouyang L, Ching WY, Su X, Garofalini SH. Phys Rev B 2005;71:235317.
[142] Painter GS, Becher PF, Shelton WA, Satet RL, Hoffmann MJ. Phys Rev B 2004;70:144108.
[143] Painter GS, Averill FW, Becher PF, Shibata N, van Benthem K, Pennycook SJ. Phys Rev B 2008;78:214206.
[144] Shibata N, Pennycook SJ, Gosnell TR, Painter GS, Shelton WA, Becher PF. Nature 2004;428:730.
[145] Pezzotti G, Painter GS. J Am Ceram Soc 2002;85:91.
[146] Chen J, Ouyang LZ, Rulis P, Misra A, Ching WY. Phys Rev Lett 2005;95:256103.
[147] Ching WY, Rulis P, Ouyang L, Misra A. Appl Phys Lett 2009;94:051907.
[148] Ching WY, Rulis P, Ouyang LZ, Aryal S, Misra A. Phys Rev B 2010;81:214120.
[149] Frolov T, Divinski SV, Asta M, Mishin Y. Phys Rev Lett 2013;110:255502.
[150] Olmsted DL, Foiles SM, Holm EA. Scripta Mater 2007;57:1161.
[151] Daruka I, Hamilton JC. Phys Rev Lett 2004;92:246105.
[152] Olmsted DL, Buta D, Adland A, Foiles SM, Asta M, Karma A. Phys Rev Lett 2011;106:046101.
[153] Udler D, Seidman DN. Phys Rev Lett 1996;77:3379.
[154] Elder KR, Katakowski M, Haataja M, Grant M. Phys Rev Lett 2002;88:245701.
[155] Elder KR, Grant M. Phys Rev E 2004;70:051605.
[156] Mellenthin J, Karma A, Plapp M. Phys Rev B 2008;78:184110.
[157] Berry J, Elder KR, Grant M. Phys Rev B 2008;77:224114.
[158] Chakrabarti DJ, Laughlin DE. Bull Alloy Phase Diagr 1984;5:148.
[159] Voce E, Hallowes APC. J Inst Met 1947;74:323.
[160] Chang L-S, Straumal BB, Rabkin E, Gust W, Sommer F. J Phase Equilibr 1997;18:128.
[161] Chang L-S, Rabkin E, Straumal BB, Baretzky B, Gust W. Acta Mater 1999;47:4041.
[162] Divinski S, Lohmann M, Herzig C, Straumal B, Baretzky B, Gust W. Phys Rev B 2005;71:104104.
[163] Duscher G, Chisholm MF, Alber U, Ruhle M. Nature Mater 2004;3:621.
[164] Wynblatt P, Chatain D, Pang Y. J Mater Sci 2006;41:7760.
[165] Cho J, Wang CM, Chan HM, Rickman JM, Harmer MP. J Mater Res 2001;16:425.
[166] Wang CM, Cargill GS, Chan HM, Harmer MP. J Am Ceram Soc 2002;85:2492.
[167] Wang CM, Cargill GS, Harmer MP, Chan HM, Cho J. Acta Mater 1999;47:3411.
[168] Fang J, Thompson AM, Harmer MP, Chan HM. J Am Ceram Soc 1997;80:2005.
[169] Cho J, Harmer MP, Chan HM, Rickman JM, Thompson AM. J Am Ceram Soc 1997;80:1013.
[170] Cho J, Chan HM, Harmer MP, Rickman JM. J Am Ceram Soc 1998;81:3001.
[171] Thompson AM, Soni KK, Chan HM, Harmer MP, Williams DB, Chabala JM, et al. J Am Ceram Soc 1997;80:373.
[172] Behera SK. PhD dissertation, Materials Science and Engineering, Lehigh University; 2010.
[173] Rohrer GS, Bojarski SA. Personal communication; 2013.
[174] Diebold U, Li SC, Schmid M. Annu Rev Phys Chem 2010;61:129.
[175] Fujishima A, Zhang XT, Tryk DA. Surf Sci Rep 2008;63:515.
[176] Henry CR. Surf Sci Rep 1998;31:231.
[177] Christensen A, Ruban AV, Stoltze P, Jacobsen KW, Skriver HL, Norskov JK, et al. Phys Rev B 1997;56:5822.
[178] Diebold U. Surf Sci Rep 2003;48:53.
[179] Lazzeri M, Vittadini A, Selloni A. Phys Rev B 2001;63:155409.
[180] Zhong Q, Vohs JM, Bonnell DA. J Am Ceram Soc 1993;76:1137.
[181] Wagner M, Kienzle O, Bonnell DA, Rühle M. J Vac Sci Technol, A 1998;16:1078.
[182] Smith J, Bonnell DA. Phys Rev B 2000;62:4720.
[183] Bonnell DA. Prog Surf Sci 1998;57:187.
[184] Tsivion D, Schvartzman M, Huth Pv, Popovitz–Biro R, Joselevich E. Science 2011;333:1003.
[185] Rohrer GS, Henrich VE, Bonnell DA. Surf Sci 1992;278:146.
[186] Kitamura S, Iwatsuki M. Jpn J Appl Phys 1995;34:L145. 2.
[187] Appelbaum JA, Baraff GA, Hamann DR. Phys Rev B 1976;14:588.
[188] Kruger P, Pollmann J. Phys Rev B 1993;47:1898.
[189] Ramstad A, Brocks G, Kelly PJ. Phys Rev B 1995;51:14504.
[190] Boland JJ. Phys Rev Lett 1990;65:3325.
[191] Brommer KD, Needels M, Larson BE, Joannopoulos JD. Phys Rev Lett 1992;68:1355.
[192] Erwin SC, Weitering HH. Phys Rev Lett 1998;81:2296.
[193] Heinz TF, Loy MMT, Thompson WA. Phys Rev Lett 1985;54:63.
[194] Lyo IW, Kaxiras E, Avouris P. Phys Rev Lett 1989;63:1261.
[195] Boland JJ. Surf Sci 1991;244:1.
[196] Brommer KD, Galvan M, Dalpino A, Joannopoulos JD. Surf Sci 1994;314:57.
[197] Bonnell DA, Garra J. Rep Prog Phys 2008;71:044501.
[198] Luo J, Chiang Y-M, Cannon RM. Langmuir 2005;21:7358.
[199] Luo J, Chiang Y-M. Acta Mater 2000;48:4501.
[200] Luo J, Chiang Y-M. J Eur Ceram Soc 1999;19:697.

[201] Johansson SAE, Wahnstrom G. Phys Rev B 2012;86:035403.
[202] Straumal B, Gust W. Mater Sci Forum 1996;207–209:59.
[203] Gupta VK, Yoon DH, Meyer III HM, Luo J. Acta Mater 2007;55:3131.
[204] Shi X, Luo J. Phys Rev Lett 2010;105:236102.
[205] Shi X, Luo J. Appl Phys Lett 2009;94:251908.
[206] Jud E, Zhang Z, Sigle W, Gauckler LJ. J Electroceram 2006;16:191.
[207] Luo J, Gupta VK, Yoon DH, Meyer HM. Appl Phys Lett 2005;87:231902.
[208] Mei QS, Lu K. Prog Mater Sci 2007;52:1175.
[209] Lee J, Tanaka T, Mori H, Penttila K. JOM 2005;57:56.
[210] Tanaka T, Hara S. Z Metallkd 2001;92:1236.
[211] Tanaka T, Hara S. Z Metallkd 2001;92:467.
[212] French RH, Parsegian VA, Podgornik R, Rajter RF, Jagota A, Luo J, et al. Rev Mod Phys 2010;82:1887.
[213] Lee JS, Klockgeter K, Herzig C. Coll Phys 1990;51:C1.
[214] Jung JI, Zhou NX, Luo J. J Mater Sci 2012;47:8308.
[215] Ad-hoc Interagency Group on Advanced Materials, Materials Genome Initiative for Global Competitiveness. Washington DC: National Science and Technology Council; July 2011.
[216] Seah MP, Hondros ED. Proc Roy Soc Lond A 1973;335:191.
[217] Pang Y, Wynblatt P. J Am Ceram Soc 2005;88:2286.
[218] Kelly TF, Miller MK. Rev Sci Instrum 2007:78.
[219] Miller MK, Forbes RG. Mater Charact 2009;60:461.
[220] Seidman DN. Annu Rev Mater Res 2007;37:127.
[221] Clarke DR, Thomas G. J Am Ceram Soc 1977;60:491.
[222] Lou LKV, Mitchell TE, Heuer AH. J Am Ceram Soc 1978;61:392.
[223] Jayaram V, Sinclair R. J Am Ceram Soc 1983;66:C137.
[224] Clarke DR, Zaluzec NJ, Carpenter RW. J Am Ceram Soc 1981;64:601.
[225] Clarke DR, Zaluzec NJ, Carpenter RW. J Am Ceram Soc 1981;64:608.
[226] Clarke DR, Zaluzec NJ. J Am Ceram Soc 1982;65:C132.
[227] Yu Z, Wu Q, Rickman JM, Chan HM, Harmer MP. Scripta Mater 2013;68:703.
[228] Winkelman GB, Dwyer C, Hudson TS, Nguyen-Manh D, Döblinger M. Appl Phys Lett 2005;87:061911.
[229] Dillon SJ, Harmer MP. J Am Ceram Soc 2007;90:996.
[230] Bhattacharyya S, Subramaniam A, Koch CT, Cannon RM, Rühle M. Mater Sci Eng, A 2006;422:92.
[231] Detor AJ, Miller MK, Schuh CA. Philos Mag 2006;86:4459.
[232] Chellali MR, Balogh Z, Schmitz G. Ultramicroscopy 2012. http://dx.doi.org/10.1016/j.ultramic.2012.12.002.
[233] Seidman DN, Krakauer BW. Acta Mater 1998;46:6145.
[234] Straumal B, Kogtenkova O, Protasova S, Mazilkin A, Zieba P, Czeppe T, et al. Mater Sci Eng, A 2008;495:126.
[235] Kogtenkova OA, Protasova SG, Mazilkin AA, Straumal BB, Zieba P, Czeppe T, et al. J Mater Sci 2012;47:8367.
[236] Straumal BB, Kogtenkova O, Zieba P. Acta Mater 2008;56:925.
[237] Rohrer GS. J Mater Sci 2011;46:5881.
[238] Mullins WW. J Appl Phys 1957;28:333.
[239] Dillon SJ, Rohrer GS. Acta Mater 2009;57:1.
[240] Handwerker CA, Dynys JM, Cannon RM, Coble RL. J Am Ceram Soc 1990;73:1371.
[241] Saylor DM, Rohrer GS. J Am Ceram Soc 1999;82:1529.
[242] Dillon SJ, Rohrer GS. J Am Ceram Soc 2009;92:1580.
[243] Li J, Dillon SJ, Rohrer GS. Acta Mater 2009;57:4304.
[244] Rohrer GS, Li J, Lee S, Rollett AD, Groeber M, Uchic MD. Mater Sci Technol 2010;26:661.
[245] Saylor DM, Morawiec A, Rohrer GS. Acta Mater 2003;51:3675.
[246] Herring C. Phys Rev 1951;82:87.
[247] Ference TG, Balluffi RW. Scripta Metall 1988;22:1929.
[248] Holm EA, Foiles SM. Science 2010;328:1138.
[249] Olmsted DL, Holm EA, Foiles SM. Acta Mater 2009;57:3704.
[250] Park CW, Yoon DY, Blendell JE, Handwerker CA. J Am Ceram Soc 2003;86:603.
[251] Yoon DY, Cho YK. J Mater Sci 2005;40:861.
[252] Wynblatt P. Annu Rev Mater Res 2008;38:173.
[253] Avishai A, Scheu C, Kaplan WD. Acta Mater 2005;53:1559.
[254] Cannon RM, Esposito L. Z Metallkd 1999;90:1002.
[255] Esposito L, Saiz E, Tomsia AP, Glaeser A. In: Tomsia AP, Cannon RM, editors. Ceramic microstructure: control at the atomic level. New York: Plenum; 1998. p. 503.
[256] Cannon RM, Rühle M, Hoffmann MJ, French RH, Gu H, Tomsia AP, et al. Ceram Trans 2000;118:427.
[257] MacLaren I, Cannon RM, Gulgun MA, Voytovych R, Popescu-Pogrion N, Scheu C, et al. J Am Ceram Soc 2003;86:650.
[258] Molodov DA, Czubayko U, Gottstein G, Shvindlerman LS, Straumal B, Gust W. Philos Mag Lett 1995;72:361.
[259] Cahn JW. Acta Metall 1962;10:789.
[260] Watanabe T. Res Mech 1984;11:47.
[261] Gleiter H. Z Metallkd 1970;61:282.
[262] Grabski MW, Kirchner HOK, Shell CA. Z Metallkd 1970;61:977.
[263] Schölhammer J, Baretzky B, Gust W, Mittemeijer E. Interf Sci 2001;9:43.
[264] Gottstein G, Molodov DA, Shvindlerman LS. Interf Sci 1998;6:7.
[265] Sigle W, Richter G, Ruehle M, Schmidt S. Appl Phys Lett 2006;89:121911.
[266] Borisov VT, Golikov VM, Shcherbedinskii GC. Fiz Met Metalloved 1964;17:881.
[267] Gupta D. Metall Trans A 1977;8A:1431.
[268] Tai K, Feng L, Dillon SJ. J Appl Phys 2013;113:193507.
[269] Morris WG. J Vac Sci Technol 1976;13:926.
[270] Olsson E, Dunlop GL. J Appl Phys 1989;66:3666.
[271] Laval JY, Pinet MH. J Phys Colloques 1986;47:C1–329.
[272] Tsunekawa H, Nakata A, Kamijo T, Okutani K, Mishra RK, Thomas G. IEEE Trans Magn 1979;15:1855.
[273] Chiang Y-M, Silverman LA, French RH, Cannon RM. J Am Ceram Soc 1994;77:1143.
[274] Straumal BB, Sluchanko NE, Gust W. Defect Diffus Forum 2001;188–190:185.
[275] Chung S-Y, Kang S-JL. Acta Mater 2003;51:2345.
[276] Choi S-Y, Yoon D-Y, Kang S-JL. Acta Mater 2004;52:3721.
[277] Fujimoto M, Chiang YM, Roshko A, Kingery WD. J Am Ceram Soc 1985;68:C.300.
[278] Nakano H, Watari K, Urabe K. J Eur Ceram Soc 2003;23:1761.
[279] Nakano H, Watari K, Kinemuchi Y, Ishizaki K, Urabe K. J Eur Ceram Soc 2004;24:3685.
[280] Nakano H, Watari K, Ishizaki K, Urabe K. Zairyo 2005;54:559.
[281] Wang CM, Cargill GS, Chan HM, Harmer MP. Acta Mater 2000;48:2579.
[282] Ramirez MO, Wisdom J, Li H, Aung YL, Stitt J, Messing GL, et al. Opt Express 2008;16:5965.
[283] Stevenson AJ, Bittel BC, Leh CG, Li X, Dickey EC, Lenahan PM, et al. Appl Phys Lett 2011;98. 051906/1.
[284] Powell-Dogan CA, Heuer AH. J Am Ceram Soc 1990;73:3684.
[285] Powell-Dogan CA, Heuer AH. J Am Ceram Soc. 1990;73:3670.
[286] Susnitzky DW, Carter CB. J Am Ceram Soc 1990;73:2485.
[287] Yoon B-K, Choi S-Y, Yamamoto T, Ikuhara Y, Kang S-JL. Acta Mater 2009;57:2128.
[288] Duval-Riviere ML, Vicens J. J Phys IV 1993;3:1417.
[289] Pezzotti G, Kleebe H-J, Ota K-I. J Am Ceram Soc 1998;81:3293.
[290] Fujimoto M, Kingery WD. J Am Ceram Soc 1985;68:169.
[291] Ma S, Harmer MP. J Am Ceram Soc 2011;94:651.
[292] Clarke DR. Ultramicroscopy 1979;4:33.
[293] Chiang Y-M, Lee J-R, Wang H. Microstructure and intergranular phase distribution in Bi_2O_3-doped ZnO. New York: Plenum; 1998. p. 131.
[294] Nakano H, Watari K, Hayashi H, Urabe K. J Am Ceram Soc 2002;85:3093.
[295] Chang LS, Rabkin E, Straumal B, Lejcek P, Hofmann S, Gust W. Scripta Mater 1997;37:729.
[296] Chang L-S, Straumal B, Rabkin E, Lojkowski W, Gust W. Acta Mater 2007;55:335.
[297] Straumal BB, Prokofjev SI, Chang LS, Sluchanko NE, Barezky B, Gust W, et al. Diffus Defect Data, Pt A 2001;194–199:1343.

[298] Gust M, Goo G, Wolfenstine J, Mecartney ML. J Am Ceram Soc 1993;76:1681.
[299] Kayyar A, Qian H, Luo J. Appl Phys Lett 2009;95:221905.
[300] Burke JE. J Am Ceram Soc 1957;40:80.
[301] Kingery WD. J Appl Phys 1959;30:301.
[302] Coble RL. J Appl Phys 1961;32:793.
[303] Rollett AD, Srolovitz DJ, Anderson MP. Acta Metall 1989;37:1227.
[304] Rollett AD, Mullins WW. Scripta Mater 1997;36:975.
[305] Park YJ, Hwang NM, Yoon DY. Metall Mater Trans A 1996;27A:2809.
[306] Kang M-K, Kim D-Y, Hwang NM. J Eur Ceram Soc 2002;22:603.
[307] Holm EA, Miodownik MA, Rollett AD. Acta Mater 2003;51:2701.
[308] Ackler HD, Chiang Y-M. J Am Ceram Soc 1997;80:1893.
[309] Kirchheim R. Acta Mater 2002;50:413.
[310] Kirchheim R. Acta Mater 2007;55:5139.
[311] Kirchheim R. Acta Mater 2007;55:5129.
[312] Detor AJ, Schuh CA. Acta Mater 2007;55:371.
[313] Chookajorn T, Murdoch HA, Schuh CA. Science 2012;337:951.
[314] Baeurer M, Weygand D, Gumbsch P, Hoffmann MJ. Scripta Mater 2009;61:584.
[315] Hayden HW, Brophy JH. J Electrochem Soc 1963;110:805.
[316] Smith JT. J Appl Phys 1965;36:595.
[317] German RM, Munir ZA. Rev Powder Metall Phys Ceram 1982;2:9.
[318] Hannink RHJ, Bando Y, Tanaka H, Inomata Y. J Mater Sci 1988;23:2093.
[319] Clarke DR. Ceram Trans 1994;44:93.
[320] Straumal BB. Arch Metall Mater 2004;49:323.
[321] Rozenburg K, Reimanis IE, Kleebe H-J, Cook RL. J Am Ceram Soc 2008;91:444.
[322] Reimanis I, Kleebe H-J. J Am Ceram Soc 2009;92:1472.
[323] Kochawattana S, Stevenson A, Lee S-H, Ramirez M, Gopalan V, Dumm J, et al. J Eur Ceram Soc 2008;28:1527.
[324] Maitre A, Salle C, Boulesteix R, Baumard J-F, Rabinovitch Y. J Am Ceram Soc 2008;91:406.
[325] Boulesteix R, Maitre A, Baumard JF, Salle C, Rabinovitch Y. Opt Mater 2009;31:711.
[326] Marya SK, Wyon G. J Phys Colloques 1975:C4–C309.
[327] Straumal B, Baretzky B. Defect Diffus Forum 2003;216–217:53.
[328] Shvindlerman LS, Lojkowski W, Rabkin EI, Straumal BB. J Phys Colloques 1990;51:C1–629.
[329] Chadwick MM, Jupp RS, Wilkinson DS. J Am Ceram Soc 1993;76:385.
[330] Wolfenstine J, Kohlstedt DL. Phys Chem Miner 1994;21:234.
[331] Lee J-H. Monatsh Chem 2009;140:1081.
[332] Harley G, Yu R, De Jonghe LC. Solid State Ionics 2007;178:769.
[333] Kang B, Ceder G. Nature 2009;458:190.
[334] Sun K, Dillon SJ. Electrochem Commun 2011;13:200.
[335] Cao JJ, MoberlyChan WJ, De Jonghe LC, Gilbert CJ, Ritchie RO. J Am Ceram Soc 1996;79:461.
[336] Ritchie RO, Zhang XF, De Jonghe LC. Mater Res Soc Symp Proc 2004;819:3.
[337] Lange FF. J Am Ceram Soc 1979;62:428.
[338] Becher PF, Painter GS, Sun EY, Hsueh CH, Lance MJ. Acta Mater 2000;48:4493.
[339] Garofalini SH, Zhang S. J Am Ceram Soc 2010;93:235.
[340] Carniglia SC. J Am Ceram Soc 1972;55:243.
[341] Fernandes CM, Willinger MG, Vieira MT, Senos AMR. Microsc Microanal 2012;18:109.
[342] Noskovich OI, Rabkin EI, Semenov VN, Straumal BB, Shvindlerman LS. Acta Metall Mater 1991;39:3091.
[343] Glickman EE, Nathan M. J Appl Phys 1999;85:3185.
[344] Sigle W, Richter G, Ruhle M, Schmidt S. Appl Phys Lett 2006;89:121911.
[345] Furukawa Y, Nada H. Advances in understanding crystal growth mechanisms. Amsterdam: Elsevier, B.V; 1997.
[346] Buffat P, Borel J-P. Phys Rev A 1976;13:2287.